M.Sc. in CE

A.N. Sakib

**MASTER OF SCIENCE IN CIVIL ENGINEERING**

COMPRESSIVE BEHAVIOUR OF DISCONTINUOUS DOUBLE STEEL TUBE CONFINED CONCRETE COLUMN

# Compressive Behaviour of Discontinuous Double Steel Tube Confined Concrete Column

**Ann Nazmun Sakib**

**Department of Civil and Environmental Engineering**
Islamic University of Technology
April, 2025

**2025**

## Recommendation of the Board of Examiners

The thesis titled "**Compressive Behaviour of Discontinuous Double Steel Tube Confined Concrete Column**" submitted by Ann Nazmun Sakib, Student ID 191051013 of Academic Year 2019-2020 has been found as satisfactory and accepted as partial fulfilment of the requirement for the degree of Master of Science in Civil Engineering.

1. Chairmen

-------------------------------------------------------------

Dr. Md. Imran Kabir
Assistant Professor
Department of Civil and Environmental Engineering (CEE)
Islamic University of Technology (IUT)

2. Member (Ex-Officio)

-------------------------------------------------------------

Dr. Shakil Mohammad Rifat
Professor and Head
Department of Civil and Environmental Engineering (CEE)
Islamic University of Technology (IUT)

3. Member

-------------------------------------------------------------

Dr. Hossain Md. Shahin
Professor
Department of Civil and Environmental Engineering (CEE)
Islamic University of Technology (IUT)

4. Member (External)

-------------------------------------------------------------

Dr. Md. Jahidul Islam
Associate Professor
Department of Civil Engineering (CE)
Military Institute of Science and Technology (MIST)

## Declaration of Candidate

It is hereby declared that this thesis has not been submitted elsewhere for the award of any Degree or Diploma.

| | |
|---|---|
| Signature of Candidate: | |
| Name of Candidate: | Ann Nazmun Sakib |
| Student Id: | 191051013 |
| Academic Year: | 2019-2020 |
| Date: | 18-04-2025 |

# Dedication

I dedicate this thesis to my parents, my brother, my sister-in-law and my two nephews, Muhammad and Muddassir.

# Table of Content

# List of Tables

# List of Figures

# List of Symbols

| Symbols | Description |
|---|---|
| $D_o$ | Diameter of outer steel tube |
| $t_o$ | Thickness of outer steel tube |
| $D_i$ | Diameter of inner steel tube |
| $t_i$ | Thickness of inner steel tube |
| $f_{yo}$ | Yield strength of outer steel tube |
| $f_{yi}$ | Yield strength of inner steel tube |
| $f_u$ | Ultimate strength of steel tube |
| $f'_{cc}$ | Compressive strength of confined concrete |
| $f_{cu}$ | Unconfined cylindrical concrete strength |
| $f_r$ | Residual stress of concrete |
| $f'_{cs}$ | Compressive strength of sandwich concrete |
| $f'_{cs}$ | Compressive strength of inner concrete |
| $\lambda_r$ | Sectional slenderness ratio |
| $\lambda$ | Global slenderness ratio |
| $\bar{\lambda}$ | Relative slenderness |
| $P_{FE}$ | Numerical predicted axial strength |
| $R_{FE}$ | Numerical predicted residual strength |
| $A_{cs}$ | Area of sandwich concrete |
| $A_{ci}$ | Area of inner concrete |
| $\xi$ | Confinement ratio |
| $\eta_s$ | Slenderness factor |
| $\eta_c$ | Confinement factor |
| $\chi$ | Slenderness reduction factor |
| $P_{GB}$ | Compressive strength of DDSTCC column by GB 50936–2014 |
| $P_{DBJT}$ | Compressive strength of DDSTCC column by DBJ/T 13-51-2010 |
| $P_{EC4}$ | Compressive strength of DDSTCC column by EC4 |
| $P_{MAN}$ | Compressive strength of DDSTCC column by modified formula |
| $\gamma_m$ | Partial safety factor |

# Acknowledgements

Glory and praise be to Allah, the Almighty, for granting me the strength, wisdom and good health to continue and complete this research. All praise belongs to Allah, the Most Gracious and Merciful, whose countless blessings have guided me throughout this journey.

I would like to extend my heartfelt gratitude to my supervisor, Dr. Md. Imran Kabir for his invaluable guidance, unwavering support and advice throughout my research journey. His faith in my abilities and patience during challenging times have been a source of motivation and encouragement.

I wish to express my sincere gratitude to Dr. Hossain Md. Shahin and Dr. Md. Jahidul Islam for dedicating their valuable time to review my research and provide thoughtful feedback.

Finally, I am deeply indebted to my family for their unwavering support, endless encouragement and understanding throughout this journey. Their love and belief in me have been a constant source of strength and I could not have accomplished this without them.

# Abstract

In this study, a new type of concrete filled tube (CFT) column knowns as discontinuous double steel tube confined concrete (DDSTCC) columns were investigated for compressive behaviour through numerical simulations and analytical modelling. Unlike conventional concrete filled steel tube (CFST) and concrete filled double steel tube (CFDST) columns, the DDSTCC column consists of inner continuous steel tube and outer discontinuous steel tube with infilled inner and sandwich concrete. The discontinuous outer steel tube enhances the confinement, higher than the continuous tube, thereby improving load bearing capacity and buckling behaviour. The numerical simulation was carried out using ABAQUS, incorporating both material and geometric nonlinearities. First, the accuracy of the finite element (FE) models was validated against experimental data in terms of load-displacement, peak loads, and failure behaviour. Then, a three-stage parametric study was conducted considering key parameters such as thickness of steel tubes, diameter of inner tube, height, strength of materials and loading eccentricity. Regarding stub and full-scale slender column, using high strength outer steel and sandwich concrete could significantly improves axial strength 20% to 24% while increasing the diameter of inner tube improves post peak stability. However, for eccentrically loaded column the moment capacity and buckling resistance was influence by thickness and diameter of inner steel tube. In terms of failure pattern, slender DDSTCC columns exhibited C-shaped buckling, with failure primarily influenced by global instability while eccentrically loaded column shows localized failure. The existing design standards EC4, GB 50936–2014, and DBJ/T 13-51-2010 applicable for CFST column fails to fully capture the unique confinement effects of DDSTCC columns. Thus, a modified analytical formula was developed,

achieving mean test-to-predicted strength ratios of 1.02 (stub) and 0.95 (full-scale) with a partial safety factor of 0.98. A comparative analysis shows that the proposed formula demonstrates a better predictive accuracy and material efficiency than other design standards. Thus, the DDSTCC columns could be a viable option for high-rise and large-span structures due to its superior confinement, enhanced compressive behaviour with stable buckling failure pattern. The findings of this study provide valuable design guideline which could shed light into the applicability of this column and guide the day-to-day design practitioners for high rise construction.

# CHAPTER 1: INTRODUCTION

## 1.1 Background

Steel-concrete composite columns combine the strengths of both materials, creating a unified structural member with enhanced performance. Reinforced concrete (RC) columns, while commonly used, are not ideal for tall buildings due to their large cross-sectional areas and brittle failure under heavy loads. On the other hand, using only structural steel may lead to premature buckling failure. As a result, the use of bare steel columns construction in the world's tallest buildings has steadily decreased since the 1960s, with composite columns emerging as the preferred choice (Gabel et al., 2015; Reddy et al., 2021). This trend underscores the growing importance of steel-concrete composite columns, which are poised to dominate in future structural design. The increasing demand for these materials further highlights the need for continued research in this area. In response, a new type of composite column system—known as the concrete-filled tube (CFT) column—was introduced in the past to effectively combining the strengths of both steel and concrete in a unified structural form. One notable example of CFT column is the concrete-filled steel tube (CFST) column (see Fig 1.1a), which usually consists of a hollow steel tube filled with concrete. Over time, various configurations have emerged to further optimize the performance of these columns. Notable among these are the concrete-filled double steel tube (CFDST) column (see Fig 1.1b) which involves two concentric steel tubes filled with concrete, and the discontinuous double steel tube confined concrete (DDSTCC) column, where the outer tube is discontinuous as illustrated in Fig 1.1c. These types of CFT columns offer a range of structural advantages over traditional RC and bare steel columns (Samarakkody et al., 2017).

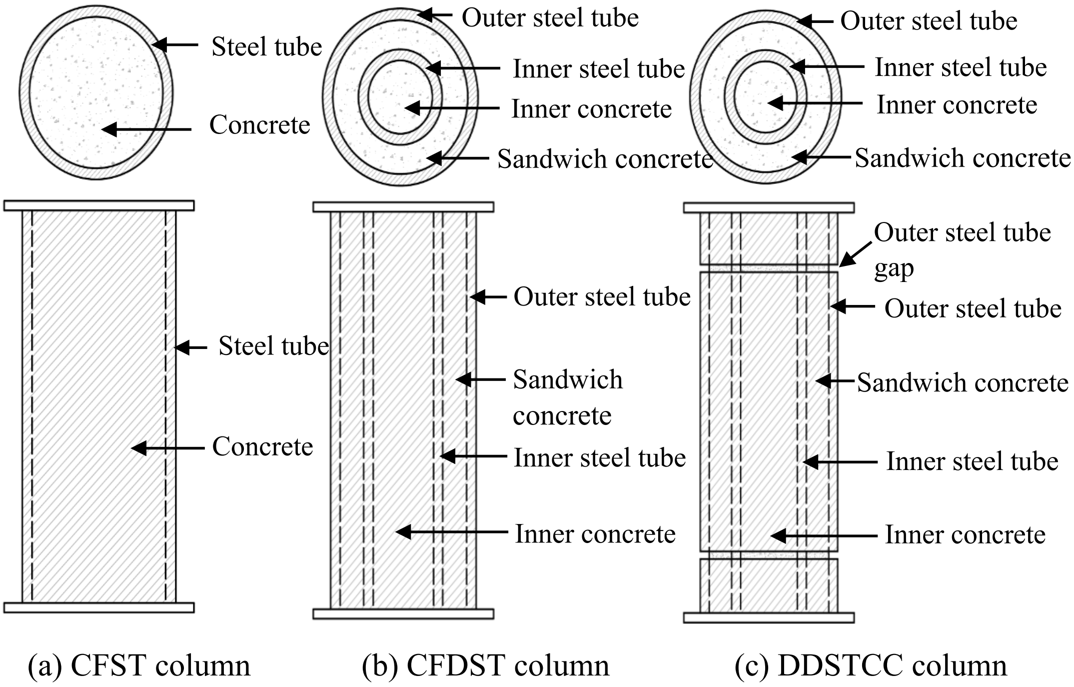


**Fig 1.1** Different types of concrete filled tube (CFT) columns

Over the past few decades, CFST columns have gained significant attention in structural engineering due to their superior load-bearing capacity, enhanced durability, and efficient use of materials. As a result, CFST columns are increasingly being utilized in the construction of high-rise buildings and large-span bridges, offering an effective solution for these demanding applications (Han et al., 2007, 2014; Liew & Xiong, 2012). The success of CFST columns can be attributed to the composite action between the steel tube and the concrete core. The steel tube serves as both formwork and longitudinal reinforcement, while also providing confinement to the concrete. This synergy between the two materials enhances the overall performance of the column, making it an efficient and cost-effective choice for modern construction (Han et al., 2014; Liang et al., 2020). By utilizing both materials, CFST columns demonstrate superior ultimate strength and enhanced post-peak behaviour when compared to RC and bare steel columns, as illustrated in Fig 1.2 and 1.3 (Han et al., 2014).

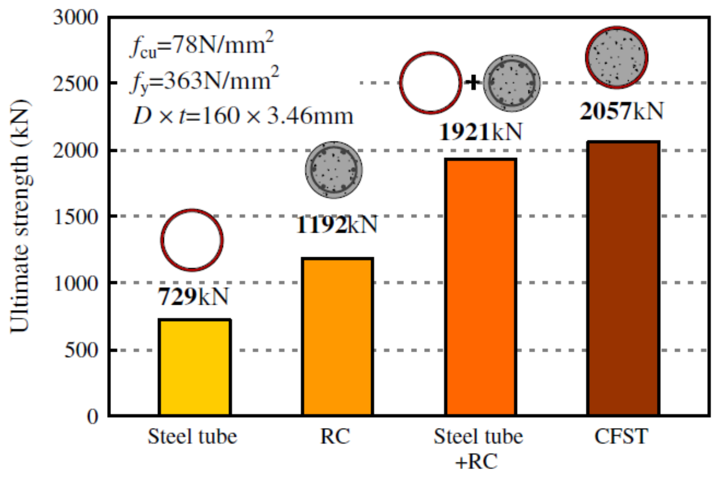


**Fig 1.2** Comparison of ultimate strength between different types of columns (Han et al., 2014)

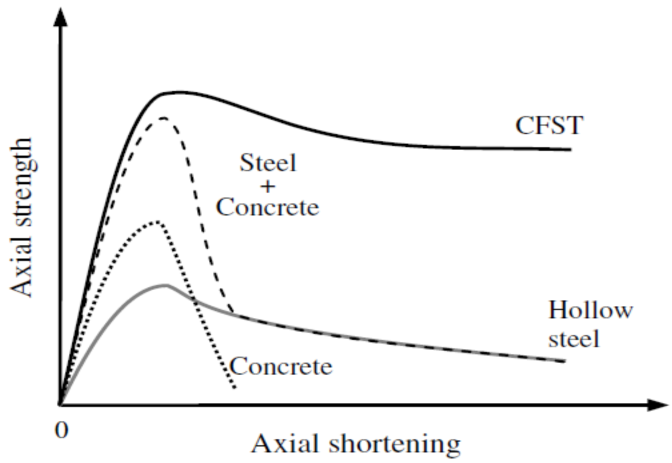


**Fig 1.3** Axial strength vs axial shortening behaviour of different types of columns (Han et al., 2014)

CFST columns are also available in various shapes, including circular, rectangular, elliptical, and hexagonal sections as shown in Fig 1.4 (Ren et al., 2014). Each shape offers distinct advantages in terms of structural behaviour and design flexibility. The circular section is particularly effective in providing confinement to the concrete core, which improves the column's load-bearing capacity and overall strength. The rectangular section, while offering less confinement than the circular shape, is especially advantageous in beam-column joint applications due to its ability to better facilitate these connections (Ibañez et al., 2018). Elliptical and octagonal sections, though less efficient in terms of confinement, are often used for aesthetic purposes, as their unique shapes do not significantly compromise the structural performance of the column (Evirgen et al., 2014; Zhu & Chan, 2018). This versatility in design allows engineers to adopt CFST columns to both structural and aesthetic requirements in a wide range of applications. Since the 1960s, extensive research has focused on CFST columns, revealing both their advantages and limitations (Han et al., 2014).

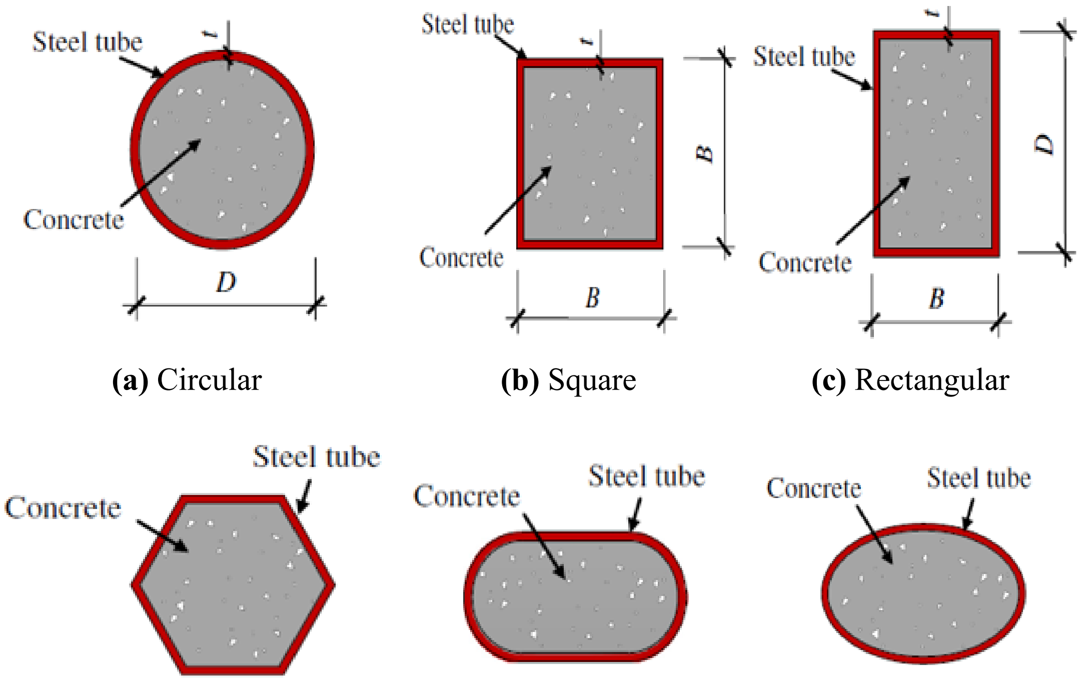


**(a)** Circular **(b)** Square **(c)** Rectangular

**(d)** Hexagonal **(e)** Elliptical

**Fig 1.4** Typical cross-sectional shapes of CFST column (Ren et al., 2014)

Despite their benefits, CFST columns require large cross-sectional areas, which can limit architectural flexibility, particularly in high-rise buildings. Additionally, the outer steel tube is susceptible to fire and corrosion, raising concerns about long-term durability and further restricting design options (Ahmed et al., 2019; Yan & Zhao, 2021; Yang et al., 2024; Wang et al., 2019). These challenges highlight the need for continued research to improve the efficiency, durability, and design versatility of CFST columns in modern construction.

These challenges are addressed through a new type of CFT column known as the concrete-filled double steel tube (CFDST) column (see Fig. 1.1b), (Liew & Xiong, 2012a; 2015b; Zheng & Tao, 2018). The CFDST features a double-tube configuration that effectively mitigates the issues associated with traditional single-tube CFST columns. The presence of two steel tubes reduces the overall cross-sectional area required, which in turn decreases the material demand and improves architectural flexibility. The double-tube configuration also enhances the confinement of the concrete core, further improving the column's load-bearing capacity and overall performance (Xiong et al., 2017; Zheng & Tao, 2018). Moreover, the outer tube offers additional protection against fire and corrosion, addressing two key durability concerns associated with CFST columns (H. Zhu et al., 2024). The applicability of CFDST columns has been extensively explored through both experimental and numerical studies by various researchers. These studies have examined the performance of CFDST columns under a various loading conditions and geometric configurations (Ahmed et al., 2020; Ekmekyapar & Al-Eliwi, 2017; Liew & Xiong, 2012; Zheng et al., 2018). Despite the advancements made with CFDST columns, one issue persists, similar to the CFST columns—early onset of local buckling in the outer steel tube at both column ends. The reason behind the early onset of local buckling in both CFST and CFDST columns is primarily attributed to the difference in Poisson's ratio between steel and concrete (Lu et al., 2022). Upon loading, the steel tube tends to expand outward more rapidly than the concrete core, leading to debonding between the two materials. Although this debonding is mitigated in the later stages of loading, it is the primary cause of reduced confinement to the concrete and the subsequent early buckling of the steel tube (Hoang & Fehling, 2017; Lu et al., 2022; Yu et al., 2009).

Towards this end, the researchers have proposed a practical solution to address this issue by discontinuing the outer steel tube at both ends of the column. By removing the tube from these regions, the outer steel tube is no longer subjected to axial load at the ends, effectively delaying the onset of local buckling and shifting it to more favourable the mid-height section of the column. This modification helps to reduce the premature buckling at the column ends, thereby enhancing the confinement of the concrete and improving the overall stability of the column (Lu et al., 2022; Yu et al., 2009). This slight adjustment resulted in an increase in confining stress and axial load capacity by up to 24% and 2%, respectively, compared to CFST column (Yu et al., 2009). Additionally, the discontinuous steel tube simplifies the beam-column joint design, making it easier for construction. With the steel tube absent at the joints, the complexity of construction is reduced, allowing for a more straightforward assembly process (J. Zhu & Chan, 2019).

Recently, Lu et al. (2022) introduced a novel CFT column design known as the discontinuous double steel tube confined concrete (DDSTCC) column as shown in Fig. 1.1c and experimentally analysed its compressive performance in compact stub sections. The DDSTCC column represents the latest advancement in CFT column design, effectively mitigating the issues associated with earlier column types. Extensive research on CFST and CFDST columns has explored their potential advantages and limitations, shedding light on the path forward for modern construction in regions such as China, Europe, and North America (Han et al., 2014; Zheng & Tao, 2018). The discontinuous double-tube configuration DDSTCC column shows a notable enhancement in both axial load and displacement capacities, achieving increases of up to 11.5% and 61.3%, respectively, over the CFDST column (Lu et al., 2022). To date, only a preliminary numerical investigation has been conducted along with the experimental work on the compressive performance of DDSTCC columns with compact sections (Lu et al., 2022). However, no study has yet addressed their compressive behaviour under eccentric loading or in full-scale slender column applications. Given their enhanced resistance to local buckling, the use of slender sections in DDSTCC columns could present a viable option, particularly from an economic perspective. Recently, high-strength slender sections are gaining popularity in modern construction due to their superior efficiency and structural performance (Nguyen et al., 2021). In this context, the DDSTCC column presents a promising solution, offering enhanced resistance to local buckling and improved load-carrying capacity. To ensure its practical application, it is essential to investigate the behaviour of DDSTCC columns under eccentric loading and for full-scale slender sections. Therefore, further research is necessary to comprehensively understand the compressive behaviour of DDSTCC columns and assess their applicability in long-span structures and high-rise buildings. For this purpose, a numerical study could be a viable option to supplement the test results for better understanding the compressive behaviour of both stub and full scale DDSTCC columns under concentric and eccentric loading.

Motivated by these facts, this thesis aims to investigate the compressive behaviour of DDSTCC columns using a numerical approach, and provide a thorough understanding of their structural performance under various loading conditions. Additionally, the research seeks to develop and propose analytical formulas to facilitate the adoption of DDSTCC columns in practical design applications.

**1.2 Objectives**

The objectives of this research are set as follows:

1. To develop a 3D Finite Element (FE) model and validate the developed FE model against the test results.
2. To carry out a parametric study by considering geometric and material strength variation.
3. To investigate the compressive behaviour of DDSTCC column under concentric and eccentric loading.
4. To develop an analytical model to predict the compressive behaviour of stub and full scale slender DDSTCC column under concentric loading.
5. To evaluate the uncertainty in material optimization and safety for both the existing standards and the proposed analytical formula.

**1.3 Scope of the Research**

This study aims to provide a comprehensive understanding of the compressive behaviour of DDSTCC columns and establish reliable design guidelines for their effective implementation in modern construction projects. A validated finite element (FE) model will be developed to simulate column behaviour under axial and eccentric loads. Key parameters will be investigated include,

i. Thickness of inner and outer steel tubes
ii. Diameter of inner steel tube

iii. Compressive strength of inner and sandwich concrete
iv. Yield strength of inner and outer steel tube
v. Column height
vi. Loading eccentricity

Initial observations from previous studies indicated that DDSTCC columns exhibit delayed and stable buckling with no signs of local buckling, highlighting their potential for improved structural performance. To explore this further, the behaviour of both compact and slender outer steel sections will be evaluated, particularly because the outer tube does not directly carry axial load but significantly influences global stability. For practical implementation, the performance of full-scale slender columns and eccentrically loaded columns will also be examined to reflect real-world design conditions. This study will adapt existing CFST guidelines to calculate the axial strength and, furthermore, propose a modified analytical model tailored to DDSTCC columns. A reliability analysis will also be conducted to ensure safety and validate the proposed design approach. The outcomes are expected to support structural engineers in adopting DDSTCC columns for high-rise and critical infrastructure projects.

### 1.4 Outline of the Thesis

This thesis is structured into six chapters, with chapter 1 is introducing the topic and the following chapters are covering the respective subjects.

1. **Chapter 1** outlines the evolution of CFT columns from CFST to DDSTCC, highlighting their development, shortcomings and the need for FE analysis to address the limitations and improve design accuracy.

2. **Chapter 2** provides an overview of previous research conducted on CFST, steel tube confined concrete (STCC), CFDST, concrete filled double skin steel tube (CFDSST) and DDSTCC column, covering experimental and numerical studies on structural performance and analytical modelling over recent decades.
3. **Chapter 3** provides the details about the development of FE models using ABAQUS CAE 6.14. It covers the creation of parts and assemblies, selection of material models, meshing, definition of surface interactions, boundary conditions, the selection of the appropriate analysis type for the simulation and verification of FE model against the test results.
4. **Chapter 4** provides a detailed discussion on the effects of various parameters—such as tube thickness, diameter, material strength, column height and loading eccentricity—on the compressive behaviour of DDSTCC columns. The chapter investigates how changes in these parameters influence the structural response of the columns under compressive loading.
5. **Chapter 5** evaluates existing design standards based on the results of the parametric study and presents a modified analytical formula along with a reliability analysis for accurately predicting the axial strength of the column with safety margin.
6. **Finally, chapter 6** provides a concluding summary of the key findings, highlighting the impact of various parameters on column performance. It also suggests directions for future research, including the effects of cyclic and fatigue loading, void defects and life cycle analysis.

# CHAPTER 2: LITERATURE REVIEW

## 2.1 Introduction

The general discussion about the significance of DDSTCC columns, including their structural efficiency and innovative applications, has already been addressed in the introduction. This chapter presents the evolution and classification of CFT columns, including CFST, steel tube confined concrete (STCC), CFDST, concrete filled double skin steel tube (CFDSST) and DDSTCC. It presents their applications in modern construction, highlights their distinct features and traces their chronological development, showcasing how advancements have contributed to improved structural performance and design versatility. Additionally, the rationale for selecting this research topic is presented, focusing on the gaps in experimental investigations and the necessity for further numerical analyses to address these limitations.

## 2.2 Development of Concrete Filled Tube (CFT) Columns

Throughout the history of construction, steel and concrete have been essential building materials, used both individually and in combination to achieve structural resilience and enhance durability of the construction projects. Combining the benefits of steel and concrete, a specific type of composite column known as the CFT column had emerged in past. Nonetheless, the CFT column presents certain limitations that have been addressed through the evaluation of various geometric configurations, including circular, square and hexagonal shapes, along with the incorporation of additional tubes and strength variations. At each stage of the evaluation process, the shortcomings of the previous steps have been effectively addressed and mitigated, resulting in a progressively improved and effective design. The CFT column is a broad term that consists several variations, including CFST, CFDST, STCC, CFDSST and the more recently developed DDSTCC column, as listed in following Fig. 2.1. A detailed discussion of these variations will follow in the next subsections.

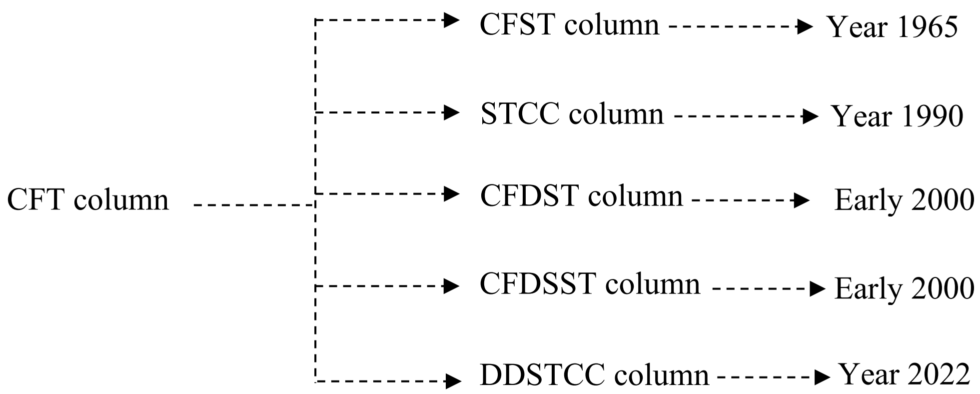


**Fig 2.1** Development of CFT columns

### 2.2.1 Research on Conventional Concrete Filled Steel Tube (CFST) Column

CFST columns were first pioneered in China, with the earliest application at the Qian men subway station in Beijing in 1966 (see Fig. 2.2a). Over the decades, their use expanded chronologically to a wide range of structures, including buildings in the 1980s to avoid large column sizes, as seen in projects in Beijing and Fujian, as well as iconic structures like the Ruifeng International Commercial Building in Hangzhou (2001) (see Fig. 2.2b). In the 1990s, CFST columns became common in bridges, starting with the Wangcang East River Bridge (1992) (see Fig. 2.2c) and later the Zhaohua Jialing River Bridge in Sichuan (see Fig. 2.2d). Today, CFST columns are integral components in numerous buildings, bridge piers, towers, and decks worldwide, demonstrating their versatility and structural efficiency (Han et al., 2014) (see Fig. 2.2e and 2.2f).

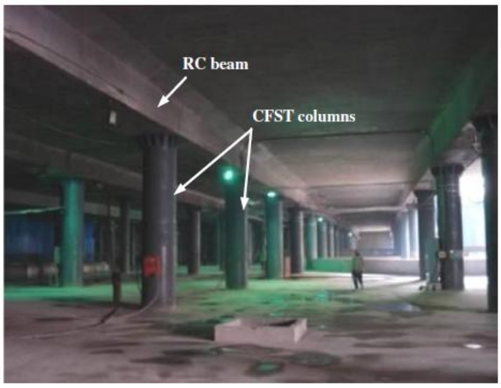


**(a)** Qian men subway station


**(b)** Ruifeng building in Hangzhou


**(c)** Wangcang East River Bridge

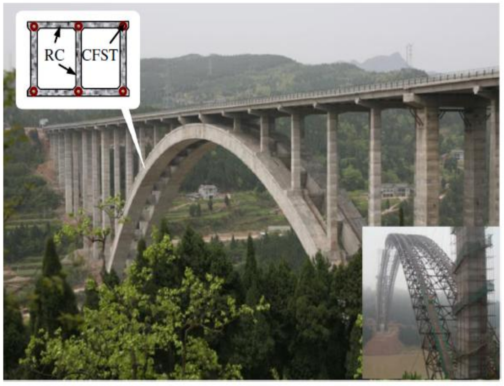


**(d)** Zhaohua Jialing River Bridge


**(e)** Zhoushan electricity pylon

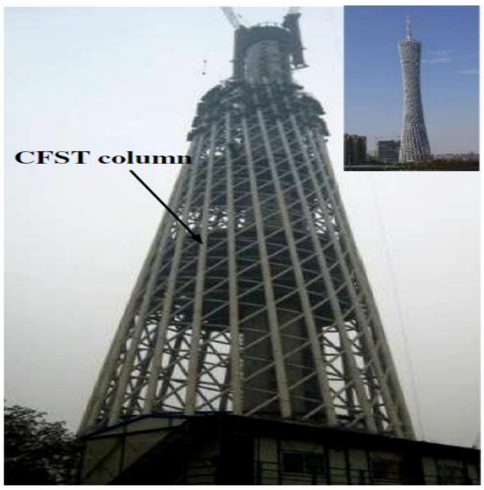


**(f)** Canton tower

**Fig 2.2** Application of CFST columns in various structural systems (Han et al., 2014).

Research on CFST columns before the year 2000 significantly advanced the understanding of axial strength and confinement effects, illustrating the evolution of their applications over time. Early studies, such as those by Furlong (1967), that investigated 13 specimens, and Gardner and Jacobson (1967), that examined 22 specimens, established foundational knowledge regarding the independent load-bearing capacities of concrete cores and steel tubes. These investigations underscored the significance of the diameter-to-thickness (D/t) ratio—specifically limiting D/t to 55—and showed that although the concrete contributed some stability to the steel tube, the anticipated interaction effects were relatively limited.

As research progressed, studies by Knowles and Park (1969), that explored 12 circular and 7 square columns with D/t ratios of 15, 22, and 59, highlighted the superior confinement capabilities of circular columns (with confinement effectiveness up to 2.0) compared to square and rectangular ones (typically below 1.0). This growing body of knowledge led to an increased appreciation for the triaxial confinement effects that enhance concrete strength, which became crucial in designing CFST structures for various applications. By the late 1970s and 1980s, researchers like Tomii et al. (1977), who investigated nearly 270 specimens with D/t ratios ranging from 19 to 75, and Sakino et al. (1985), who tested 18 circular specimens with D/t ratios from 18 to 192, were examining the performance of CFST columns under simultaneous loading conditions. These studies further confirmed the material's load-bearing advantages, underscoring the benefits of CFST columns in diverse structural applications. With further research, the behaviour of CFST columns under combined loading conditions—such as axial, bending, and pure torsional loads—was explored by Han et al. (2007) who highlighted the significant impact of composite action on the stability and strength of these columns. In addition, Nie et al. (2013) studied eight CFST columns under combined compression, bending, and cyclic torsional loading, observing that while the columns exhibited good seismic performance, rectangular sections showed strength degradation of 9% compared to circular section due to local buckling. Ibañez et al. (2018) studied twelve CFST stub columns with circular, square, and rectangular cross-sectional shapes, using both normal-strength (C30) and high-strength (C90) concrete infills. Their study highlighted that circular column exhibited uniform outward local buckling with high ductility index (DI ≈ 3.5) and strong composite action, while square and rectangular columns experienced inward corner buckling and shear cracking, showing lower ductility index (DI ≈ 2.0–2.5) and weaker confinement and interaction between steel and concrete. In addition, octagonal, polygonal, and elliptical CFST columns also have been studied by various researchers, including Hossain and Chu (2019), Patel et al. (2016), and Ren et al. (2014). Again, using high-strength concrete and steel was not restricted by code limitations and is applied in projects like the Petronas Towers, The Sail at Marina Bay, Techno Station, Hong Kong International Commerce Centre, and Shanghai World Financial Center. Thus, Liew et al. (2016), conducted a study on CFST columns using ultra-high strength concrete (up to 190 MPa) and high tensile steel (up to 780 MPa), proposing a design guide based on an extension of EC4 to cover higher material strengths. They have proposed that for high-rise CFST columns, adopting a concrete strength reduction factor of 0.8 and ignoring confinement effects for ultra-high strength concrete (90–190 MPa), combined with 550 MPa steel, enhances resistance to axial and bending loads while reducing material use, welding, and overall construction costs. Recently, Nguyen et al. (2021) conducted two separate studies—one focusing on the sectional slenderness and the other on the global slenderness effects of high-strength CFST columns, utilizing both experimental and numerical analyses, and evaluated against design codes. High-strength CFST columns with b/t > 35 suffer early local buckling, using compatible materials can delay this, with square CFST columns (150 MPa concrete, 690 MPa steel, $\lambda_e = 60$, b/t = 36) being optimal for strength, space, and cost efficiency. In the following year, Nguyen et al. (2021) conducted another study specifically on eccentrically loaded CFST columns with high-strength constituents and evaluated their interaction behaviour in relation to existing design standards. The cumulative findings from these studies not only provided a strong theoretical framework but also facilitated the widespread adoption of CFST columns in modern construction practices, particularly in seismic-prone areas and large infrastructure projects.

### 2.2.2 Research on Concrete Filled Double Steel Tube (CFDST) Column

Compared to CFST columns, the use of CFDST columns in construction is relatively rare due to limited design guidelines. In Germany, CFDST columns have been applied in notable projects, including the Wuppertal City Hall extension (circular tubes), Commerzbank Tower, Frankfurt (1997, triangular columns), (see Fig. 2.3a), and Berlin Central Station (rectangular tubes). More recently, CFDST columns were utilized in China, such as in the Guangzhou Fortune Center (2015), (see Fig. 2.3b), featuring square cells with embedded circular tubes to enhance load capacity and stiffness (Zheng et al., 2018).

**(a)** Commerzbank Tower, Frankfurt **(b)** Guangzhou Fortune Center

**Fig 2.3** Application of CFDST columns in various structural systems (Zheng et al., 2018)

The limited application of CFDST columns indicate a gap in practical usage, and there have also been a limited number of studies conducted in recent decades to explore their true potential and usefulness. Among these studies, Liew and Xiong (2012), conducted 27 tests, including 8 on CFDST columns, to evaluate their potential use in construction. The study compared them with CFST columns, assessed the applicability of EC4 (1994) for design, and investigated the performance of UHPC in enhancing the 14.6 % of load capacity of CFDST columns. Another study by Xiong et al. (2017) evaluated high-strength steel and concrete by testing 56 different types of circular and square CFST and CFDST columns, with concrete strengths up to 190 MPa and steel strengths up to 780 MPa. Their findings revealed that CFDST column exhibited a notable improvement in ultimate resistance, ranging from 11% to 22%, which was significantly higher compared to CFST column, whose increase ranged from only 2.6% to 10.7% using UHPC. The research further aimed to determine if plastic cross-sectional resistance could be applied at the ultimate limit state for CFSTs made with high- and ultra-high-strength materials, resulting in design recommendations for accurately predicting the behaviour of short CFST and CFDST columns. The behaviour of core and sandwich concrete is different from the concrete section present in CFST columns. To address this, Ahmed et al. (2019) proposed a confinement pressure model through a numerical study and introduced a new strength degradation parameter to improve the understanding of these unique concrete behaviours. In addition, the potential benefits of the double circular steel tube configuration include its ability to repair CFST columns while achieving performance levels that closely resemble those of pure CFDST columns (Ekmekyapar and Al-Eliwi, 2017). The load-bearing capacity of the repaired CFST columns was only 5.36% to 7.50% lower than that of CFDST columns, indicating that the double-tube repaired configuration closely matches the strength of CFDST columns. Most of the works investigated the behaviour of concentrically loaded columns, however Ahmed et al. (2019) were the first to explore the structural responses of eccentrically loaded circular CFDST short columns through both experimental and numerical studies considering eccentricities (e) ranging from 0 to 30 mm. Their findings showed that as eccentricity increased from 0 to 10 mm, the ultimate strength decreased by approximately 13%. A mathematical model using fiber analysis was developed to accurately simulate axial load-moment-curvature relationships and strength envelopes, with results validated against experimental data. A research group carried out a series of experimental and numerical analyses to study the behaviour of slender CFDST columns under eccentric loading, considering the use of high-strength materials and the effects of fire and ambient temperatures (Albero et al., 2021), (Ibañez et al. 2017), (Romero et al. 2015). However, experimental work on long columns remains limited due to the challenges in test setup, leading most studies to rely on numerical methods. Recently, Wang et al. (2022) tested 16 CFST and CFDST slender column specimens with both square and circular sections under concentric and eccentric loading with eccentricity ratio ($e/D_o$) of 0 to 0.4. Results showed that circular CFDST columns exhibited a 12% increase in strength, while square CFDST columns showed about a 7% improvement compared to their CFST counterparts. However, as the eccentricity ratio increased, the strength of the columns decreased by approximately 19%, with this reduction becoming more pronounced as the slenderness ratio increased, indicating a combined influence of eccentricity and slenderness on structural performance. CFDST columns, while structurally efficient, face some disadvantages, including susceptibility to corrosion, especially in humid or marine environments, and sensitivity to high temperatures that can reduce the steel's strength during events like fires. For this reason, using stainless steel for the outer tube of CFDST columns is a good choice, as it offers greater durability and longevity. Various studies have found that using stainless steel for the outer tube in CFDST columns can achieve up to twice the fire protection compared to conventional CFDST columns and significantly enhance the buckling performance, particularly for slender columns (Wang et al., 2018; Hassanein et al., 2017). Despite these benefits, CFDST columns are prone to early buckling at both ends, and debonding between the concrete core and steel tubes can reduce the confinement effect during the initial loading stages, potentially impacting their overall stability and load-bearing capacity.

### 2.2.3 Research on Concrete Filled Double Skin Steel Tube (CFDSST) Column

CFDSST members, also known as "steel-concrete-steel sandwich tubular" structures, consist of two concentric steel tubes with a concrete core between them as illustrated in Fig 2.4. Developed to improve upon CFST members, CFDSST members address limitations of traditional steel tubes by expanding their potential uses and enhancing structural performance.

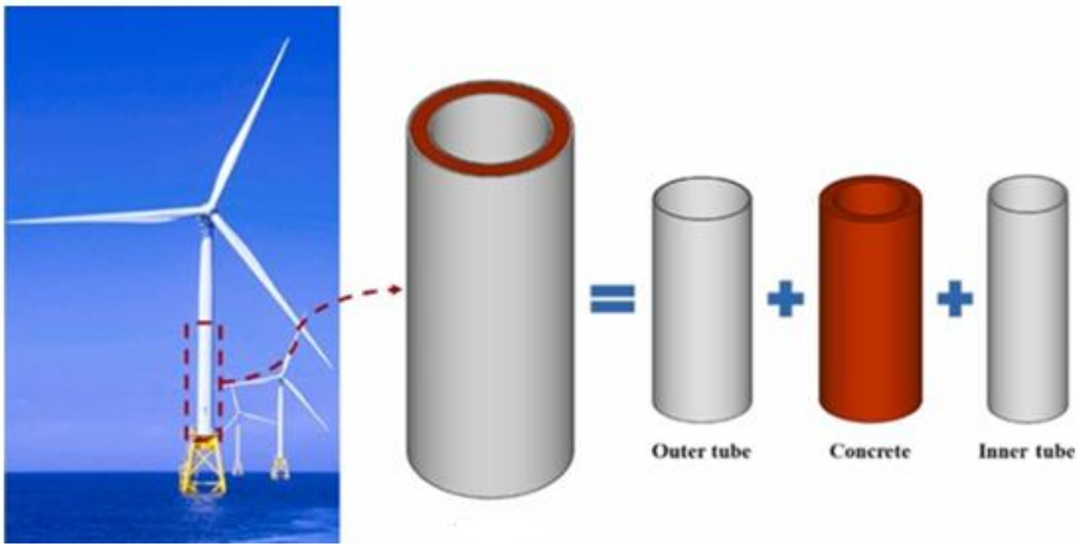


**Fig 2.4** General view of CFDSST column (Jin et al., 2024)

CFDSST columns are suitable for applications such as bridge piers, railway viaducts, offshore platforms, wind turbine installation, high voltage pole and blast-resistant shelters as shown in Fig 2.5. They offer various advantages such as increased section modulus, enhanced stability, lighter weight, good damping, and cyclic performance, along with improved fire resistance due to the protective sandwiched concrete (Sugimoto et al 1997; Han et al., 2014). Recently, Japan has used CFDSST columns in bridge piers to reduce structural weight and enhance earthquake resilience through greater energy absorption capacity (Zhao & Grzebieta, 2002).


**(a)** High voltage pole

**(b)** Wind turbine installation


**(c)** A CFDSST electrical pole

**Fig 2.5** Application of CFDSST columns in various structural systems (Han et al., 2014)

Uenaka et al. (2009) investigated the axial compression behaviour of CFDST stub columns, which consist of concentric steel tubes with concrete filled between them. The study primarily focused on the effects of inner-to-outer diameter ratio ($D_i/D_o$), ranging from 0 to 0.73, and the diameter-to-thickness ratio ($D_o/t_o$), ranging from 73 to 176, on the mechanical behaviour of the columns. The predominant failure modes were local buckling of both tubes, coupled with shearing failure of the filled concrete.

Analytical equations were developed to predict the ultimate compressive strength based on the yielding strengths of the steel tubes and core concrete. It was observed that columns with larger inner tube diameters exhibited reduced ductility and more complex buckling behaviour. The proposed equations showed strong predictive accuracy, with a statistical correlation factor r = 0.96 and an average predicted-to-experimental strength ratio of approximately 1.02. In another study by Ekmekyapar and Hasan (2019), the influence of the inner steel tube on the mechanical performance of CFDSST columns under axial compression was investigated. The study involved testing sixteen specimens with varying D/t ratio and concrete strengths (normal and high strength). The results demonstrated that the inner steel tube significantly enhances the compression capacity of CFDSST columns, with capacity increases ranging from 18.95% to 65.44%. However, thinner inner tubes (D/t = 23.93) were found to suffer from early local buckling, limiting their confinement effect and performance. In contrast, thicker inner tubes (D/t = 10.45) provided better composite action and contributed efficiently to the column's overall performance, even with high-strength concrete. The study also highlighted that the presence of the inner tube is critical for the confinement of the concrete, with the outer tube alone being insufficient for adequate confinement. Furthermore, prediction methods such as EC4 (1994) and AISC (2016) showed better accuracy for CFDSST columns compared to traditional CFST column. Recent studies have explored various geometric configurations of CFDSST columns, such as circular, rectangular, and mixed-section designs (Elchalakani et al., 2002; Zhao & Grzebieta, 2002; Tao & Han, 2005). A new dodecagonal section has been proposed, offering improved local buckling resistance compared to square sections and advantages in fabrication and connection surface flatness over circular sections. Testing on double-skin CFDSST columns with dodecagonal sections showed that, for stub columns, the outer tube buckled like circular sections, while the inner tube buckled at the flat edges. The study found that dodecagonal-section columns perform similarly to circular ones with variation under 2% and can be designed using existing circular-section equations with appropriate adjustments for material areas (Chen et al., 2014). While the CFDSST column offers lightweight and efficient performance, it has been increasingly used in China for electricity transmission towers (see Fig 2.5a) with tapered sections (Han et al., 2014; (Li et al., 2012). This design reduces steel usage and foundation costs compared to traditional straight columns. The failure mode of tapered CFDSST columns occurs near the smallest section, similar to straight ones, and stress analysis has led to formulas for calculating their ultimate strength, enhancing design accuracy (Li et al., 2012). Though numerous experimental and numerical studies have been conducted on the shape and concentric loading of CFDSST columns, the torsional behaviour remains critical for large transmission lines and poles. Huang et al. (2013) investigated the torsional behaviour of CFDSST columns using two setups: one with circular hollow sections (CHS) for both inner and outer tubes, and another with CHS as the inner tube and square hollow sections (SHS) as the outer tube. Their results showed a 20% improvement in torsional capacity compared to double square hollow tube (DSHT) columns, with increased hollow and steel ratios further enhancing torsional performance. Though CFDSST columns have a relatively low strength-to-weight ratio, they exhibit both inward and outward buckling of the outer and inner tubes under heavy loads (Pagoulatou et al., 2014). As a result, these columns are not commonly used in high-rise construction. Instead, they are more favourable for single-tube-like structures or applications requiring moderate load-bearing capacity.

### 2.2.4 Research on Steel Tube Confined Concrete (STCC) Column

Steel tube confined concrete (STCC) columns are a distinct variant of CFT columns, where the concrete core primarily carries the load while the surrounding steel tube acts solely as a confining shell as shown in Fig 2.6. The concept of STCC columns, much like CFST columns, was initially explored in the 1980s, with notable contributions from Tomii, M. (1985). Their research introduced the innovative idea of disconnecting the steel tube at the beam-column joint (see Fig. 2.7), with the goal of relieving the axial stress in the steel tube induced by external forces.

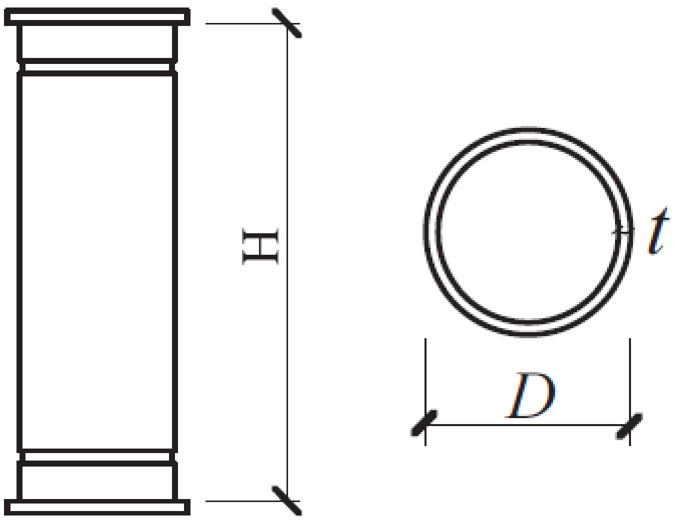


**Fig 2.6** Geometric configuration of steel tube confined concrete column

Despite the similarities in their basic structure, the behaviour of CFST and STCC columns differs primarily due to the slight geometric modification in the design, particularly in terms of the confinement mechanism.

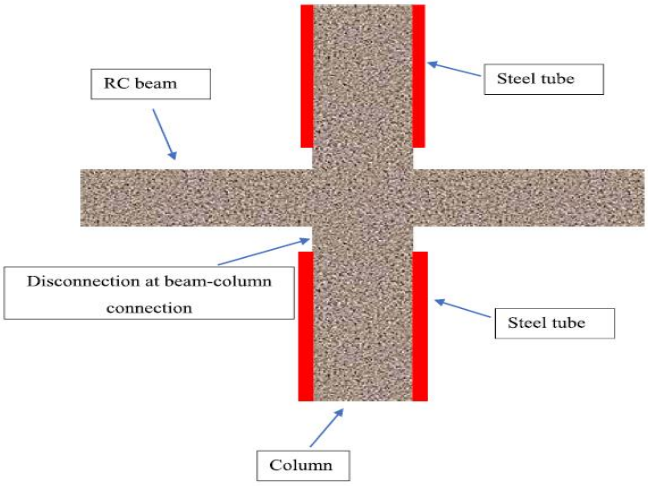


**Fig 2.7** Beam-column construction joint of STCC column (Tomii, M. 1985)

O'Shea and Bridge (2000) investigated this confinement mechanism in STCC columns under three different loading conditions, as illustrated in Fig. 2.8.

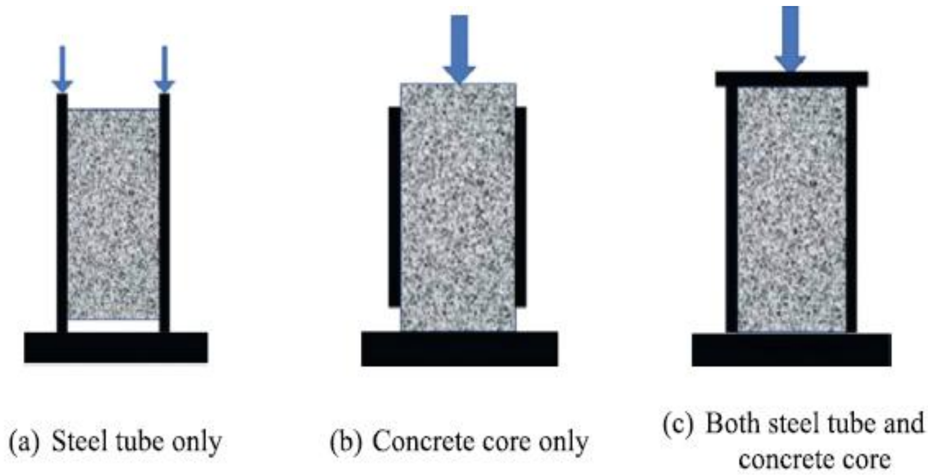


**Fig 2.8** Different loading condition (O'Shea and Bridge, 2000)

This experimental finding highlighted the behaviour of columns under varying loading conditions. When no load is applied to the steel tube, radial expansion due to Poisson's effect causes separation between the tube and the concrete core, resulting in a lack of confinement. However, when the load is applied solely to the concrete, the steel tube effectively confines the core, significantly enhancing its compressive strength. In contrast, when both the tube and concrete core are loaded simultaneously, confinement occurs only if the concrete expands beyond the tube, which can reduce hoop stress and confining pressure. Han et al. (2007) conducted an extensive experimental study on 46 specimens subjected to axial local compression. Their findings revealed that The ultimate strength of the columns decreased by about 13% as the local compression area ratio (ß) increased from 1 to 16 and the D/t increased from 52 to 105. Additionally, they observed that circular steel tubes provided better confinement to the concrete core than square tubes, setting the stage for further theoretical research. J. Zhu and Chan (2019) studied the performance of various CFST and STCC columns, including circular, rectangular, and octagonal shapes, under monotonic loading with varying D/t, L/D, and material strength parameters. The study found that circular and octagonal STCC columns performed similarly to, and slightly better than, their CFST counterparts, while rectangular STCC columns showed about 8% lower strength, likely due to reduced confinement. It concluded that existing CFST design formulas could be adapted for STCC columns with some modifications using a confinement coefficient (k=1.36); however, for rectangular columns, the formulas were not applicable as they overestimated strength by up to 50%.

Unlike CFST columns, no generalized formula existed for STCC columns, and the confinement mechanism had not been thoroughly explored. In 2010, Yu et al. (2009) made a pioneering advancement by introducing the first theoretical model specifically for circular STCC columns. Their study also examined the confinement behaviour of both STCC and CFST columns under bonded and unbonded conditions. Results showed that STCC columns provide enhanced load-bearing capacity, primarily due to increased confining stress. Notably, STCC columns begin to offer effective confinement from the early stages of loading. Although the steel tube in STCC columns carries about 6% less axial force than in CFST columns, the confining stress is approximately 25% higher, and the core concrete carries 2.5% more axial load. Overall, these factors contribute to a 2% increase in the total load-carrying capacity of STCC columns compared to their CFST counterparts. In the same year, De Oliveira et al. (2009) studied the confinement of circular STCC columns with varying concrete strengths from 30 MPa to 100 MPa and D/t ratios of 58 to 220. They found that columns with normal strength concrete (C30, C60) showed good ductility without losing capacity after peak load, while high-strength concrete columns (C80, C100) did not exhibit the same behaviour. They also noted that thicker steel tubes were necessary for proper confinement in high-strength concrete columns. To improve predictions for slender columns (L/D > 3), they introduced a correction factor ($\lambda_o$), with the analytical model showing a 5.2% difference when compared to experimental results from O'Shea and Bridge (2000).

Despite the various benefits of STCC columns, the application of STCC columns was limited as depicted in Fig 2.9. In CFST columns, the outer steel tube acts as longitudinal reinforcement, providing ductility. However, for STCC columns, the gap region between the steel tube and concrete core is particularly vulnerable to seismic activity and cyclic loading, often leading to concrete shear failure in this area. To address this issue, conventional reinforcement has been used, resulting in the development of Steel-Confined Reinforced Concrete Columns (STRCC) (Wei et al., 2020). For this reason, discontinuous steel in column is primarily used for retrofitting purposes, it is not suitable for high-rise structures.

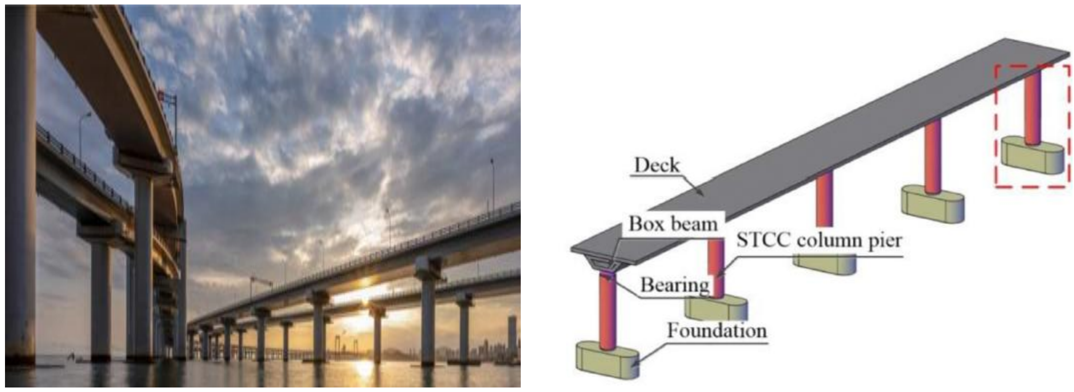


**Fig 2.9** Xinghai bay bridge at dalian, China (Qiyun et al. 2021)

### 2.2.5 Research on Discontinuous Double Steel Tube Confined Concrete (DDSTCC) Column

The previous sections discussed the evolution of CFST, CFDST, CFDSST and STCC Columns and reviewed extensive experimental research conducted on these column types over the years. While these columns have proven effective, one major disadvantage remains: they are prone to early buckling under certain conditions. In 2022, a new column type was introduced, known as the discontinuous double steel tube confined concrete (DDSTCC) column as shown in Fig 2.10.

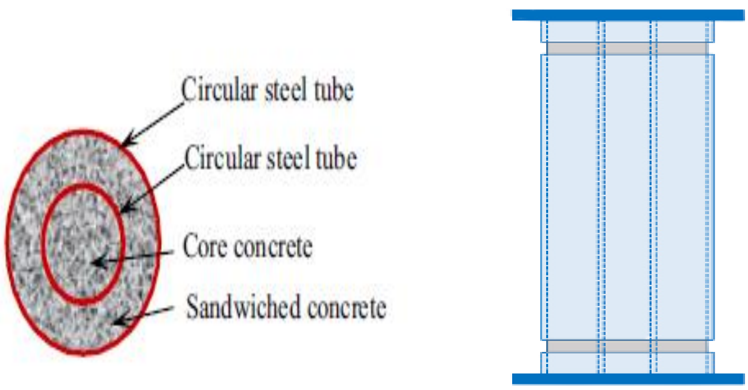


**Fig 2.10** Schematic view of DDSTCC column (Lu et al., 2022)

This innovative column design addresses some of the limitations of its predecessors by incorporating a unique structure with discontinuous outer steel tubes, which enhances confinement and improves overall stability. The DDSTCC column is expected to mitigate early buckling issues, offering improved durability and load-bearing capacity in structural applications. The comparative study between CFST, STCC, CFDST, and DDSTCC columns indicates that the use of discontinuous tubes significantly improves confinement, resulting in more uniform buckling behaviour (Lu et al., 2022).

### 2.2.6 Numerical and Analytical Study on Different Types of CFT Column

Experimental studies on concrete-filled steel tube (CFST) columns have been significantly enriched by numerical investigations, providing a deeper understanding of their behaviour under various loading conditions. Alongside these, analytical methods have been developed to improve performance assessment and to inform the formulation of design guidelines specifically for CFST columns.

#### 2.2.6.1 CFST column

Ellobody et al. (2005) conducted one of the earliest large-scale numerical analyses on axially loaded CFST circular stub columns, exploring concrete strengths ranging from 30 to 110 MPa and D/t ratios between 15 and 80 for compact sections. Their finite element (FE) model, with a mean $P_{FE}/P_{EC4}$ ratio of 0.9 and a coefficient of variation (COV) of 0.096, showed strong predictive accuracy. Comparison with design codes revealed that ASCE and AS 2327 codes were generally conservative, while the EC4 code tended to be unconservative. Liang and Fragomeni (2009) developed models for confined concrete in CFST columns to enhance axial load predictions. Their study found that increasing steel yield strength significantly improved axial capacity, with performance indices of 0.345, 0.399, and 0.48 corresponding to steel grades of 350 MPa, 450 MPa, and 690 MPa, respectively. They introduced a strength reduction factor based on D/t ratios—lower D/t ratios enhanced strain hardening, while higher D/t ratios reduced strength (from 0.9 to 1.1). Their analytical model also addressed the impact of confinement, especially in high-strength concrete applications. In a separate study, Liang (2010) developed a new numerical model for high-strength circular CFST slender beam-columns. Unlike previous models for short columns, this one accounted for slenderness effects, loading eccentricities, initial geometric imperfections, and the influence of high-strength materials and concrete confinement. The model could generate load-deflection curves and axial load-moment interaction diagrams, offering a more complete and precise analysis framework. Nguyen et al. (2021) conducted a numerical study of 180 slender CFST columns and proposed a new form factor based on relative slenderness and concrete strength for better load prediction. Their design optimization recommended using grade 150 concrete, grade 690 steel, and a section slenderness ($\lambda_e$) of 60 for optimal performance and cost efficiency. Lam et al. (2012) numerically analyzed inclined tapered CFST columns under axial compression, considering inclination angles from 0° to 9° and taper angles from 0° to 4°. They proposed a reduction factor ($\alpha$) for axial capacity, which showed a nearly linear decrease with increasing angles—particularly pronounced in inclined columns.

#### 2.2.6.2 STCC column

In contrast, research on steel tube confined concrete (STCC) columns has been relatively limited. Yu et al. (2009) were among the pioneers in applying analytical and numerical methods to STCC columns. Their findings indicated that STCC columns provide positive confinement, improving load-carrying capacity by approximately 2% compared to circular CFST columns. However, for square sections, STCC columns exhibited slightly lower axial strength but superior ductility. Based on these insights, they proposed confinement-based analytical formulas valid for steel yield strengths (fy) of 235–345 MPa and concrete compressive strengths ($f_{cu}$) of 30–60 MPa. Expanding on this, Hoang and Fehling (2017) examined STCC columns using a wider range of material strengths—steel fy from 185.7 to 460 MPa and concrete fc from 16.7 to 200 MPa—with D/t ratios between 15.9 and 220.93. They observed that while increasing concrete strength raised ultimate load and stiffness, it reduced confinement efficiency. Specifically, strength enhancement ratios ($f_{cc}/f_c$) decreased by 15%–30% for high strength concrete (HSC) and 34%–62% for ultra high strength concrete (UHSC) compared to normal strength concrete (NSC). Meanwhile, increasing steel strength improved confinement by 21%–33% for NSC and 10%–19% for HSC, but had minimal impact on UHSC. In another study, Hoang et al. (2018) developed new analytical models to predict axial strength while accounting for these effects.

#### 2.2.6.3 CFDST column

Ahmed et al. (2019) created a fiber element-based numerical model for high-strength Circular CFDST short columns, validated against 29 experimental datasets. Their parametric study varied outer-to-inner diameter ratios ($D_o/D_i$) from 700 mm to 140 mm and steel yield strength ($f_y$) from 250 MPa to 450 MPa. The model incorporated confinement in both the core and sandwiched concrete and introduced a novel confining pressure model along with a strength degradation parameter for post-peak behaviour. The resulting simplified analytical expression closely matched Liang (2010) formulation and outperformed several design codes. Kabir et al. (2025) analyzed short and long CFDST columns under axial load, reporting axial strength improvements of up to 36% for short columns and 30% for long ones. Ductility increased by 10%–40%, and toughness by up to 57% with optimal configurations. They proposed a modified squash strength formula, which aligned more closely with experimental results than existing codes, with predicted-to-tested strength ratios of 0.99 for stub columns and 1.1 for long columns. Hossain et al. (2017) investigated slender CFDST columns with slenderness ratios between 46 and 191, emphasizing intermediate and long columns. Their study revealed that EC4 significantly underestimates strength in slender sections. As a remedy, they proposed a modified version of the EC4 model, which improved prediction accuracy—achieving a mean prediction ratio of 0.95.

#### 2.2.6.4 CFDSST column

Confinement behaviour differs notably among CFST, CFDST, and CFDSST columns. Ahmed et al. (2019) previously proposed a confinement pressure model for CFDST columns. For CFDSST columns, a separate study (Ahmed et al., 2021) introduced a numerical confinement model based on hollow steel ratios. When comparing predicted-to-test strength ratios, the modified EC4 (0.99) and original EC4 (0.95) models outperformed others such as ACI 318–11 (0.77), AISC 360–16 (0.80), DBJ

13–51-2010 (0.83), and AIJ (0.95). Pagoulatou et al. (2014) numerically investigated circular CFDSST stub columns under axial compression. Their study showed that CFDSST columns are lighter yet exhibit about 12% higher load-bearing capacity than CFST columns. A new EC4 based formula was proposed and validated against numerical results, demonstrating reliable strength predictions. In another study, Liang (2016) evaluated several confinement pressure models for sandwich concrete proposed by Tao et al. (2004), Hu and Su (2011), and Uenaka et al. (2009). Among them, the Hu and Su (2011) model most accurately predicted compressive loads across varying geometric parameters, although it is constrained by specific outer and inner D/t ratios.

A comparative summary of the analytical models proposed by different researchers is presented in Table 2.1.

Table 2.1 Summary of analytical models for different types of columns

| Column type | Analytical formulation | Reference |
|---|---|---|
| CFST | $P_u = (\gamma_c f_c' + 4.1 f_{rp}) A_c + \gamma_s f_{sy} A_s$ | (Liang and Fragomeni, 2009) |
| STCCC | $P_u = (1.14 + 1.34\xi) f_c' A_c$ | (Yu et al, 2009) |
| CFDST | $P_u = (\gamma_{sc} f_{cs}' + 4.1 f_{rps}) A_{cs} + \gamma_{so} f_{so} A_{so} + (\gamma_{si} f_{ci}' + 4.1 f_{rpi}) A_{ci} + \gamma_{si} f_{si} A_{si}$ | (Ahmed et al, 2019) |
| CFDSST | $P_u = (\gamma_{sc} f_{cs}' + 4.1 f_{rps}) A_{cs} + \gamma_{so} f_{so} A_{so} + \gamma_{si} f_{si} A_{si}$ | (Liang, 2016) |

### 2.3 Research Gaps

As discussed in previous sections, various types of CFT columns have been investigated through experimental, numerical, and analytical methods, with a focus on understanding the specific variations in strength, load-carrying capacity, and geometric configurations. Performance and investigation of different types of columns which have been used in high rise building construction is presented in Table 2.2. Table 2.2 demonstrate that the performance of DDSTCC columns is comparable to that of CFDST and CFDSST columns.

**Table 2.2** Summary of different parameters of CFT column

| Parameters | CFST | STCC | CFDST | CFDSST | DDSTCC |
|---|---|---|---|---|---|
| Section size | Large | Large | Small | Small | Small |
| Fire resistance | Fair | Fair | Excellent | Excellent | Yet to report |
| Construction ability | Fair | Excellent | Moderate | Moderate | Excellent |
| Anti corrosion | Fair | Fair | Moderate | Moderate | Moderate |
| Seismic behaviour | Good | Not good | Excellent | Excellent | Yet to report |
| **Investigation** | | | | | |
| Concentrically loading | Already done | Already done | Already done | Already done | Already investigated |
| Eccentrically loading | Already done | Already done | Already done | Already done | Yet to report |
| Slender long column | Already done | Already done | Already done | Already done | Yet to report |
| Analytical work | Already done | Already done | Already done | Already done | Yet to report |
| Cyclic loading | Already done | Already done | Already done | Already done | Yet to report |

However, key aspects, such as behaviour under eccentric loading, the performance of full-scale slender columns, and the analytical formulation for calculating axial strength, remain unexplored. Thus, further investigation is essential to fully understand the behaviour of these column types. To the best of the authors' knowledge, only one experimental study, along with one numerical analysis, has been conducted to date on these columns. However, research on this advancement has been limited, focusing primarily on compact sections of stub columns. The potential for using discontinuous tube designs in non-compact, slender sections and examining the full-scale column behaviour remains largely unexplored. In the past, compact sections were predominantly considered in practical structures, even when local buckling was not a significant concern. However, with the increasing demand for architectural and structural applications, particularly in large structures, there has been a significant rise in the use of slender sections (An et al., 2012), (see Fig 2.11). Given the enhanced buckling resistance observed, these columns could present a viable solution for broader structural applications. For practical use, additional research is required to investigate the behaviour of full-scale slender columns.


**Fig 2.11** A practical application of CFT column with high slenderness ratio (An et al., 2012)

Thus, a comprehensive analytical formulation addressing these behaviours is crucial for advancing the structural applications of DDSTCC columns. While initial findings are promising, further studies are essential to optimize and understand the full potential of these columns under diverse scenarios. Further experimental investigations could be supplemented by numerical simulations to explore the full capabilities of DDSTCC columns across various section types, loading conditions.

### 2.4 Summary

Previous work on different types of CFT column has been summarized and potential research gap and scope of future work of DDSTCC column has been identified in this chapter. Extensive research was conducted on other column types, however DDSTCC columns require further investigation. Thus, this chapter outlines the direction to numerically and analytically investigate the compressive behaviour of DDSTCC column.

# CHAPTER 3: FINITE ELEMENT MODELLING

## 3.1 Introduction

The primary objective of this research is to enhance the understanding of the compressive behaviour of DDSTCC columns through a comprehensive numerical analysis. By using computational modelling, this study seeks to gain deeper insights into the compressive behaviour of both full-scale and stub DDSTCC columns under various loading and structural conditions, including concentric and eccentric loading scenarios. For this purpose, ABAQUS 6.14, a widely recognized and versatile FE software package, is employed to conduct detailed simulations and analyses of the DDSTCC columns. The study is based on tests conducted by Lu et al. (2022) serving as a reliable basis for the development and validation of FE models. The numerical models would supplement the experimental results by providing further insights into the performance of DDSTCC columns, particularly in conditions that are challenging to replicate in experiments. In this chapter, detailed tests by Lu et al. (2022) along with the sequential development of FE model and validation of FE models are discussed in the following sections.

## 3.2 Overview of the Experimental Study Performed by Lu et al. (2022)

In previous study of Lu et al. (2022) eighteen specimens of different types of CFT columns were fabricated with different geometric configuration and material property to assess their overall structural performance under pure axial load. Among these, seven specimens were classified as DDSTCC columns. These columns were prepared with a fixed outer steel tube diameter of 206 mm and the inner steel tube diameter was varied between 80 to 158 mm. Variation in thickness of both steel tubes were considered in 7 different sets with a range of 2 to 5 mm. In addition, a consistent concrete mix of 67.7 MPa was used for casting both the inner and sandwich concrete. The column had an overall height of 600 mm. The outer steel tube was separated into three sections by 10 mm wide girth strips, cut 40 mm away from each column's end. The geometric details and material strengths of DDSTCC columns are summarized in Table 3.1.

**Table 3.1** Details of test specimens

| Column designation | Outer tube | Inner tube | Steel yield strength | | Concrete strength | Height, h (mm) |
|---|---|---|---|---|---|---|
| | $D_o \times t_o$ (mm) | $D_i \times t_i$ (mm) | $f_{yo}$ (MPa) | $f_{yi}$ (MPa) | $f_{cu}$ (MPa) | |
| ST3-D80-4 | 206 × 3 | 80 × 4 | 208 | 205 | 67.6 | 600 |
| ST3-D106-3 | 206 × 3 | 106 × 3 | 208 | 208 | 67.6 | 600 |
| ST3-D158-2 | 206 × 3 | 158 × 2 | 208 | 206 | 67.6 | 600 |
| ST3-D106-4 | 206 × 3 | 106 × 4 | 208 | 205 | 67.6 | 600 |
| ST3-D106-5 | 206 × 3 | 106 × 5 | 208 | 204 | 67.6 | 600 |
| ST4-D106-3 | 206 × 4 | 106 × 3 | 205 | 208 | 67.6 | 600 |
| ST5-D106-3 | 206 × 5 | 106 × 3 | 204 | 208 | 67.6 | 600 |

Two loading plates were placed at each end of the column to ensure a pin support condition and uniform distribution of load. Finally, the columns were instrument for testing and placed under a Universal Testing Machine (UTM) to apply a 20 mm monotonic displacement-controlled load. Various LVDTs were placed at different locations on the column and strain gauges were also attached to the steel surface to collect displacement and strain data. These measurements were continuously monitored by a dynamic data acquisition system. The displacement was recorded by four LVDTs placed at each corner of the loading plates. Besides, several strain gauges were attached to the mid height surface of outer and inner steel tubes to measure hoop and longitudinal strains during the tests. In brief, eight horizontal and four vertical strain gauges on the outer steel tube along with four hoop strain gauges on the inner steel tube were evenly distributed around the circumference. Further details and clarification regarding the test setup are shown in Fig. 3.1 (Lu et al., 2022).

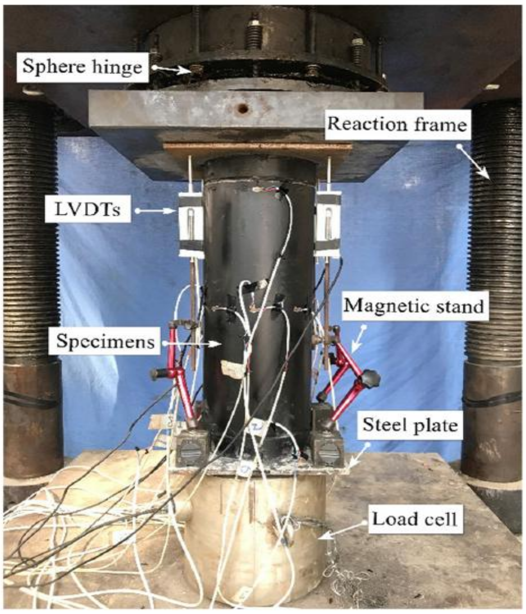


**Fig 3.1** Test setup by Lu et al. (2022)

### 3.3 Development of FE Model

#### 3.3.1 Parts and Assembly

In the FE model of a DDSTCC column, the column structure was divided into 6 distinct parts to accurately represent the complex interactions and behaviours of each component. The FE model included an outer steel tube, an inner steel tube, an inner concrete core, a sandwich concrete layer and two column capitals, each treated as a separate part in the FE assembly. The concrete components, including the inner concrete core and the sandwich concrete layer were modelled as solid deformable elements. This approach captures the three-dimensional deformation and stress distribution within the concrete, allowing for a more realistic simulation of its compressive behaviour and potential cracking under load. The steel tubes, both the outer, inner tubes and column capitals were modelled as shell deformable elements, which effectively represent the thin-walled structure of the steel and allow for accurate depiction of buckling and other failure modes in the tube walls. Creating these parts also involved defining the geometry and assigning material properties specific to each element type. In assembling the FE model, the inner concrete core was positioned at the center of the column, surrounded by the inner steel tube. The sandwich concrete layer was placed between the inner steel tube and the outer steel tube, creating the composite structure. The column capitals were placed at each end of the column with a 10 mm gap from the outer steel tube. The assembly of the DDSTCC column parts, including the concrete core, inner and outer steel tubes, sandwich concrete, and column capitals is shown in Fig. 3.2.

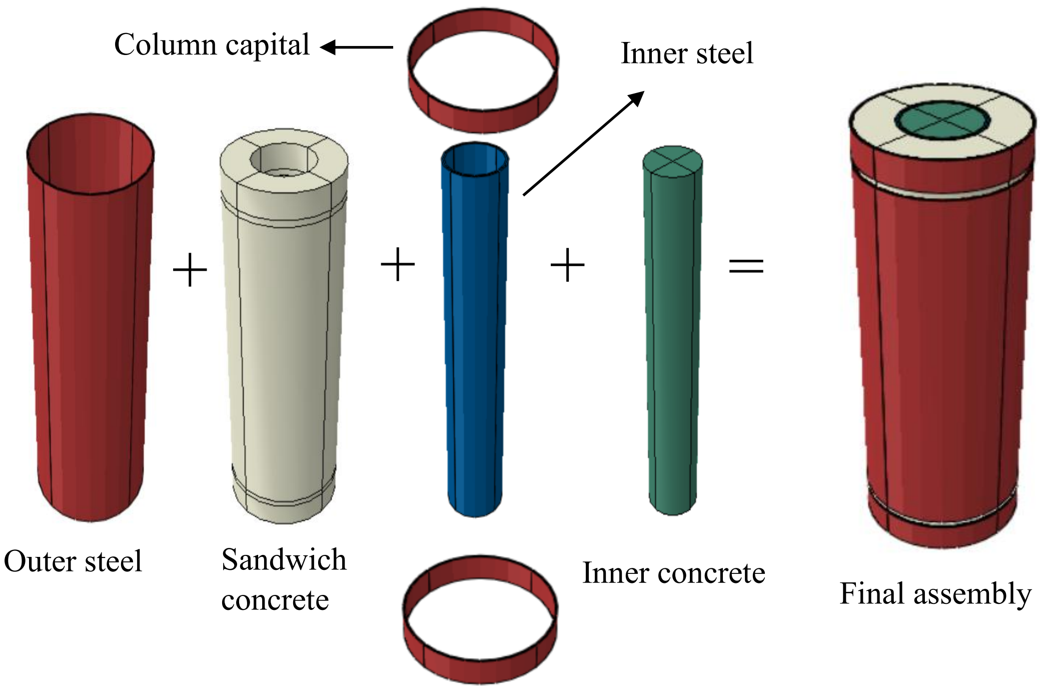


**Fig 3.2** Assembly of different parts in FE model

This layered assembly accurately reflects the structural layout of the DDSTCC column with the test setup, facilitating precise analysis of load transfer and confinement effects.

### 3.3.2 Constitutive Material Models

#### 3.3.2.1 Steel

The behaviour of steel tubes under loading can be categorized into three distinct phases: elastic, plastic, and strain hardening. Various models had been developed to represent these behaviours, including the elastic-plastic model and the elastic-perfectly plastic model with linear hardening. While these models have minimal impact on the axial strength of columns, they induce slight variations in the overall behaviour. Among these, the model proposed by Tao et al. (2013) is widely regarded as a convenient and straightforward approach. Thus, this model was adopted in this study to simulate the stress-strain behaviour of the steel tubes. The elastic phase was represented using a linear stress-strain relationship, characterized by a modulus of elasticity (E) of 200 GPa and a Poisson's ratio of 0.3. The stress-strain relationship is illustrated in Fig. 3.3 and represented through Eq. (3.1).

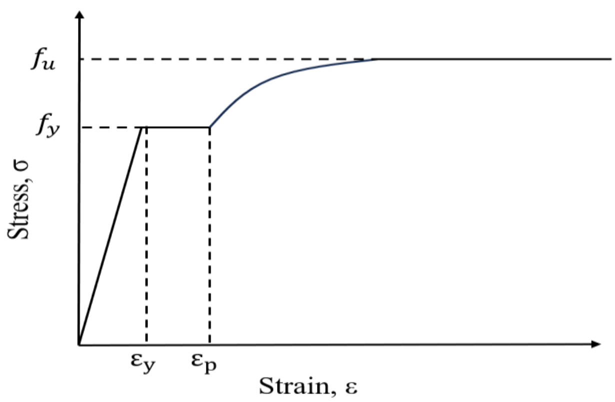


**Fig 3.3** Constitutive material model for steel tube

$$\sigma = \begin{cases} E_s\varepsilon & 0 \le \varepsilon < \varepsilon_y \\ f_y & \varepsilon_y \le \varepsilon < \varepsilon_p \\ f_u - (f_u - f_y) \cdot \left(\frac{\varepsilon_u - \varepsilon}{\varepsilon_u - \varepsilon_p}\right)^p & \varepsilon_p \le \varepsilon < \varepsilon_u \\ f_u & \varepsilon \ge \varepsilon_u \end{cases} \tag{3.1}$$

Where, $\varepsilon_y$ , $\varepsilon_p$ , $\varepsilon_u$ are the yield strain, hardening strain and ultimate strain respectively.

#### 3.3.2.2 Concrete

The concrete damage plasticity (CDP) model in ABAQUS was employed to incorporate the compressive and tensile stress-strain response of concrete into the FE model. When subjected to loading, the concrete experiences triaxial compression, while the steel tube is predominantly under biaxial stress conditions. This interaction between concrete and steel leads to an enhanced mechanical response, known as confinement effect imposed by the steel tube. To effectively simulate this confinement effect, a two-stage stress-strain model was adopted, representing the stress-strain behaviour of concrete as depicted in Fig 3.4. Initially, the curve rises linearly to the compressive strength $f_c'$ followed by a strain-hardening phase extending to the confined compressive strength $f_{cc}'$ as proposed by Mander et al. (1988).

$$\sigma_c = \frac{f_{cc}'\lambda(\varepsilon_c/\varepsilon_{cc}')}{\lambda - 1 + (\varepsilon_c/\varepsilon_{cc}')^{\lambda}} \tag{3.2}$$

In this equation, $\sigma_c$ corresponds to the compressive stress at a given strain $\varepsilon_c$. The term $f_{cc}'$ signifies the peak compressive strength of confined concrete at strain $\varepsilon_{cc}'$. λ governs the initial slope and the shape of the curve.

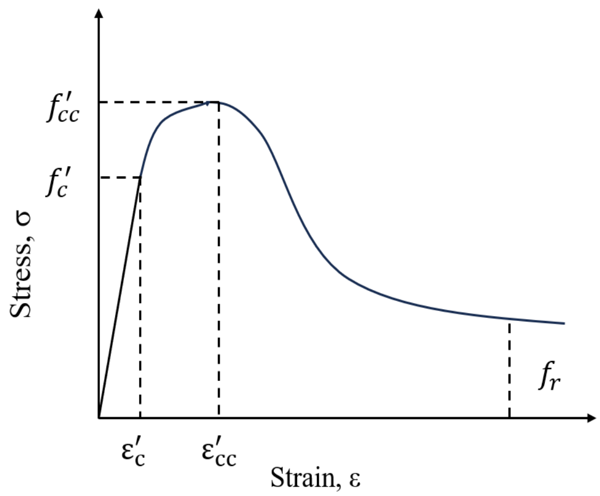


**Fig 3.4** Constitutive material model for concrete

The confined compressive strength $f'_{cc}$ surpasses the unconfined compressive strength $f'_c$ primarily because of the confinement effect imposed by the steel tube, which restricts lateral expansion and concurrently increases the corresponding strain $\varepsilon'_{cc}$ in the concrete. The unconfined cylindrical concrete strength $f'_c$ is converted from cubic strength $f_{cu}$ by

$$f'_c = \left[0.76 + 0.2log_{10}\left(\frac{f_{cu}}{19.6}\right)\right] f_{cu} \tag{3.3}$$

The lateral confining pressure can be determined using established concrete models proposed by various researchers such as Abed et al. (2012), Hu and Su (2011) and Tang et al. (1996). The confining pressure experienced by sandwich concrete exhibits notable distinctions from that of core concrete, primarily because the sandwich concrete is subjected to confinement from both the inner and outer steel tubes. However, several pressure models employed to calculate the confining pressure for sandwich concrete primarily account for the effect of the outer steel tube. Notably, Hu and Su (2011) and Tang et al. (1996) have developed more accurate models for this purpose, with Hu and Su (2011) model being particularly comprehensive as it considers both the inner and outer steel tubes, yet it does not incorporate yield strength and imposes constraints on the D/t ratio. The recent confining model proposed by Yan et al. (2021) had been utilized to calculate the lateral confining pressure of inner and sandwich concrete as it consider both the geometry and material properties of both steel tubes.

$$f'_{cc} = \gamma_c f'_c + 2.2\lambda {f'_c}^{0.3} \sigma_{ru}^{0.81} \tag{3.4}$$

where $f_{rp} = 2.2\lambda {f'_c}^{0.3} \sigma_{ru}^{0.81}$ indicates the lateral confining pressure induced by steel tube (Yan et al. 2021). Here, $\sigma_{ru}$ represents the circumferential stresses of the steel tube at the maximum axial load and the strength reduction factor $\gamma_c$ is based on column size, expressed as $\gamma_c = 1.85 D_c^{-0.135}$ (Yan et al., 2021; Liang, 2008). $D_c$ denotes the core diameter of concrete represented as $D_i - 2t_i$ for inner concrete and $D_o - 2t_o - D_i$ for sandwich concrete.

The descending branch of stress strain curve as shown in Fig 3.4 was adopted by incorporating the formula proposed by Binici (2005) as expressed:

$$\sigma_c = f_r + (f'_{cc} - f_r) exp\left[-\left(\frac{\varepsilon_c - \varepsilon'_{cc}}{\alpha}\right)^{\beta}\right] \tag{3.5}$$

Here, $f_r$ is the residual stress as shown in Fig 3.4. The additional parameters $\beta$ is taken as 1.2 and $\alpha$ is calculated through the following Eq. 3.6.

$$\alpha = 0.04 - \frac{0.036}{1+e^{6.08\xi - 3.49}} \tag{3.6}$$

Here, ξ is the confinement effect acting upon the concrete $\left(\xi = \frac{A_s f_y}{A_c f_c'}\right)$, depends on the material strength and geometric area of steel and concrete (Tao et al., 2013).

In this study, the uniaxial tensile response was assumed to be linear until the concrete's tensile strength, defined as $0.1f_c'$, was reached. After this failure stress was exceeded, the model characterized the tensile softening response with Fracture Energy (GF) obtained from Tao et al. (2013).

$$G_f = (0.0469d_{max}^2 - 0.5d_{max} + 26)\left(\frac{f_c'}{10}\right)^{0.7} N/m \tag{3.7}$$

The values for various parameters utilised in CDP and constitutive models are listed in Table 3.2 (Tao et al., 2013).

**Table 3.2** Values of various parameters used in constitutive models

| Properties | Values | Reference |
|---|---|---|
| Young's modulus of steel (GPa) | 200 | |
| Poisson's ratio (Steel) | 0.3 | |
| Poisson's ratio (Concrete) | 0.2 | |
| Dilation angle | $30^0$ | |
| Flow potential eccentricity | 0.1 | |
| Ratio of the compressive strength under biaxial loading to uniaxial compressive strength | 1.16 | (Tao et al., 2013) |
| Ratio of the second stress invariant on the tensile meridian to that on the compressive meridian | 0.667 | |

### 3.3.3 Interactions, Constraints and Boundary conditions

In the FE model, accurately defining the interaction between different elements is essential for simulating load transfer and deformation. For normal (normal-to-surface) behaviour, a hard contact interaction was established to prevent penetration between the concrete and steel elements under compressive forces. This method allows the transfer of normal forces while effectively capturing the confinement effect in situations like concrete and steel interaction, where the concrete is confined by the steel reinforcement. The interaction can be further modified by adjusting the contact stiffness and considering frictional effects, depending on the scenario. For tangential behaviour, a friction model with a friction coefficient of 0.4 was applied, representing the slip resistance at the steel-concrete interface, allowing realistic shear transfer while accommodating controlled relative sliding. In FE model, steel tubes were defined as master surfaces due to their higher stiffness, while the concrete surfaces were set as slave surfaces to ensure precise load transmission and accurate interaction. The primary surfaces involved in this interaction include the inner and outer surfaces of the inner steel tube, the interface with the concrete sandwiched between the steel tubes, the inner surface of the outer steel tube, the inner surface of the column capital, and the outer surface of the concrete core. In total, five critical contact interfaces are defined as shown in Fig 3.5.

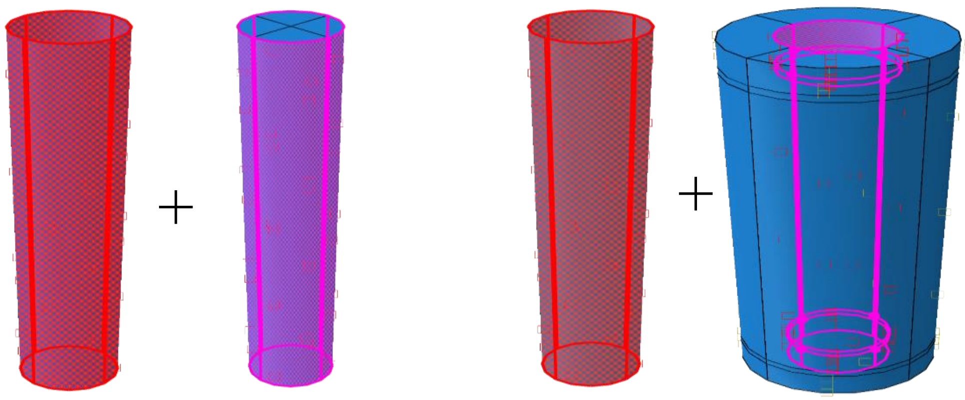


Inner steel Inner concrete

(a) Inner steel to inner concrete

Inner steel Sandwich concrete

(b) Inner steel to sandwich concrete

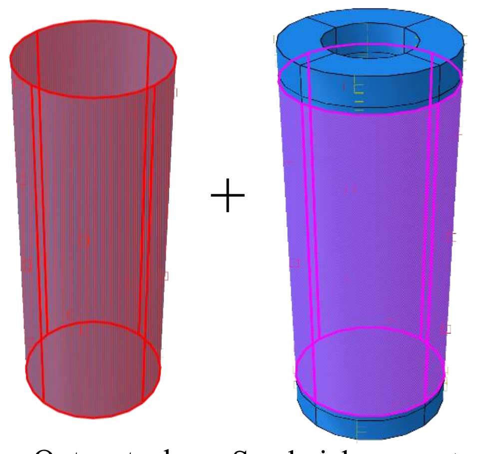


**(c)** Outer steel to sandwich concrete

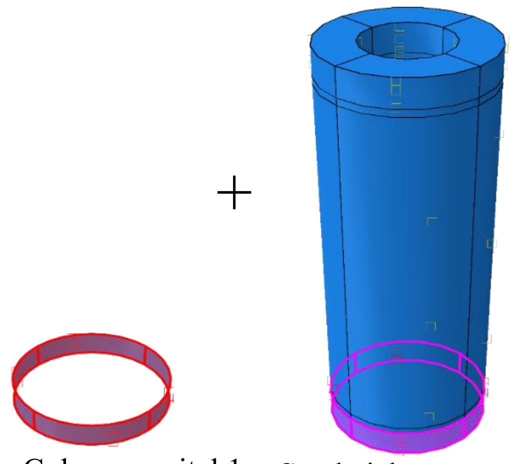


**(d)** Column capital to sandwich concrete

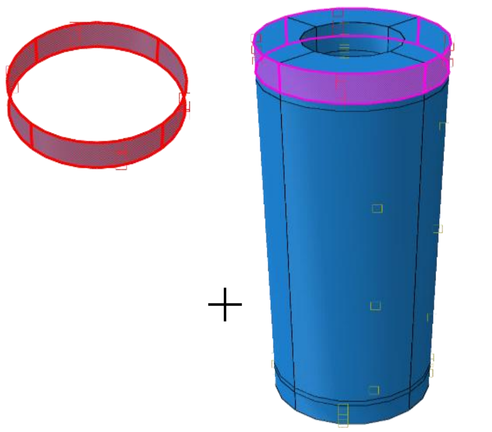


**(e)** Column capital to sandwich concrete

**Fig 3.5** Interaction between different parts in FE model

This interaction setup enabled coherent load sharing within the DDSTCC column model, contributing to a realistic simulation of its structural performance. In FE model, two reference points (RFs) were created at the top and bottom of the column. These RFs were connected to column ends using rigid body constraints for concentric loading (Fig. 3.6a) and coupling constraints for eccentric loading to ensure accurate load transfer (Fig. 3.6b).

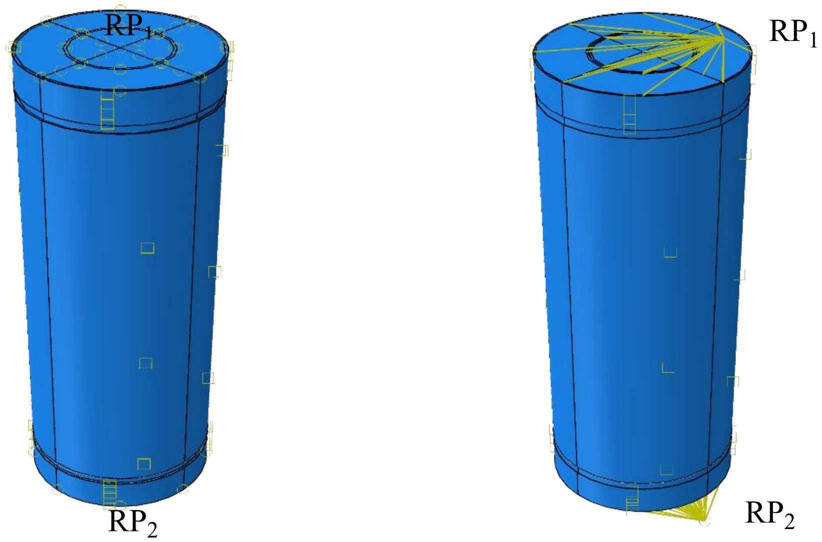


**(a)** Rigid body constraints **(b)** Coupling constraints

**Fig 3.6 Constraints**

At the top reference point, a displacement-controlled load of 20 mm was applied (similar to experimental setup discussed in section 3.2) while the rotation was allowed along all axes ($UR_1 \neq UR_2 \neq UR_3 \neq 0$), but lateral movement was restricted in transverse axis ($U_1 = U_3 = 0$).

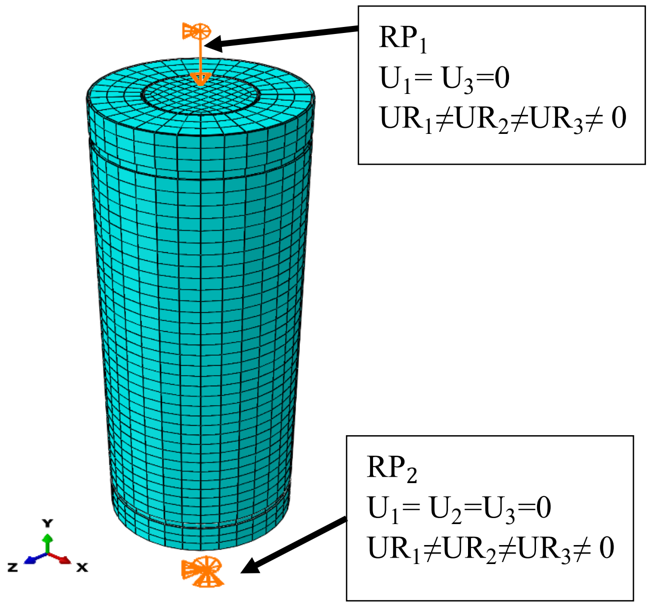


**Fig 3.7** Boundary conditions applied in the FE model

Meanwhile, a pin condition was imposed at the bottom reference point by restricting translations in each direction ($U_1= U_2= U_3= 0$) yet permitting rotation along all three axes ($UR_1\neq UR_2\neq UR_3\neq 0$) as shown in Fig. 3.7.

### 3.3.4 Element Type and Meshing

In the FE analysis selecting appropriate element types and meshing strategies is essential for capturing structural behaviour accurately under loading conditions. For the concrete, 8-node hexahedral solid elements (C3D8R) were used to effectively represent the three-dimensional stress state within the concrete. As reduced-integration solid elements, C3D8R elements helped to mitigate shear locking, a common issue in high-aspect-ratio elements, while maintaining good computational efficiency. For the outer and inner steel tubes, S4R elements—4-node shell elements with reduced integration were employed. Shell elements are well-suited for thin-walled structures such as steel tubes, enabling efficient modelling of bending, shear and membrane actions. Because, the reduced integration in S4R elements prevents overestimation of stiffness in thin shells, supporting a stable and realistic simulation. Finally, a mesh sensitivity study was conducted on the ST5-D106-3 specimen to determine the optimal meshing configuration for accurate results with reduced computational time and improved convergence. The study highlighted the importance of node-to-node matching across different elements, which significantly contributed to computational efficiency and model stability. Based on this analysis, a meshing scheme was adopted that includes 32 elements along the circumference of the steel and concrete and an element size of 20 mm in the longitudinal direction. This configuration balance between accuracy and computational efficiency, ensuring reliable results while minimizing processing time. Fig. 3.8 illustrates the details of the mesh sensitivity study, cross-sectional and a 3D view of the meshing.

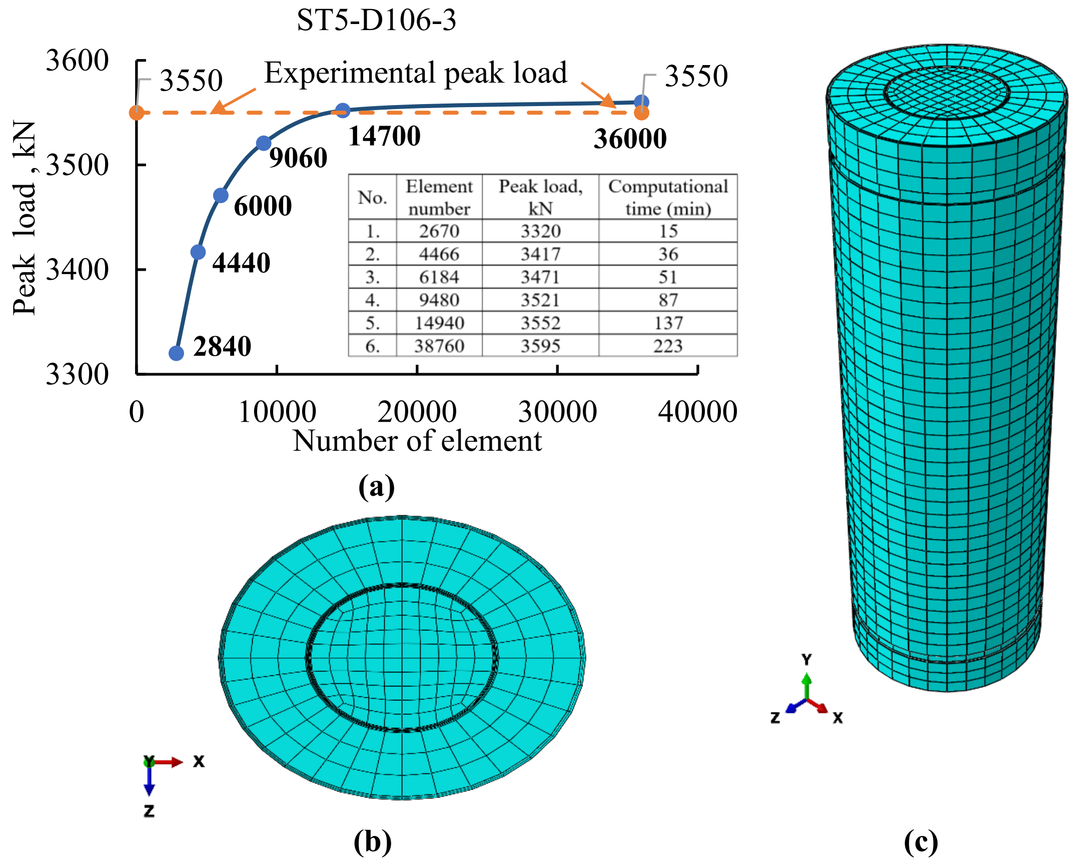


| No. | Element number | Peak load, kN | Computational time (min) |
|---|---|---|---|
| 1. | 2670 | 3320 | 15 |
| 2. | 4466 | 3417 | 36 |
| 3. | 6184 | 3471 | 51 |
| 4. | 9480 | 3521 | 87 |
| 5. | 14940 | 3552 | 137 |
| 6. | 38760 | 3595 | 223 |

**Fig 3.8 (a)** Mesh sensitivity analysis; **(b)** Cross sectional view of meshing **(c)** Meshing of the developed FE model (3D view)

### 3.3.5 Analysis Techniques

Different analytical techniques were employed for the stub and full-scale slender column simulations to accurately capture their structural behaviour. For the stub column, static general procedure was selected, as this method is well-suited for stub columns where global buckling effects are negligible. In contrast, for the full-scale slender column, initial geometric imperfections were incorporated into the analysis, as global buckling in slender columns is significantly influenced by these imperfections.

To account for this, a two-step approach was implemented. In the first step, a buckling analysis using linear perturbation was performed to identify the critical buckling mode shape. Following this, the nodal displacements corresponding to the critical buckling mode were extracted and applied to the main model as initial imperfections, scaled by a factor of L/1000 (where *L* represents the column height). The scale factor, selected from L/250, L/500, L/1000, or L/2000, was used to define the magnitude of initial imperfections. Among these, a scale factor of L/1000 was commonly used in most literature as it offers a balance between computational efficiency and the accuracy of the buckling analysis (Zhao et al., 2020; Wang et al., 2022). This modified model was then analysed using the static general procedure, providing a realistic representation of buckling behaviour under applied loads. Fig. 3.9 illustrates the critical buckling shape obtained from the linear perturbation buckling analysis.

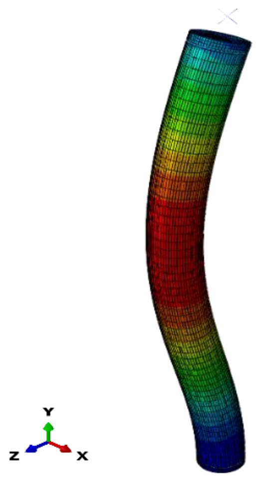


**Fig 3.9** First eigenmode of full-scale slender column

### 3.4 Validation of the FE Model

In order to validate the FE model, seven models were developed following the detailed material properties, geometrical configurations as summarized in Table 3.1. The FE simulation results were compared with test results, focusing on key features such as axial load, load-displacement behaviour, and failure modes, to assess the accuracy and reliability of the model. The results from this comparative study are presented and discussed in the following subsections, highlighting the similarities or discrepancies between the FE simulations and test results.

### 3.4.1 Comparison of Axial Strength

The axial strength of the developed FE model was determined using the result post-processing module in Abaqus. The axial force at $RP_2$ (as shown in Fig. 3.6) was extracted from the field output and the maximum value represents the simulated axial strength of the column. The comparison between the simulated FE results and the test results obtained by Lu et al. (2022) is presented in Table 3.3.

**Table 3.3** Comparison of test and predicted axial strength of DDSTCC column

| Designation | Axial strength from test, $P_{test}$ (kN) | Axial strength from FE analysis, $P_{FE}$ (kN) | $P_{FE}/P_{test}$ |
|---|---|---|---|
| ST3-D80-4 | 2808 | 2880 | 1.025 |
| ST3-D106-3 | 2828 | 2983 | 1.054 |
| ST3-D158-2 | 2872 | 2983 | 1.038 |
| ST3-D106-4 | 2991 | 2989 | 0.999 |
| ST3-D106-5 | 3099 | 2901 | 0.936 |
| ST4-D106-3 | 3106 | 3249 | 1.046 |
| ST5-D106-3 | 3574 | 3552 | 0.993 |
| | | Mean | 1.013 |
| | | Standard deviation (SD) | 0.038 |
| | | Coefficient of variance (COV) | 0.037 |

The FE model's predictive accuracy was demonstrated by an average $P_{FE}/P_{test}$ ratio of 1.013, accompanied by a low coefficient of variation (COV) of 0.037 and a standard deviation (SD) of 0.038. These values indicated that the FE models consistently predicted the test axial strength with high accuracy and minimal variability, confirming the reliability of the FE model in simulating the behaviour of DDSTCC columns under compressive loading conditions.

### 3.4.2 Comparison of Load vs Displacement Behaviour

The load-displacement behaviour of the FE model was obtained through the result post-processing module in Abaqus. Axial loads were collected at $RP_2$, and the corresponding displacement values were recorded at $RP_1$ as shown in Fig. 3.6. Then, the load-displacement data was then plotted and compared with the test results as presented in Fig. 3.9. The behavioural patterns observed in both the FE simulations and tests were analysed across several key aspects, including initial stiffness, axial strength, post-peak behaviour and overall load-displacement trends. The initial stiffness of the FE models was found to be in good agreement with the test results. Besides, the peak axial strength was observed at nearly the same displacement in both the FE simulations and the test results, demonstrating strong consistency. As for the post-peak behaviour, the FE models were able to predict stable and reasonably accurate post-peak responses, aligning closely with the test behaviour. Upon closer inspection, it was noted that two specific column ST3-80-4 and ST3-D106-5, exhibited a sudden drop in load after reaching the axial strength, followed by a recovery in residual strength at the final displacement.

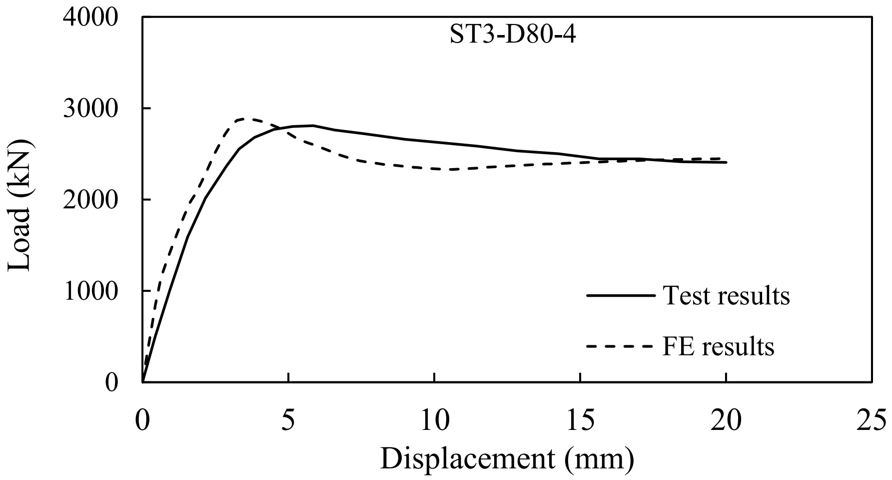


**(a)** ST3-D80-4

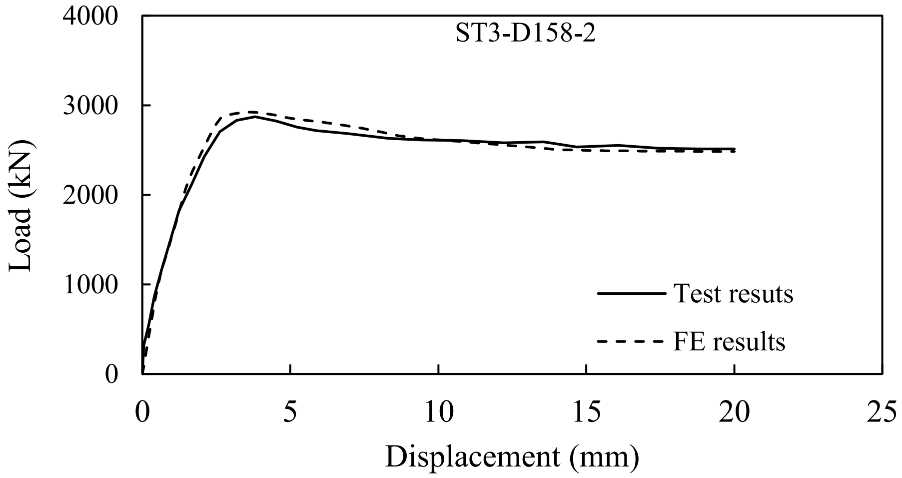


**(b)** ST3-D158-2

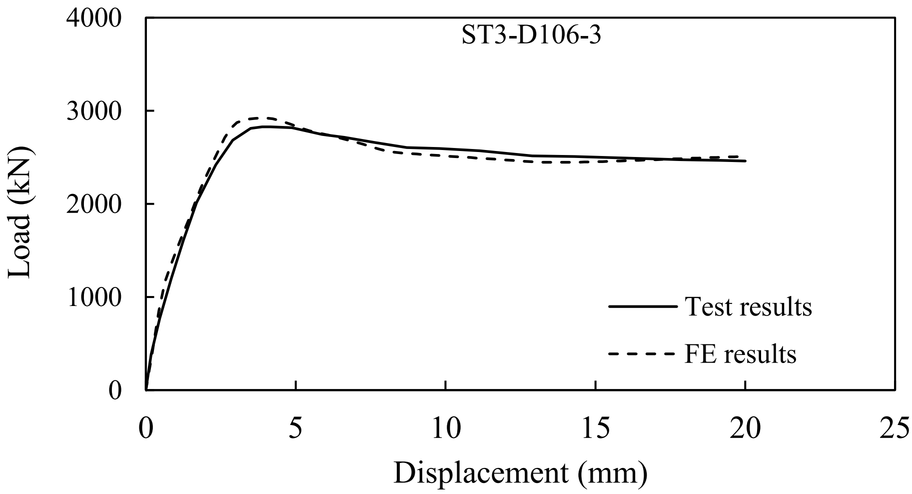


**(c)** ST3-D106-3

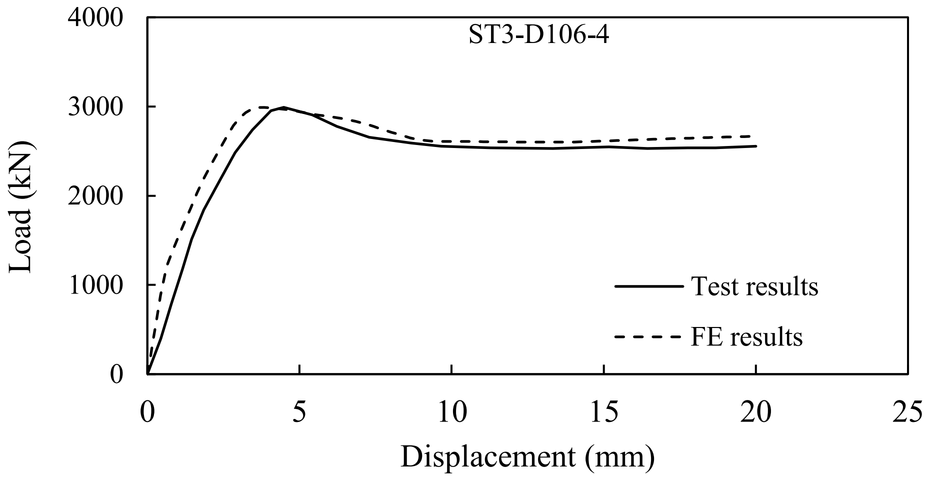


**(d)** ST3-D106-4

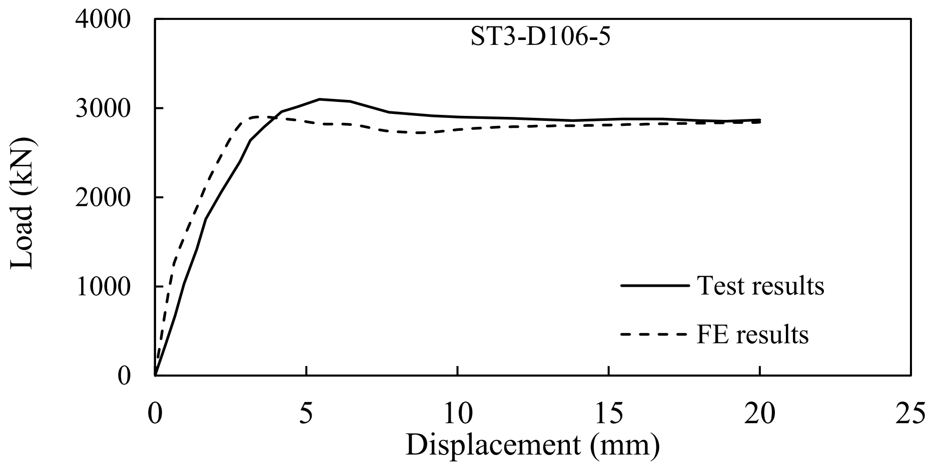


**(e)** ST3-D106-5

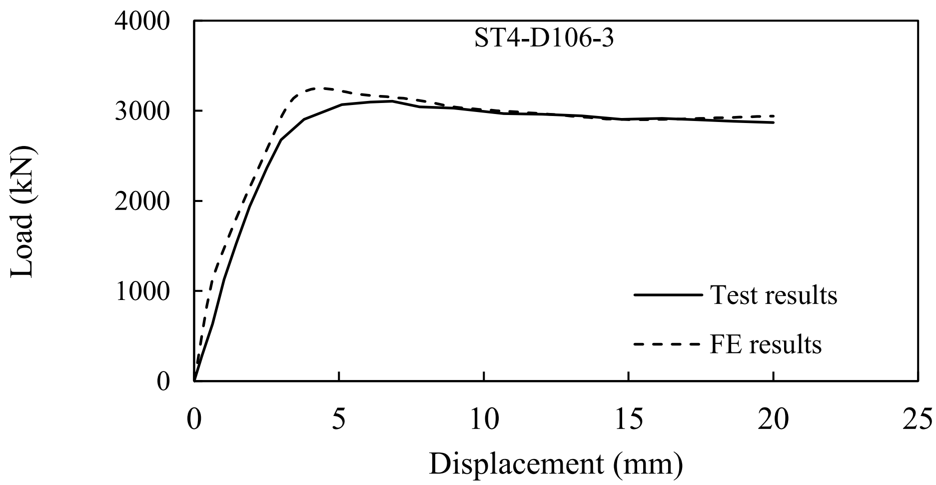


**(f)** ST4-D106-3

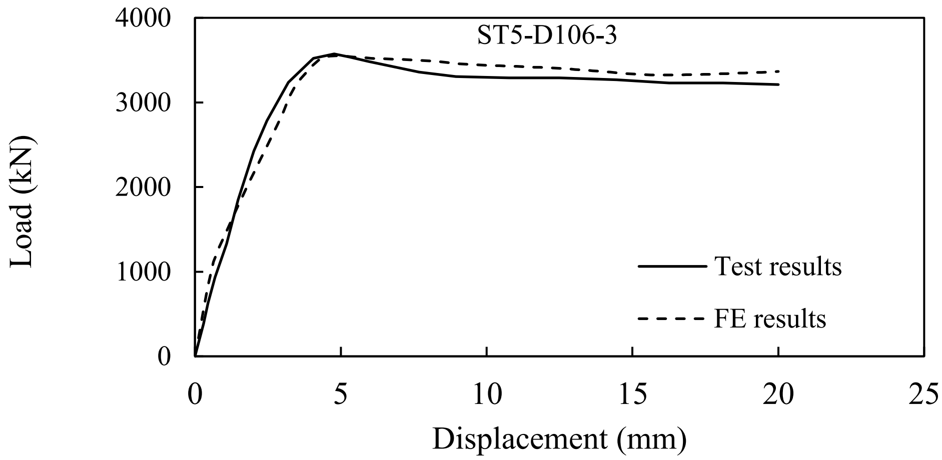


**(g)** ST5-D106-3

**Fig 3.10** Comparison between the test and FE results

This behaviour, although not observed in all specimens, suggests some differences in the post-peak response between certain FE models and test results. The overall load versus displacement behaviour of the FE models aligned well with the test results, demonstrating consistency in trends and key features.

### 3.4.3 Prediction of Failure Modes

The accuracy of the FE model in predicting the failure behaviour of the test specimens was further analysed by comparing the FE simulated failure modes with the test observations as shown in Fig. 3.10. The location and pattern of buckling obtained in the FE simulations closely resembled those in the test specimens, with failure occurring near the mid-height region of the columns. The stress band distribution further supported the accuracy of the simulation, as it highlights concentrated stress near the buckling location, consistent with the test results. Additionally, the stress band dispersed along the height of the column, with minimal stress observed near the column capital region.

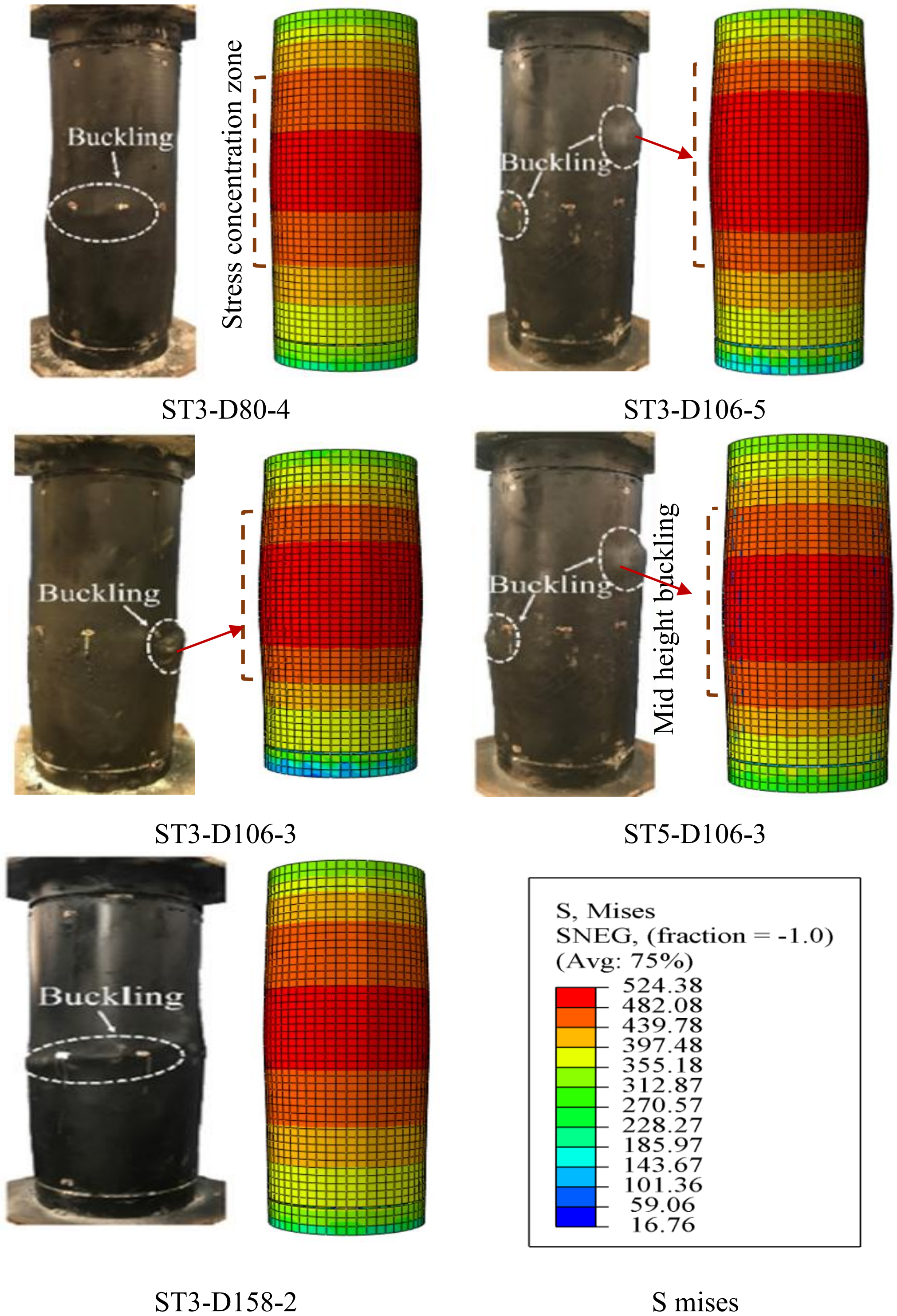


**Fig 3.11** Comparison of failure mode between test and FE results

This distribution suggested that the FE simulation is capable of accurately predicting the distinct failure patterns, including the localization of stress and the progression of failure, in a manner similar to the test observations.

### 3.5 Summary

In summary, this chapter outlines the step-by-step procedure for developing the FE model, including the selection of appropriate material models and the determination of an optimal mesh size. The FE model demonstrates strong accuracy across all key aspects, making it suitable for further parametric studies. Consequently, the model has been adopted for extensive parametric investigation in chapter 4.

# CHAPTER 4: INVESTIGATION ON COMPRESSIVE BEHAVIOUR OF DDSTCC COLUMN^

## 4.1 Introduction

In chapter 3, FE models were developed and validated to ensure their accuracy and reliability in simulating the compressive behaviour of the column. The present chapter 4 adopted the validated FE model to conduct an extensive parametric investigation on compressive behaviour of concentrically and eccentrically loaded stub and concentrically loaded full scale slender DDSTCC column. The results of this parametric study are discussed in detail, highlighting the effects of different variables and their interactions. The insights gained from this study will serve as the basis for the analytical formulations presented in chapter 5.

---

^The findings discussed in this chapter have been disseminated through the following publications:

1. Sakib, A. N., & Kabir, Md. I. (2025). Behaviour and design of discontinuous double steel tube confined concrete columns for concentric and eccentric loading. *Structures*, *79*, 109511. https://doi.org/10.1016/j.istruc.2025.109511
2. Nazmun Sakib, A., & Imran Kabir, Md. (2024). Compressive Behaviour of Slender Discontinuous Double Steel Tube Confined Concrete Column Under Concentric Loading. *Lecture Notes in Civil Engineering*, 127–136. https://doi.org/10.1007/978-3-031-63280-8_14

## 4.2 Brief Overview of the Parametric Study

The validated FE model was employed for conducting the extensive parametric study. In this parametric study, the behaviour of three different types of columns were investigated:

i. The behaviour of compact and slender sections of stub columns,
ii. The performance of full-scale slender columns and
iii. The behaviour of eccentrically loaded stub columns.

Various geometric and material parameters were considered to gain an in-depth understanding of their influence on the compressive behaviour of studied columns. The geometric parameters included the steel tube diameter, tubes wall thickness and column height, while the material properties were the strength of the concrete and steel tubes. Additionally, the effects of loading eccentricity were taken into account for eccentrically loaded stub column. The geometry and material parameters for each phase were chosen in such a way so that for stub column both compact and non-compact sections were present. This was maintained by comparing the sectional slenderness ratio ($D_o/t$) against the slenderness limit $\lambda_r = \frac{0.19E_s}{F_y}$ (AISC, 2010). For full scale columns, global slenderness ratio $\lambda$=4L/$D_o$ greater than 22 were classified as slender columns (Zhao et al., 2020; Wang et al., 2022). To ensure consistency in the analysis, the outer steel tube diameter was fixed at 300 mm for stub columns and 250 mm for full-scale columns. The wall thickness of the steel tubes was varied between 2 to 4 mm. For stub columns, a fixed height of 1000 mm was used, while for full-scale columns four different heights ranging from 1000 mm to 6000 mm were considered.

The yield strength of the steel tube was varied between 255 to 690 MPa, while the compressive strength of the concrete ranged from 40 to 90 MPa, allowing a combination of both normal and high strength constituents. In the parametric study, the columns were subjected to a 20 mm displacement load, consistent with validation and experimental models. The developed FE model is organized into 25 distinct groups, denoted as G1 through G25. Each group focuses on varying one specific parameter while keeping all other parameters fixed. The details of each phase are outlined in **Tables 4.1 to 4.3** and are discussed in the following sections. The columns were categorized using a specific designation format: “xloxt-ixt-sxx-cxx”.

i. The first term, “xl,” specifies the type and height of the column, with the type indicating whether it is a stub, full-scale, or eccentrically loaded column.
ii. The next three characters, “oxt,” describe the outer steel tube’s dimensions, where “x” represents its diameter, and “t” denotes its thickness.
iii. The term “ixt” refers to the dimensions of the inner steel tube, with “xt” specifying its diameter and thickness.
iv. The component “sxx” indicates the strength of the steel tubes, with “xx” representing the strength of both the outer and inner steel tubes.
v. Lastly, “cxx” corresponds to the strength of the concrete, where “xx” reflects the strengths of the sandwich concrete and inner concrete layers.

For instance, the designation S1O33-I13-S44-C66 refers to a stub column with a height of 1000 mm. It has an outer steel tube diameter of 300 mm and a thickness of 3 mm, an inner steel tube diameter of 150 mm with a thickness of 3 mm, a steel tube strength of 420 MPa, and a concrete strength of 60 MPa. Similarly, L3O23-I13-S33-C66 refers to a full-scale slender column with a height of 3000 mm, while the other terms correspond to stub columns. For eccentrically loaded columns, an additional term, “x,” was incorporated to denote the $e/D_o$ ratio, where e represents the eccentricity and $D_o$ is the outer steel tube’s diameter. For example: ElO33-I13-S4-C6-0 represents an eccentrically loaded column with an $e/D_o$ ratio of 0. To analyze variations in performance across different column types, control specimens were selected based on their balanced properties. These include:

i. S1O33-I13-S44-C66 for stub columns, presented in **Table 4.1**
ii. L3O23-I13-S33-C66 for full-scale columns, shown in **Table 4.2**
iii. ElO33-I13-S4-C6-0 for eccentrically loaded columns, detailed in **Table 4.3**

**Table 4.1** Summary of compact and slender section of stub columns

| Group | Column designation | Height, h (mm) | Outer steel tube | | Inner steel tube | | Steel yield strength | | Concrete strength | | Section type | $\lambda_r$ | $P_{FE}$ (kN) | $R_{FE}$ (kN) |
|---|---|---|---|---|---|---|---|---|---|---|---|---|---|---|
| | | | $D_o \times t_o$ (mm) | $D_o / t_o$ (mm) | $D_i \times t_i$ (mm) | $D_i / t_i$ (mm) | $f_{yo}$ (MPa) | $f_{yi}$ (MPa) | $f'_{cs}$ (MPa) | $f'_{ci}$ (MPa) | | | | |
| | S1O34-I13-S44-C66 | | 300 × 4 | 75 | | | | | | | C | | 6952 | 6469 |
| G1 | S1O33-I13-S44-C66 | 1000 | 300 × 3 | 100 | 150 × 3 | 50 | 420 | 420 | 60 | 60 | S | 90 | 6120 | 5416 |
| | S1O32-I13-S44-C66 | | 300 × 2 | 150 | | | | | | | S | | 5430 | 4615 |
| | S1O33-I14-S44-C66 | | | | 150 × 4 | 37.5 | | | | | S | | 6375 | 5640 |
| G2 | S1O33-I13-S44-C66 | 1000 | 300 × 3 | 100 | 150 × 3 | 50 | 420 | 420 | 60 | 60 | S | 90 | 6120 | 5416 |
| | S1O33-I12-S44-C66 | | | | 150 × 2 | 75 | | | | | S | | 5952 | 4925 |
| | S1O33-I23-S44-C66 | | | | 225 × 3 | 75 | | | | | S | | 6755 | 6055 |
| G3 | S1O33-I13-S44-C66 | 1000 | 300 × 3 | 100 | 150 × 3 | 50 | 420 | 420 | 60 | 60 | S | 90 | 6120 | 5416 |
| | S1O33-I.73-S44-C66 | | | | 75 × 3 | 25 | | | | | S | | 5755 | 4429 |
| | S1O33-I13-S74-C66 | | | | | | 690 | | | | C | 55 | 7592 | 6950 |
| G4 | S1O33-I13-S44-C66 | 1000 | 300 × 3 | 100 | 150 × 3 | 75 | 420 | 420 | 60 | 60 | S | 90 | 6120 | 5416 |
| | S1O33-I13-S24-C66 | | | | | | 255 | | | | S | 149 | 5260 | 4575 |
| | S1O33-I13-S47-C66 | | | | | | | 690 | | | S | | 6562 | 5990 |
| G5 | S1O33-I13-S44-C66 | 1000 | 300 × 3 | 100 | 150 × 3 | 50 | 420 | 420 | 60 | 60 | S | 90 | 6120 | 5416 |
| | S1O33-I13-S42-C66 | | | | | | | 255 | | | S | | 5860 | 5090 |
| | S1O33-I13-S44-C46 | | | | | | | | 40 | | S | | 5586 | 5263 |
| G6 | S1O33-I13-S44-C66 | 1000 | 300 × 3 | 100 | 150 × 3 | 50 | 420 | 420 | 60 | 60 | S | 90 | 6120 | 5416 |
| | S1O33-I13-S44-C96 | | | | | | | | 90 | | S | | 7331 | 5724 |
| | S1O33-I13-S44-C64 | | | | | | | | | 40 | S | | 5745 | 5198 |
| G7 | S1O33-I13-S44-C66 | 1000 | 300 × 3 | 100 | 150 × 3 | 50 | 420 | 420 | 60 | 60 | S | 90 | 6120 | 5416 |
| | S1O33-I13-S44-C69 | | | | | | | | | 90 | S | | 6522 | 5480 |

**Table 4.2** Summary of full-scale slender columns

| Group | Column designation | Height, h (mm) | Outer steel tube | | Inner steel tube | | Steel yield strength | | Concrete strength | | λ | $P_{FE}$ (kN) |
|---|---|---|---|---|---|---|---|---|---|---|---|---|
| | | | $D_o \times t_o$ (mm) | $D_o / t_o$ (mm) | $D_i \times t_i$ (mm) | $D_i / t_i$ (mm) | $f_{yo}$ (MPa) | $f_{yi}$ (MPa) | $f'_{cs}$ (MPa) | $f'_{ci}$ (MPa) | | |
| G8 | L3O24-I13-S33-C66 | 3000 | 250 × 4 | 62.5 | 125 × 3 | 41.6 | 350 | 350 | 60 | 60 | 48 | 3460 |
| | L3O23-I13-S33-C66 | | 250 × 3 | 83.3 | | | | | | | | 3270 |
| | L3O22-I13-S33-C66 | | 250 × 2 | 62.5 | | | | | | | | 2950 |
| G9 | L3O23-I14-S33-C66 | 3000 | 250 × 3 | 83.3 | 125 × 4 | 31.2 | 350 | 350 | 60 | 60 | 48 | 3290 |
| | L3O23-I13-S33-C66 | | | | 125 × 3 | 41.6 | | | | | | 3270 |
| | L3O23-I12-S33-C66 | | | | 125 × 2 | 62.5 | | | | | | 3124 |
| G10 | L3O23-I13-S37-C66 | 3000 | 250 × 3 | 83.3 | 125 × 3 | 41.6 | 350 | 690 | 60 | 60 | 48 | 3670 |
| | L3O23-I13-S33-C66 | | | | | | | 350 | | | | 3270 |
| | L3O23-I13-S32-C66 | | | | | | | 210 | | | | 3071 |
| G11 | L3O23-I13-S73-C66 | 3000 | 250 × 3 | 83.3 | 125 × 3 | 41.6 | 690 | 350 | 60 | 60 | 48 | 3930 |
| | L3O23-I13-S33-C66 | | | | | | 350 | | | | | 3270 |
| | L3O23-I13-S23-C66 | | | | | | 210 | | | | | 2940 |
| G12 | L3O23-I13-S33-C46 | 3000 | 250 × 3 | 83.3 | 125 × 3 | 41.6 | 350 | 350 | 40 | 60 | 48 | 2680 |
| | L3O23-I13-S33-C66 | | | | | | | | 60 | | | 3270 |
| | L3O23-I13-S33-C96 | | | | | | | | 90 | | | 4000 |
| G13 | L3O23-I13-S33-C64 | 3000 | 250 × 3 | 83.3 | 125 × 3 | 41.6 | 350 | 350 | 60 | 40 | 48 | 3120 |
| | L3O23-I13-S33-C66 | | | | | | | | | 60 | | 3270 |
| | L3O23-I13-S33-C69 | | | | | | | | | 90 | | 3360 |
| G14 | L3O23-I1.73-S33-C66 | 3000 | 250 × 3 | 83.3 | 175 × 3 | 58.33 | 350 | 350 | 60 | 60 | 48 | 3340 |

| | | | | | | | | | | | |
|---|---|---|---|---|---|---|---|---|---|---|---|
| | L3O23-I13-S33-C66 | | | | 125 × 3 | 41.6 | | | | | | 3270 |
| | L3O23-I.73-S33-C66 | | | | 75 × 3 | 25 | | | | | | 3050 |
| G15 | F1O23-I13-S33-C66 | 1000 | 250 × 3 | 83.3 | 125 × 3 | 41.6 | 350 | 350 | 60 | 60 | 16 | 4250 |
| | F3O23-I13-S33-C66 | 3000 | | | | | | | | | 48 | 3270 |
| | F4O23-I13-S33-C66 | 4500 | | | | | | | | | 72 | 2940 |
| | F6O23-I13-S33-C66 | 6000 | | | | | | | | | 96 | 2370 |
| G16 | F1O23-I13-S22-C66 | 1000 | 250 × 3 | 83.3 | 125 × 3 | 41.6 | 210 | 210 | 60 | 60 | 16 | 3440 |
| | F3O23-I13-S22-C66 | 3000 | | | | | | | | | 48 | 2750 |
| | F4O23-I13-S22-C66 | 4500 | | | | | | | | | 72 | 2420 |
| | F6O23-I13-S22-C66 | 6000 | | | | | | | | | 96 | 1950 |
| G17 | F1O23-I13-S66-C66 | 1000 | 250 × 3 | 83.3 | 125 × 3 | 41.6 | 690 | 690 | 60 | 60 | 16 | 6340 |
| | F3O23-I13-S66-C66 | 3000 | | | | | | | | | 48 | 4250 |
| | F4O23-I13-S66-C66 | 4500 | | | | | | | | | 72 | 3920 |
| | F6O23-I13-S66-C66 | 6000 | | | | | | | | | 96 | 3370 |
| G18 | F1O23-I13-S33-C44 | 1000 | 250 × 3 | 83.3 | 125 × 3 | 41.6 | 350 | 350 | 40 | 40 | 16 | 3510 |
| | F3O23-I13-S33-C44 | 3000 | | | | | | | | | 48 | 2580 |
| | F4O23-I13-S33-C44 | 4500 | | | | | | | | | 72 | 2450 |
| | F6O23-I13-S33-C44 | 6000 | | | | | | | | | 96 | 2200 |
| G19 | F1O23-I13-S33-C99 | 1000 | 250 × 3 | 83.3 | 125 × 3 | 41.6 | 350 | 350 | 90 | 90 | 16 | 5382 |
| | F3O23-I13-S33-C99 | 3000 | | | | | | | | | 48 | 4220 |
| | F4O23-I13-S33-C99 | 4500 | | | | | | | | | 72 | 2940 |
| | F6O23-I13-S33-C99 | 6000 | | | | | | | | | 96 | 2870 |
| G20 | F1O23-I.73-S33-C66 | 1000 | 250 × 3 | 83.3 | 75 × 3 | 25 | 350 | 350 | 60 | 60 | 16 | 4050 |
| | F3O23-I.73-S33-C66 | 3000 | | | | | | | | | 48 | 3140 |
| | F4O23-I.73-S33-C66 | 4500 | | | | | | | | | 72 | 2780 |
| | F6O23-I.73-S33-C66 | 6000 | | | | | | | | | 96 | 2250 |

**Table 4.3** Summary of eccentrically loaded stub columns

| Group | Column designation | Height, h (mm) | Outer steel tube | | Inner steel tube | | Steel yield strength | Concrete strength | $e/D_o$ | Moment, $M_{FE}$ (kN-m) | Axial load, $P_{FE}$ (kN) |
|---|---|---|---|---|---|---|---|---|---|---|---|
| | | | $D_o \times t_o$ (mm) | $D_o / t_o$ (mm) | $D_i \times t_i$ (mm) | $D_i / t_i$ (mm) | $f_y$ (MPa) | $f_c'$ (MPa) | | | |
| G21 | ElO33-I13-S4-C6-0 | 1000 | 300 × 3 | 100 | 150 × 3 | 50 | 420 | 60 | 0 | 0 | 6119 |
| | ElO33-I13-S4-C6-0.10 | | | | | | | | 0.1 | 133 | 4420 |
| | E1O33-I13-S4-C6-0.20 | | | | | | | | 0.2 | 200 | 3320 |
| | E1O33-I13-S4-C6-0.35 | | | | | | | | 0.35 | 221 | 2210 |
| | E1O33-I13-S4-C6-0.45 | | | | | | | | 0.45 | 182 | 1355 |
| G22 | E1O34-I13-S4-C6-0 | 1000 | 300 × 4 | 75 | 150 × 3 | 50 | 420 | 60 | 0 | 0 | 6952 |
| | E1O34-I13-S4-C6-0.10 | | | | | | | | 0.1 | 155 | 5150 |
| | E1O34-I13-S4-C6-0.20 | | | | | | | | 0.2 | 226 | 3780 |
| | E1O34-I13-S4-C6-0.35 | | | | | | | | 0.35 | 233 | 2222 |
| | E1O34-I13-S4-C6-0.45 | | | | | | | | 0.45 | 200 | 1490 |
| G23 | E1O33-I14-S4-C6-0 | 1000 | 300 × 3 | 100 | 150 × 4 | 37.5 | 420 | 60 | 0 | 0 | 6375 |
| | E1O33-I14-S4-C6-0.10 | | | | | | | | 0.1 | 139 | 4679 |
| | E1O33-I14-S4-C6-0.20 | | | | | | | | 0.2 | 225 | 3436 |
| | E1O33-I14-S4-C6-0.35 | | | | | | | | 0.35 | 228 | 2172 |
| | E1O33-I14-S4-C6-0.45 | | | | | | | | 0.45 | 220 | 1630 |
| G24 | E1O33-I.73-S4-C6-0 | 1000 | 300 × 3 | 100 | 75 × 3 | 25 | 420 | 60 | 0 | 0 | 5622 |
| | E1O33-I.73-S4-C6-0.10 | | | | | | | | 0.1 | 124 | 4152 |
| | E1O33-I.73-S4-C6-0.20 | | | | | | | | 0.2 | 186 | 3105 |
| | E1O33-I.73-S4-C6-0.35 | | | | | | | | 0.35 | 188 | 1790 |
| | E1O33-I.73-S4-C6-0.45 | | | | | | | | 0.45 | 142 | 1050 |

| | | | | | | | | | | | |
|---|---|---|---|---|---|---|---|---|---|---|---|
| G25 | E1O33-I23-S4-C6-0 | 1000 | 300 × 3 | 100 | 225 × 3 | 75 | 420 | 60 | 0 | 0 | 6754 |
| | E1O33-I23-S4-C6-0.10 | | | | | | | | 0.1 | 142 | 4760 |
| | E1O33-I23-S4-C6-0.20 | | | | | | | | 0.2 | 218 | 3650 |
| | E1O33-I23-S4-C6-0.35 | | | | | | | | 0.35 | 238 | 2270 |
| | E1O33-I23-S4-C6-0.45 | | | | | | | | 0.45 | 237 | 1754 |

Note: $D_o$ and $D_i$ represent the diameter of outer and inner steel tube, $t_o$ and $t_i$ represent the thickness of outer and inner steel tube. $f_{yo}$ and $f_{yi}$ represent the yield strength of outer and inner steel tube, $f'_{cs}$ and $f'_{ci}$ denotes the compressive strength of sandwich and inner concrete. Compact and slender section are denoted by "C" and "S". $P_{FE}$ and $R_{FE}$ are the axial and residual strength of column (for **Table 4.1 to 4.3**)

### 4.3 Behaviour of Compact and Slender Sections of Stub Columns

This section investigates the influence of various geometric and material parameters on the compressive behaviour of compact and slender sections of stub columns. The local slenderness was analysed within the groups G1 to G7 as presented in Table 4.1, with outer steel tube diameter and thickness were carefully selected to include a combination of compact and slender sections for a comprehensive evaluation. The local slenderness ratio ($D_o/t$) was compared against the slenderness limit $\lambda_r = \frac{0.19E_s}{F_y}$, as specified in AISC 360-10 (2010). The effect of slenderness on the compressive behaviour of the columns was examined in detail and failure patterns were systematically identified. Additionally, the influence of specific parameters on structural performance was assessed through the analysis of load versus displacement behaviour. The key insights into the impact of local slenderness on the overall behaviour and failure mechanisms of the columns are discussed below:

#### 4.3.1 Effect of Steel Tube Thickness

The effect of the thicknesses of both the outer and inner steel tubes, was analysed by varying the thickness between 2 to 4 mm, while keeping the diameter constant. As shown in Fig 4.1a, the load-bearing capacity of the columns significantly increased with an increase in the thickness of the outer steel tube. In particular, a 28% improvement in load-bearing capacity was observed when the thickness of the outer tube was increased from 2 to 4 mm. This enhancement can be attributed to the outer tube's increased ability to resist outward buckling, which directly contributed to the overall strength of the column. On the other hand, as depicted in Fig. 4.1b, a relatively modest increase of 7% in load-bearing capacity was observed when the thickness of the inner steel tube was increased. This suggests that the contribution of the inner tube to the overall strength is less significant compared to that of the outer tube.

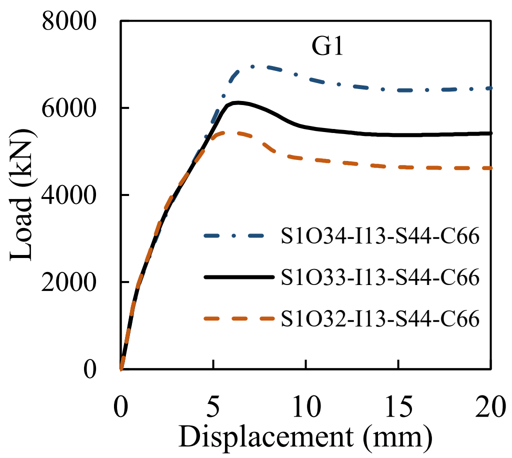


**(a)** Outer steel tube thickness

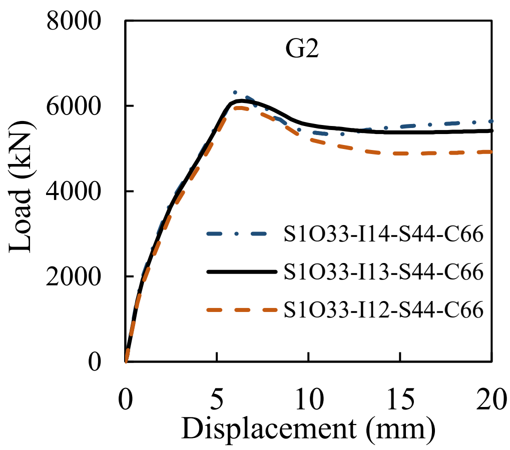


**(b)** Inner Steel tube thickness

**Fig 4.1** Effect of steel tube thickness

Unlike the increased thickness of outer steel tube, the thicker inner steel tube contributed much to the overall cross-sectional capacity of the column but had a relatively minimal effect on the confinement of the surrounding concrete. This implies that while the increased thickness of the inner tube enhanced strength, its influence on the confinement of the concrete is less pronounced compared to the outer tube, which is more crucial in preventing buckling and enhancing the column's stability.

### 4.3.2 Effect of Variation in Inner Steel Tube Diameter

The influence of diameter variations in the inner steel tube was investigated by selecting tube diameters ranging from 75 mm to 225 mm. These diameters were chosen based on the inner-to-outer diameter ratio ($D_i/D_o$)values of 0.25, 0.5, and 0.75, respectively. These ratios were chosen to evaluate their influence on the compressive behaviour particularly in terms of load distribution, structural stability, and the interaction with the surrounding concrete confinement. The effect of varying inner tube diameters on the column's overall response under compressive loads is illustrated in Fig 4.2.

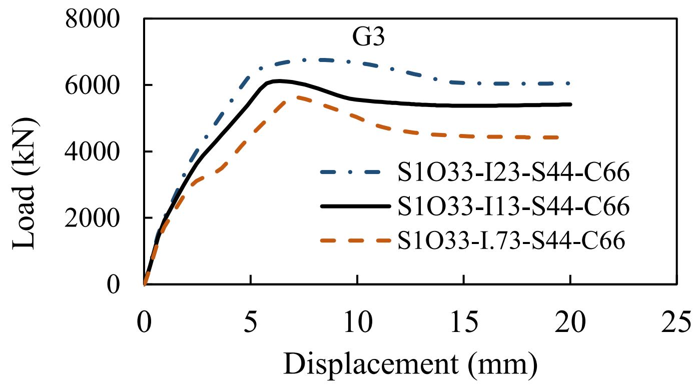


**Fig 4.2** Effect of diameter variation in inner steel tube

The results of the analysis revealed that the load-deformation behaviour was significantly influenced by the level of confinement provided by the different tube sizes. Columns with higher $D_i/D_o$ ratios, particularly those with a ratio of 0.75, demonstrated a 17% increase in peak strength, a 37% improvement in residual strength, and enhanced stability in the post-peak region (see Fig. 4.2). The increased ratio resulted in a larger inner steel tube, which reduced the area of the sandwich concrete but allowed better confinement from both the inner and outer steel tubes. Additionally, the higher $D_i/D_o$ ratio led to a greater steel area, contributing positively to the overall load-bearing capacity of the column. Conversely, as the $D_i/D_o$ ratio decreased from 0.75 to 0.25, a gradual reduction in initial stiffness was observed. This reduction was primarily attributed to the smaller inner steel tube, which offered less confinement and contributed to a decrease in the column's overall stiffness. These findings highlight the significant importance of the $D_i/D_o$ ratio that influence the initial stiffness and compressive performance of the columns. Note that the variation in the diameter of the outer steel tube was not considered, as the significant changes occur in the concrete and steel areas, which will obviously enhance the compressive performance. Also, as overall outer dimensions are not constant, a direct comparison is not meaningful.

### 4.3.3 Effect of Variation in Steel Tube Strength

Fig. 4.3a and 4.3b illustrate the influence of varying the yield strength of steel tubes on the load-displacement response of the stub columns. Specifically, the yield strength of the steel tubes was varied between 255 to 690 MPa. The results showed a noticeable difference in axial strength due to variation in yield strength the outer steel tubes (see Fig. 4.3a). For the outer steel tube, an increase in yield strength from 255 MPa to 690 MPa led to a significant enhancement in load-bearing capacity, with a 44% increase in strength. This improvement can be attributed to the outer tube's role in resisting outward buckling and providing greater structural stability under compressive loads.

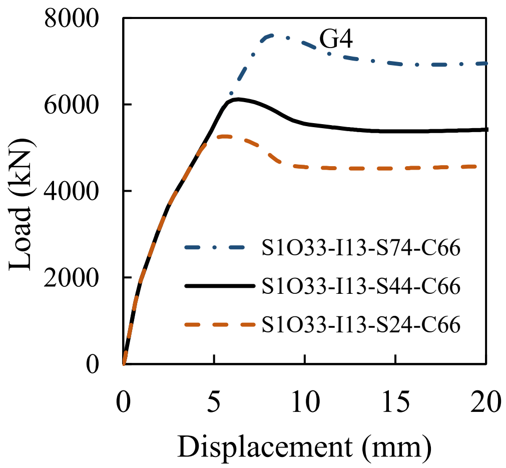


**(a)** Outer steel tube strength

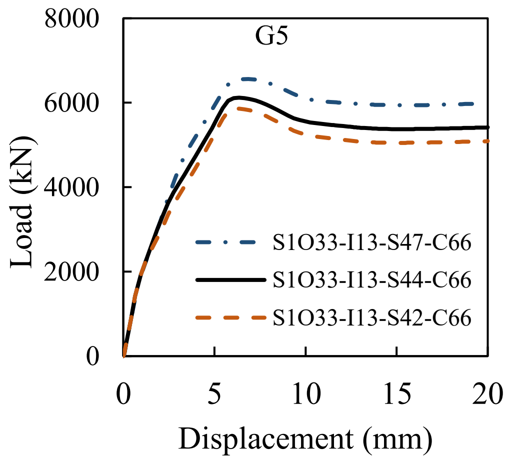


**(b)** Inner steel tube strength

**Fig 4.3** Effect of steel tube strength

In contrast, the increase in yield strength of the inner steel tube resulted in a more modest strength gain of only 12% as shown in Fig. 4.3b. This comparatively smaller increase can be explained by the fact that the inner tube's primary function is to carry axial loads, while its ability to confine the concrete core is more limited. Despite the higher yield strength, the inner tube did not significantly improve the confinement of the surrounding concrete, which is a key component in the overall load-bearing capacity. Additionally, only minor changes in the initial stiffness of the column were observed with variations in the strength of the inner tube.

These findings highlight the differing roles of the inner and outer tubes in determining the column's performance. While both tubes contribute to the overall strength and stiffness, the outer steel tube plays a more significant role in enhancing the load-bearing capacity, particularly when its yield strength is increased. This difference underscores the importance of the outer tube's strength in improving the column's ability to withstand compressive forces, while the inner tube's impact on the load-bearing capacity is relatively less pronounced.

### 4.3.4 Effect of Variation in Concrete Strength

The influence of concrete strength was examined, with concrete strength varied between 40 to 90 MPa. Three key observations can be made based on the results presented in Fig 4.4a and 4.4b. Firstly, the use of high-strength concrete in the sandwich layer (S1O33-I13-S44-C**9**6) resulted in a marked improvement of 31% in axial strength, compared to only 13% for the inner layer (S1O33-I13-S44-C6**9**). This improvement demonstrates the benefit of using high-strength concrete in the sandwich layer, leading to an increased load-bearing capacity.

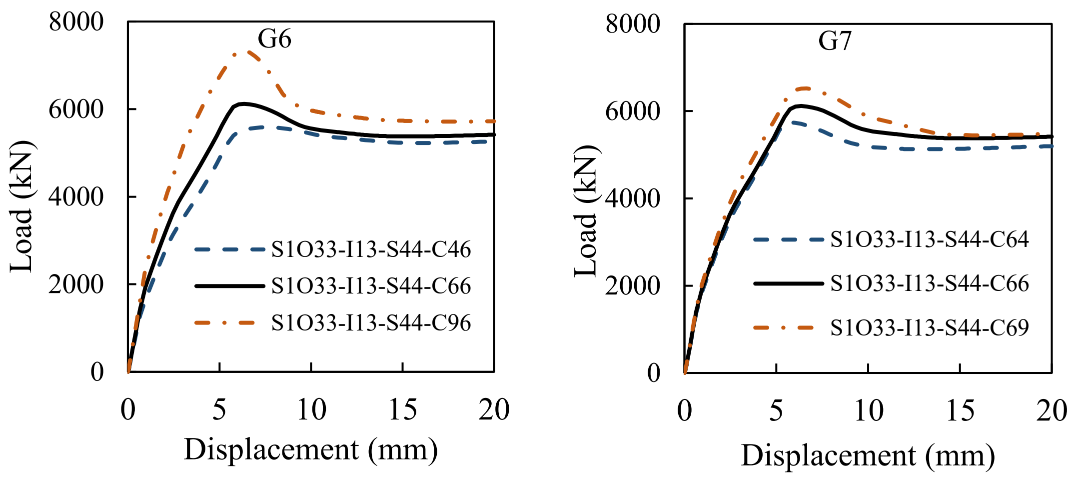


**(a)** Sandwich concrete

**(b)** Inner concrete

**Fig 4.4** Effect of variation in concrete strength

Secondly, while the residual strength remained relatively consistent across all cases (around 5700 kN to 5300 kN), a notable difference in post-peak behaviour was observed. In particular, when high-strength concrete was used in the sandwich layer (S1O33-I13-S44-C**9**6), there was a pronounced and steep drop of 28% in residual strength, while the inner concrete (S1O33-I13-S44-C6**9**) experienced only a 19% drop. This suggests that high-strength concrete in the sandwich layer is more prone to progressive damage leading to a more significant reduction in strength as the load is applied.

Finally, the initial stiffness of the columns was significantly affected by the strength of the sandwich concrete. This was particularly evident from the steeper slope in the load-displacement curve when high-strength concrete was used in the sandwich layer. The increased strength of the sandwich concrete contributed to a higher initial stiffness, highlighting its importance in the early stages of load application.

### 4.3.5 Overall Variation in Axial and Residual Strength of Stub Columns

A detailed comparison of the variations in axial strength and residual strength observed across the different groups (G1 to G7) in this phase is presented in Fig 4.5. The results clearly demonstrate that, out of 15 columns simulated, those incorporating high-strength materials in the outer steel tube and sandwich concrete exhibited the highest axial strengths. Specifically, the column with high-strength outer steel and concrete (i.e. S1O33-I13-S**7**4-C66) achieved a 24% increase in axial strength, while the column with high-strength concrete in the sandwich layer (S1O33-I13-S44-C**9**6) showed a 20% increase, both compared to the control column as marked in Fig 4.5.

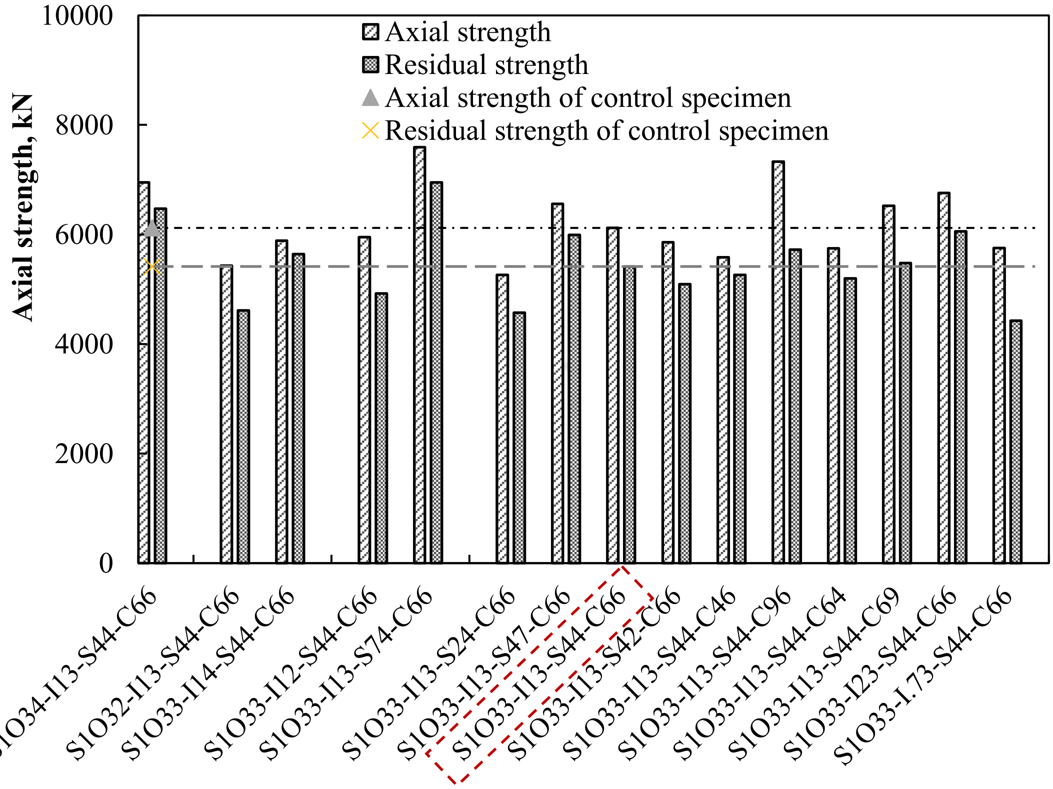


**Fig 4.5** Variation in axial strength and residual strength compared to control column for stub column

The behaviour observed was notably varied for each case in terms of residual strength. Despite the substantial increase in axial strength, the column with high-strength concrete in the sandwich layer (i.e. S1O33-I13-S44-C**9**6) exhibited only a modest improvement in residual strength, with a 6% increase over the control column. In contrast, the column with high-strength outer steel (i.e. S1O33-I13-S**7**4-C66) not only achieved a 28% increase in residual strength over the control column (5416 kN) but also exhibited a residual strength (6950 kN) that surpassed the control column's axial strength (6120 kN) by 13%. This highlights the exceptional performance of the high-strength outer tube in both axial strength and residual strength.

On the other hand, the column with normal-strength outer steel (S1O33-I13-S**2**4-C66) demonstrated a reduction of 14% in axial strength and a 15% decrease in residual strength compared to the control column. This indicates that, among the various parameters considered, the strength of the outer steel tube had the most significant impact on both axial strength and residual strength, showing the greatest variation in structural performance.

Additionally, the column with a smaller diameter inner tube (S1O33-I**.7**3-S44-C66) exhibited the lowest residual strength, with an 18% decrease compared to the control column. This emphasizes the critical role of the inner-to-outer diameter ratio ($D_i$/ $D_o$) in determining the column's damage tolerance and durability after initial failure, as a smaller diameter inner tube leads to reduced confinement and, consequently, lower residual strength.

## 4.4 Performance of Full-Scale Slender Columns

In this part of the analysis, the performance of full-scale slender columns was comprehensively evaluated to examine the influence of various parameters such as diameter and thickness of steel tubes, strength of concrete and steel as well as the effect of different slenderness ratios $\lambda$ on failure modes and overall compressive behaviour. The analysis was conducted in two distinct phases to provide a detailed understanding of the slenderness effects and the interplay of other influencing parameters.

In the Phase-I, columns from the G8 to G14 group were modelled with a fixed slenderness ratio of 48, which corresponds to a typical column height of 3000 mm commonly used in practical applications. The main objective of this phase was to analyze the influence of various geometric and material parameters on the compressive strength of these columns.

In the Phase-II, based on the insights gained in Phase I, columns from the G14 to G20 group were modelled with varying slenderness ratios, ranging from 16 to 96. In this phase, the geometry and material strength of the columns were kept constant, and the impact of different slenderness ratios on compressive performance was examined in detail.

### 4.4.1 Phase I: Effect with Fixed Slenderness Ratio

Fig. 4.6 presents the load-displacement response of the full-scale slender columns (G8 to G14). The overall elastic behaviour of these columns was similar to that observed in the stub columns as illustrated in Fig 4.1 to 4.4). However, variations in axial strength and post-peak behaviour were observed, which can be attributed to the differences in slenderness ratio ($\lambda$), as well as the geometric and material properties of the columns. Notably, columns with high-strength inner or outer steel tubes, or high-strength sandwich concrete, achieved the highest axial strengths. For instance, the column L3O23-I13-S33-C**9**6 (90 MPa-sandwich concrete) demonstrated a 49% increase in peak strength, as shown in Fig. 4.6e, while L3O23-I13-S**7**3-C66 (690 MPa-outer steel tube) exhibited a 33% increase, as depicted in Fig. 4.6d. These findings underscore the significant role of the outer steel tube and sandwich concrete strength in enhancing axial strength capacity. Although these results aligned with expected behaviour, a different trend was observed in the post-peak response. Notably, after reaching their axial strength, the columns exhibited distinct post-peak behaviour. For example, specimen L3O23-I13-S3**7**-C66 experienced a rapid and steep reduction in load capacity, dropping by 39% (from 3670 kN to 2230 kN). This highlights the susceptibility of high-strength steel to buckling under heavy loading scenarios. In contrast, column L3O23-I13-S33-C**9**6 showed an initial sudden drop in load-bearing capacity, followed by a more gradual decline of 51% (from 4000 kN to 1936 kN), which suggests that high-strength concrete tends to undergo sudden crushing failure after axial strength is reached. Upon closer inspection of Fig. 4.6, it is evident that most columns across all groups exhibited a general trend of decreasing residual strength, despite improvements in material properties and geometric configurations. However, column L3O23-I13-S73-C66 was an exception. This column demonstrated a relatively smaller reduction in load-bearing capacity—only a 17% decrease (from 3930 kN to 3251 kN)—which can be attributed to the use of a high-strength outer steel tube, as shown in Fig. 4.6d.

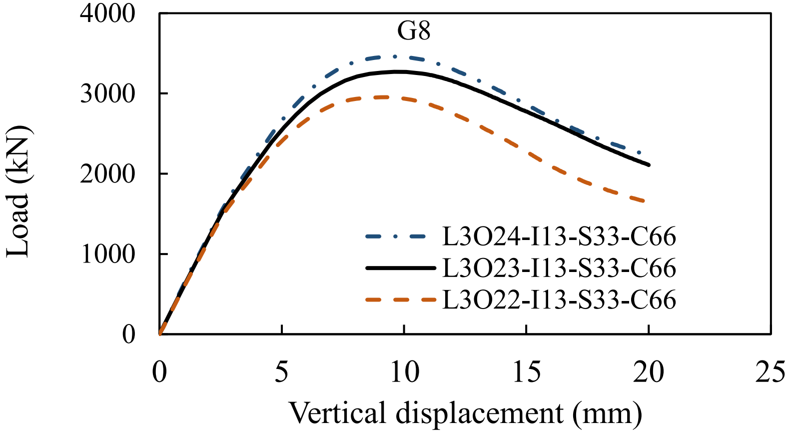


**(a)** Effect of outer steel tube thickness

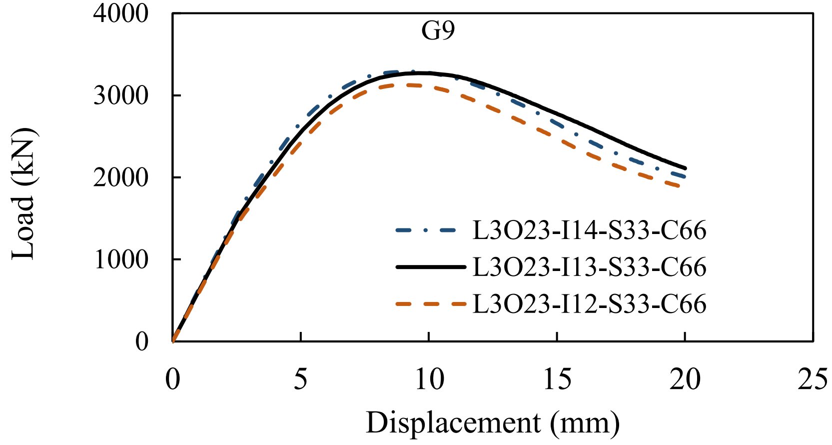


**(b)** Effect of inner steel tube thickness

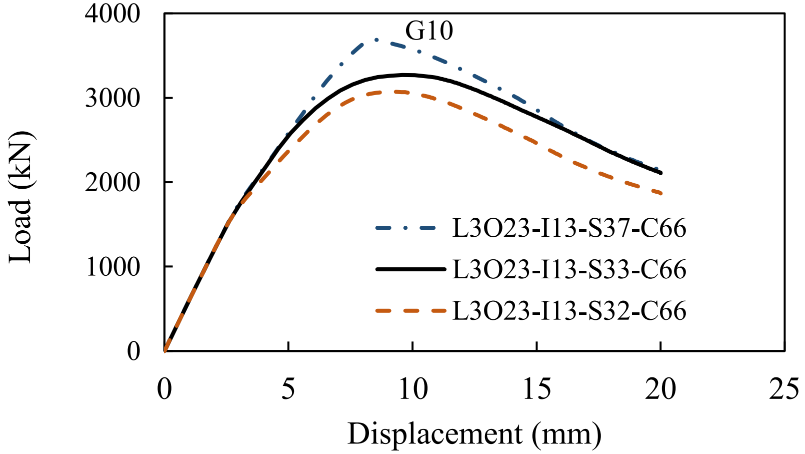


**(c)** Effect of inner steel tube strength

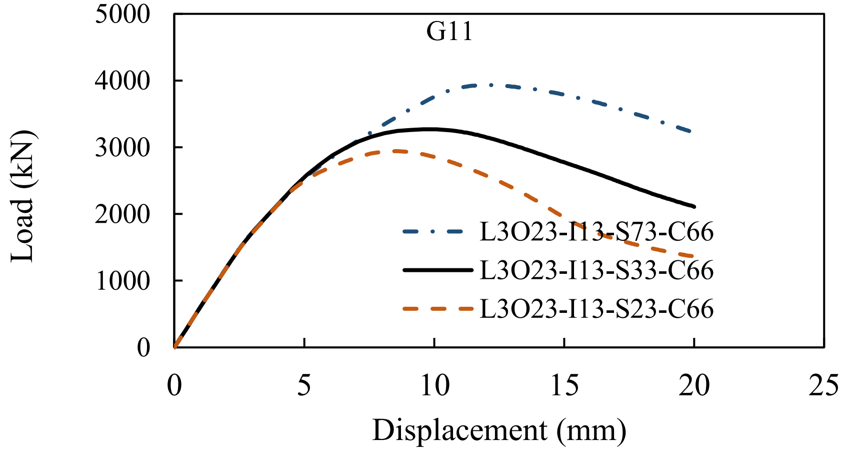


**(d)** Effect of outer steel tube strength

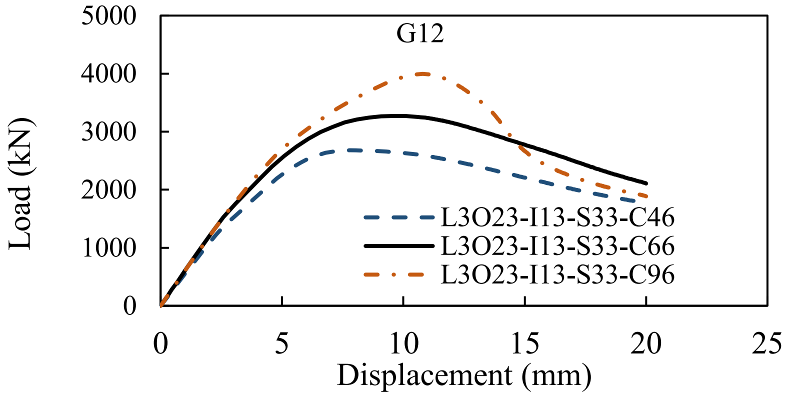


**(e)** Effect of sandwich concrete strength

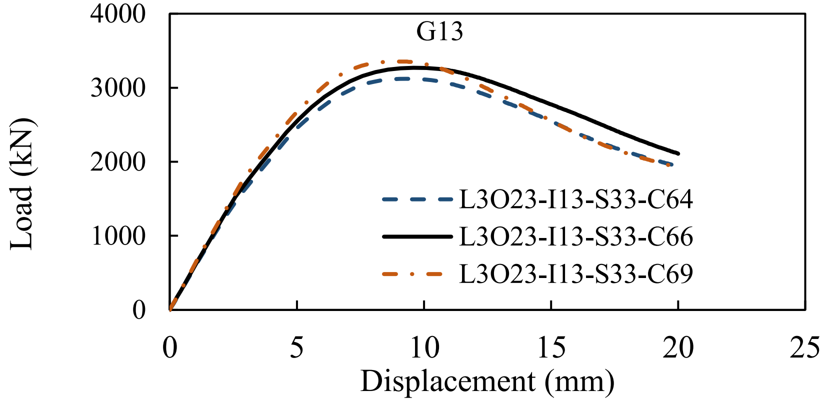


**(f)** Effect of inner concrete strength

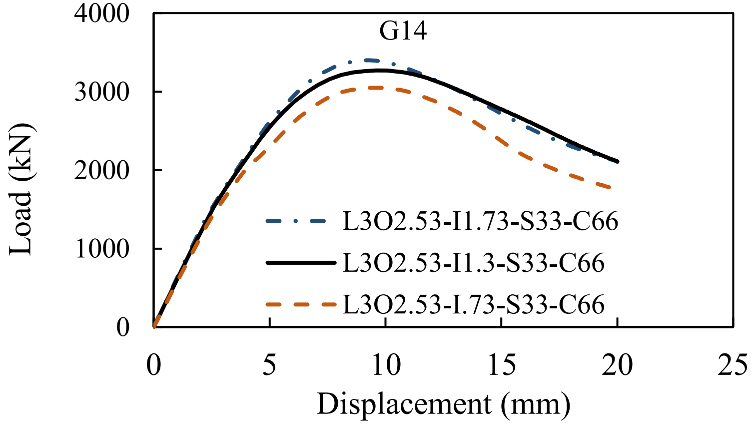


**(g)** Effect of diameter of inner steel tube

**Fig 4.6** Load vs displacement response of full-scale slender column (G8-G14)

### 4.4.2 Phase II: Effect of Varying Slenderness Ratio

Fig. 4.7 presents the correlation between the slenderness ratio and the relative axial load ratio ($P_{sl}/P_s$) of slender columns ($P_{sl}$) to stub columns ($P_s$), providing insights into how their load-bearing capacities change as slenderness increases. As anticipated, all groups exhibited a downward trend, indicating that the $P_{sl}/P_s$ ratio decreases with increasing slenderness. This decline is primarily attributed to the greater susceptibility to buckling in slender columns. However, slight discrepancies were observed between different groups, suggesting variations in their sensitivity to changes in slenderness.

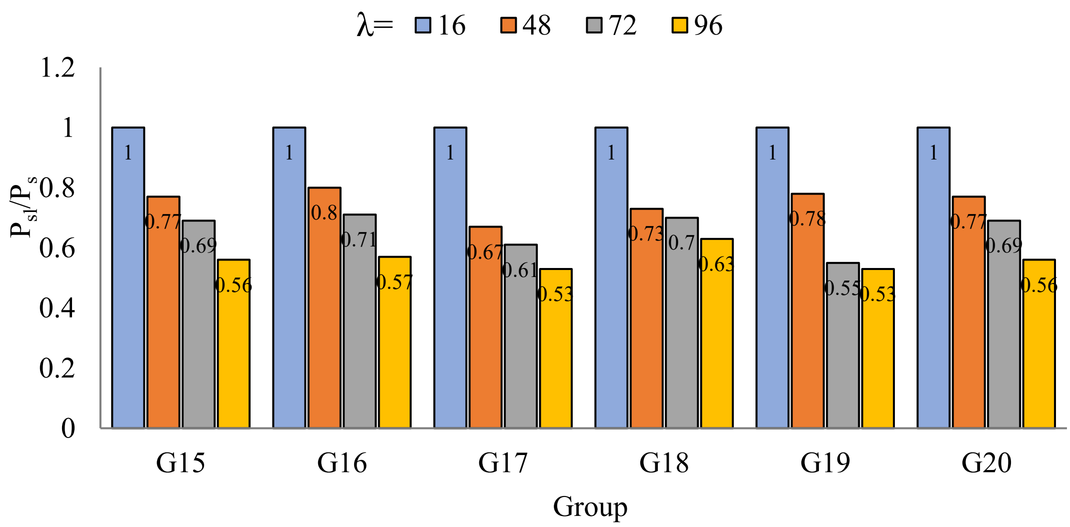


**Fig 4.7** Correlation between the relative axial strength ($P_{sl}/P_s$) and slenderness ratio

The G17 and G19 groups displayed the lowest ratios among all the columns, with a sharp drop that indicates these columns are particularly sensitive to increases in slenderness. This behaviour is likely due to less favourable geometric or material properties in these columns. In detail, G17 uses 690 MPa in both steel tubes, while G19 employs 90 MPa in both concrete. The results suggest that both high-strength steel and concrete may not perform optimally in columns with higher slenderness ratios, likely because of their inherent brittleness or lower capacity to resist buckling under increased slenderness.

In contrast, the G16 (210 MPa steel and 60 MPa concrete) and G18 (350 MPa steel and 40 MPa concrete) groups demonstrated that normal-strength steel and concrete can enhance the stability of columns with higher slenderness. These materials improve the column’s resistance to buckling, maintaining a relatively high axial load ratio even as slenderness increases. This combination of materials appears to counterbalance the potential instability associated with slender columns, offering a more effective design solution in such cases. These findings highlight the importance of selecting appropriate material strengths for columns with varying slenderness ratios to optimize both stability and load-bearing capacity.

### 4.5 Behaviour of Eccentrically Loaded Stub Columns

The compressive behaviour of eccentrically loaded DDSTCC stub columns was comprehensively analysed by considering a wide range of eccentricity ratios ranging from 0 to 0.45. These eccentricity ratios were carefully selected to ensure that the Load-Moment Interaction curve (P-M curve) exceeded the balanced failure conditions, allowing for a detailed evaluation of the column’s performance under combined axial and bending loads.

#### 4.5.1 Effect of Varying Eccentricity Ratio

This section investigates the compressive behaviour of the stub columns with varying $e/D_o$ ratios, as represented by the Load-Moment (P-M) interaction curve. The analysis focused on how the thickness of the steel tubes and the diameter of the inner steel tube influence the compressive performance of the columns. As shown in Fig. 4.8a, increasing the thickness of the outer steel tube (G22) results in higher load and moment capacities as compared to increasing the thickness of the inner steel tube (G23). This observation suggests that the outer steel tube plays a more significant role in enhancing the overall structural capacity under load.

The balanced failure zone, which is indicative of the region where the column maintains stable performance under combined axial load and moment, was found to be consistent across all groups. The $e/D_o$ ratio within the balanced failure zone was approximately 0.35 as maximum capacity of load and moment is achieved as shown in Fig 4.8. For instance, in G23, this corresponds to a load of 2172 kN and a moment of 228 kN-m. Fig. 4.8b illustrates the variations in the P-M curve for different inner steel tube diameters. A larger inner steel tube diameter (225 mm) demonstrated a higher axial strength and moment compared to smaller diameters. In particular, the P-M interaction for G25, at $e/D_o$ ratios of 0.35 and 0.45, remains within the balanced failure zone, indicating that the column can effectively resist buckling under eccentric loads. This behaviour suggests that higher $e/D_o$ ratios may lead to tensile failure, as the eccentricity increases and the column becomes more susceptible to lateral instability.

These findings imply that using a larger diameter for the inner steel tube improves the column's ability to resist eccentric loading, thereby enhancing its overall compressive performance and stability.

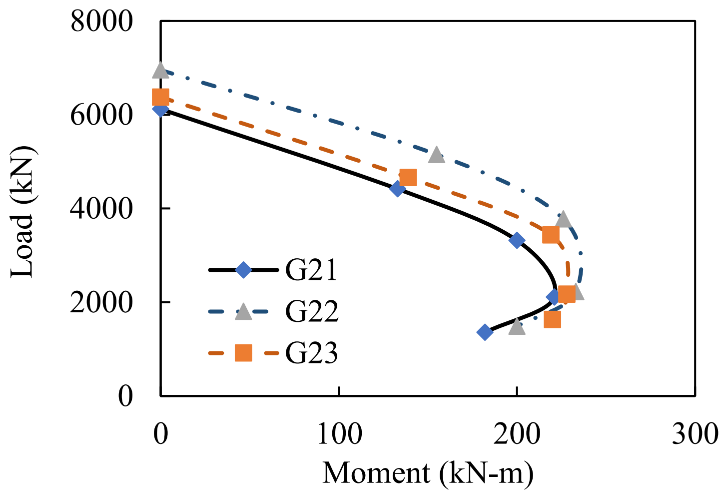


**(a)** Effect of steel tube thickness

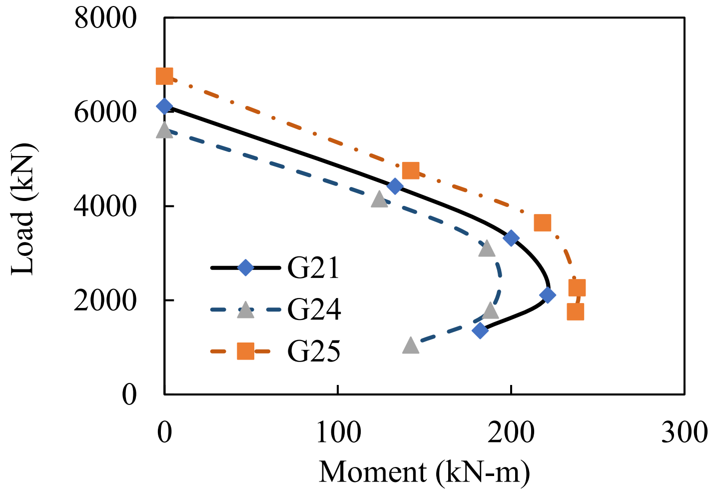


**(b)** Effect of steel tube diameter

**Fig 4.8** P-M interaction curve for eccentrically loaded column

### 4.5.2 Influence of Eccentricity Ratio on Relative Axial Strength

Fig. 4.9 illustrates the ratio of peak load with eccentricity ($P_e$) to axial strength with zero eccentricity ($P_o$), plotted against different $e/D_o$ ratios. Fig. 4.9a and 4.9b show a gradual decrease in the relative axial strength ($P_e/P_o$) ratio as the eccentricity ratio $e/D_o$ increases (0 to 0.45).

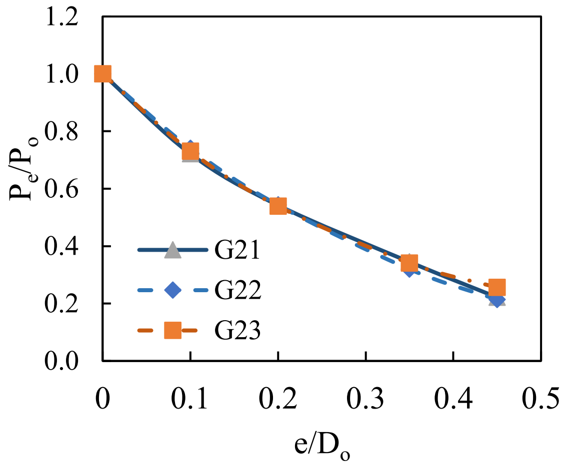


**(a)** Effect of steel tube thickness

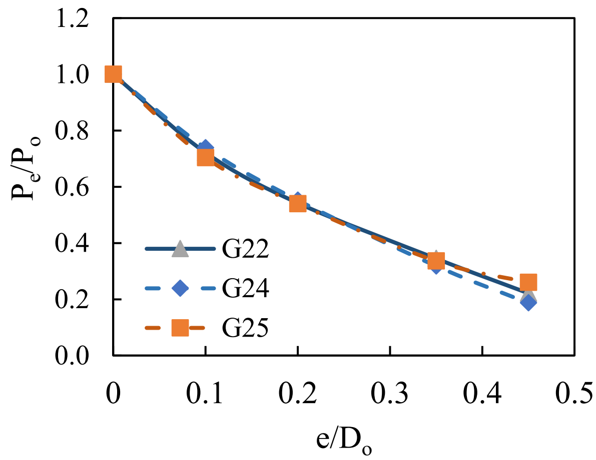


**(b)** Effect of steel tube diameter

**Fig 4.9** Correlation between the relative axial strength ($P_e/P_o$) and eccentricity ratio ($e/D_o$)

As seen in Fig 4.9a, the decline in the relative axial strength is nearly identical for each group (G21, G22, G23) up to an $e/D_o$ ratio of 0.2, where the relative axial strength decreases from 1 to 0.54. Beyond an $e/D_o$ ratio of 0.2, the relative axial strength continues to decrease for all groups (G21, G22, G23), but the rate of decrease begins to diverge slightly. Group G22 (outer steel tube thickness of 4 mm) closely followed G21, with a difference of less than 0.01 throughout the entire range. However, G23 (inner steel tube thickness of 4 mm) performed about 13% (0.25) better than G21

(0.22) at higher eccentricity ratios of 0.45, indicating a better performance in resisting eccentric loading.

In Fig. 4.9b, the relative axial strength for all groups (G21, G24, G25) follows a decreasing trend as the eccentricity ratio increases. At an $e/D_o$ ratio of 0.1, G25 (with an inner steel tube diameter of 75 mm) shows a slight drop in performance compared to G21 and G24, while G24 (with an inner steel tube diameter of 225 mm) maintains a marginally higher relative axial strength than G22. When the $e/D_o$ ratio reaches 0.2, all groups converge to nearly the same relative axial strength value, indicating very similar performance across all configurations. However, when the $e/D_o$ ratio reaches to 0.45, G25 showed a relative load of 0.26, which is approximately 18% higher than G21's value of 0.22, while G24's performance at the same eccentricity ratio is lower by the same percentage.

Thus, the relative load ratios for all groups were nearly identical at an $e/D_o$ ratio of 0.2. However, with a thicker and larger diameter inner steel tube, the relative load increased by approximately 13% to 18% compared to the control column group (G21).

For eccentrically loaded columns, the use of a thicker inner steel tube and a larger diameter proves to be particularly beneficial. These modifications enhance the column's stability and stiffness, which are crucial for handling the additional stresses that arise from eccentric loading. As the eccentricity increases, the difference in performance becomes more pronounced, demonstrating the effectiveness of these design improvements. However, it is important to note that the material parameters must also be thoroughly evaluated to ensure the structural integrity of the column.

### 4.6 Failure Behaviour of DDSTCC Columns

Distinct failure behaviours were observed for stub columns, full-scale slender columns, and eccentrically-loaded columns due to variations in the parameters, slenderness and eccentricity ratios. These differences in failure modes are attributed to the varying geometrical and loading characteristics of the columns, which significantly influence their compressive response under loading. The subsequent subsections will discuss these failure behaviours in detail.

#### 4.6.1 Failure Behaviour of Stub Columns

The failure behaviour of the stub column closely resembled the results observed in the tests as shown in Fig 3.10 and Fig 4.10. However, in addition to the failure patterns, the stress concentration and the damage to the concrete were also thoroughly evaluated. High stress concentrations were observed in both the inner and outer steel tubes. The stress distribution within the outer steel tube was more widely dispersed compared to the inner concrete core, suggesting a differential response between the two tubes. In addition, the damage index for the sandwich concrete revealed that it was approximately 19% more vulnerable to compression damage than the inner concrete (Fig 4.10d and Fig 4.10e). This increased susceptibility of the sandwich concrete to compression damage can be attributed to its positioning and the differential stress distribution within the system.

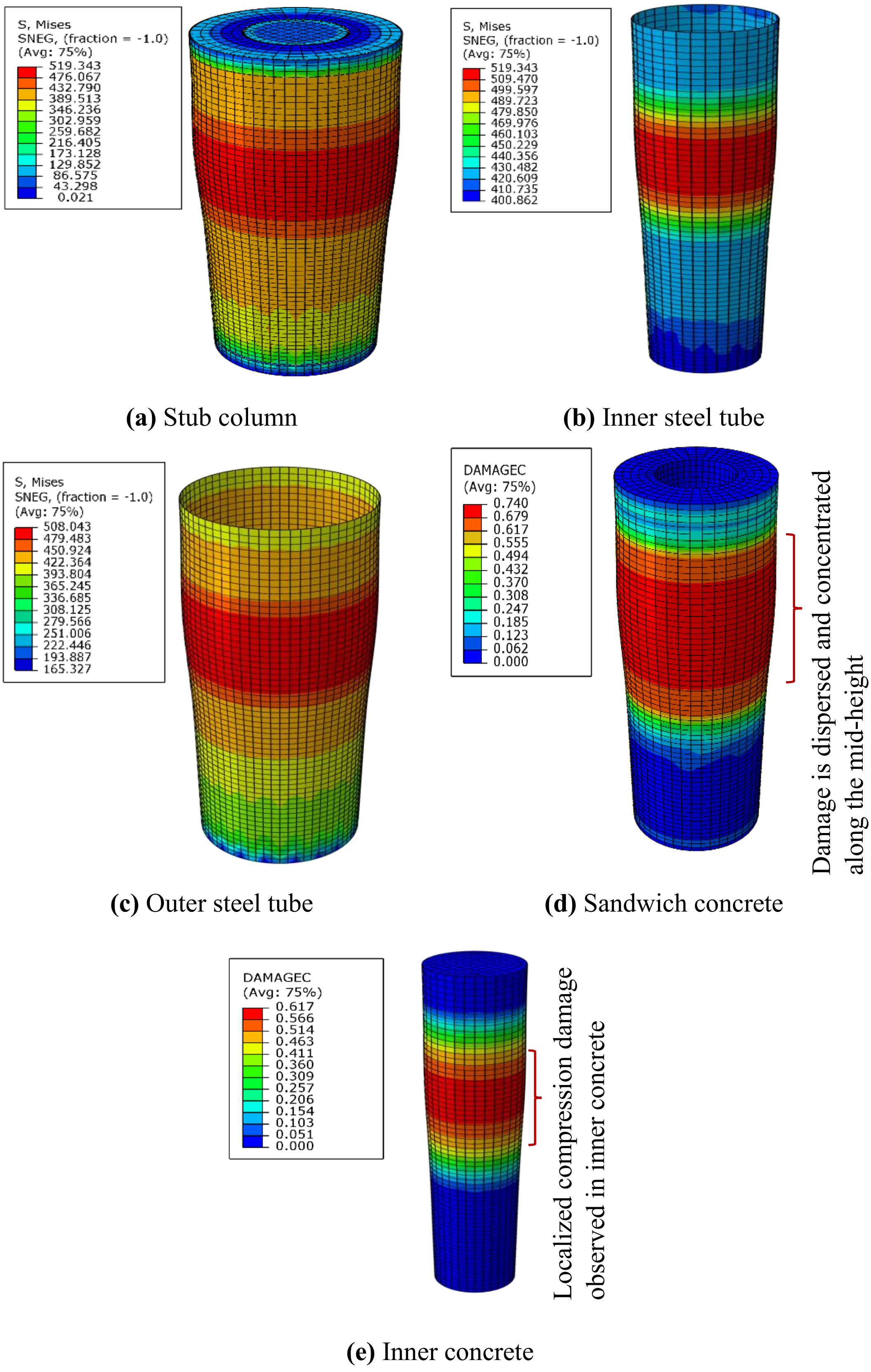


**(a)** Stub column

**(b)** Inner steel tube

**(c)** Outer steel tube

**(d)** Sandwich concrete

**(e)** Inner concrete

**Fig 4.10** Typical failure behaviour of stub columns

### 4.6.2 Failure Behaviour of Full-Scale Slender Columns

In the case of the full-scale column as depicted in Fig. 4.11, the failure behaviour was notably different from those obtained for the stub column. Here, global buckling followed a C-shaped pattern, which was more pronounced due to the scale of the column and the interaction between the materials. The inner steel tube exhibited a more significant buckling response, with substantial mid-height deflection, compared to the outer tube. This observation suggests that the inner steel tube played a more critical role in resisting axial loads and consequently experienced greater deformation as shown in Fig 4.11b. In contrast, the buckling of the outer steel tube was less pronounced and was primarily influenced by the behaviour of the surrounding concrete and the inner steel tube. The outer steel tube, not being directly subjected to axial loads, showed less localized deformation. In terms of concrete damage, both the inner and sandwich concrete exhibited localized compression damage at the mid-height region, close to the area where buckling occurred (refer to Fig. 4.11d and Fig 4.11e).

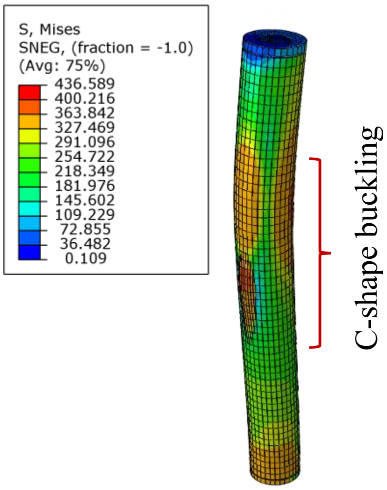


**(a)** Full scale slender column

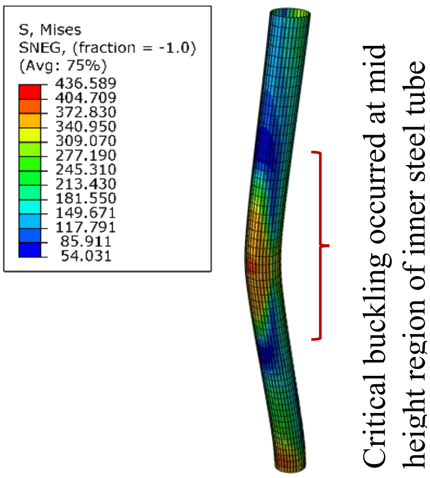


**(b)** Inner steel tube

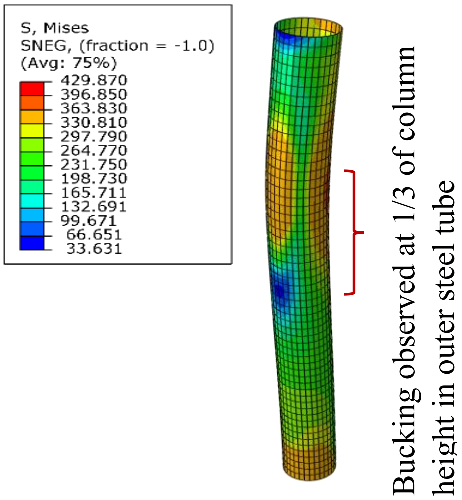


**(c)** Outer steel tube

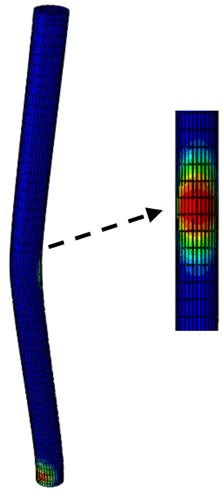

**(d)** Inner concrete

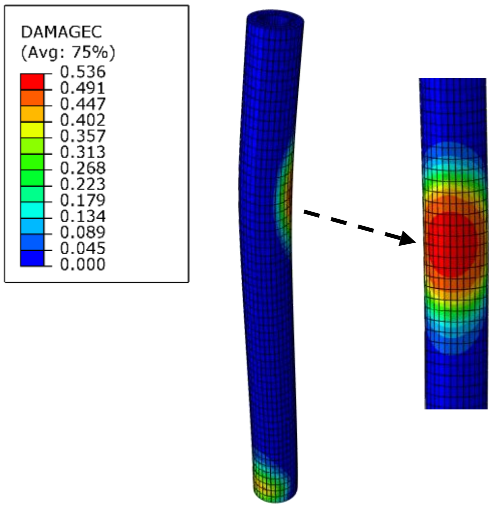


**(e)** Sandwich concrete

**Fig 4.11** Typical failure behaviour of full-scale slender columns

Similar to the stub column, the damage contour analysis revealed that the sandwich concrete sustained roughly 19% more damage than the inner concrete, highlighting the consistent vulnerability of the sandwich layer across different column types.

### 4.6.3 Failure Behaviour of Eccentrically Loaded Columns

The failure behaviour of the eccentrically loaded column as illustrated in Fig. 4.12 was notably different from that observed in the stub and full-scale columns, displaying a more complex failure pattern. The stress distribution in this case was concentrated along the eccentricity axis, with particular intensification near the gap between the outer steel tube and the column capital. In this localized region, concrete compression damage was particularly evident. As the eccentricity increased, the gap between the outer steel tube and the column capital reduced, and in some cases, the gap overlapped, further affecting the stress distribution as depicted in Fig 4.12a. On the opposite side of the eccentricity axis, a separation between the outer steel tube and the concrete was observed, resulting in a differential distribution of stress and damage. For high eccentricity ratios, the top portion of the inner steel tube experienced local deformation, leading to significant distortion in the material (see Fig 4.12b). The sandwich concrete in this case showed an unprecedented level of damage compared to the inner concrete. This disparity in damage is likely due to the higher eccentricity ratio of the applied load, which causes a more pronounced bending effect on the sandwich concrete, making it more prone to failure.

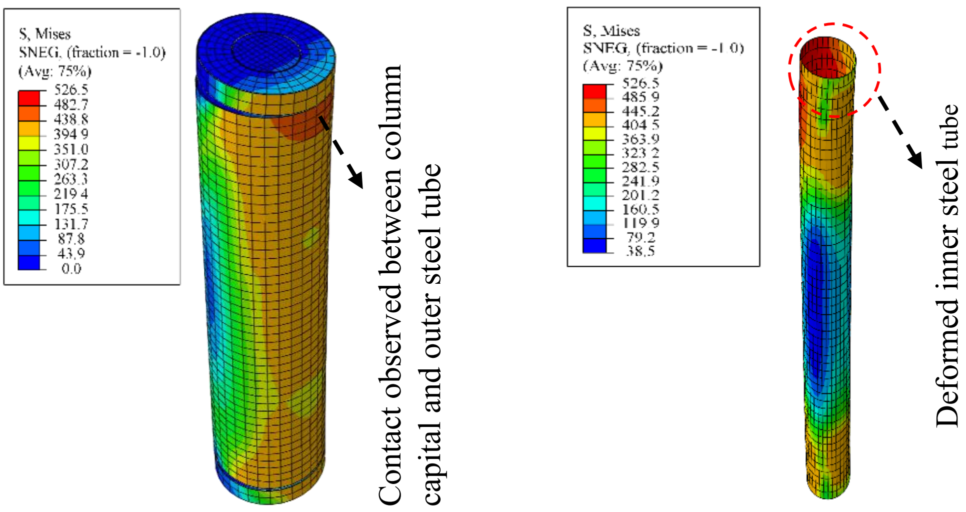


**(a)** Eccentrically loaded column

**(b)** Inner steel tube

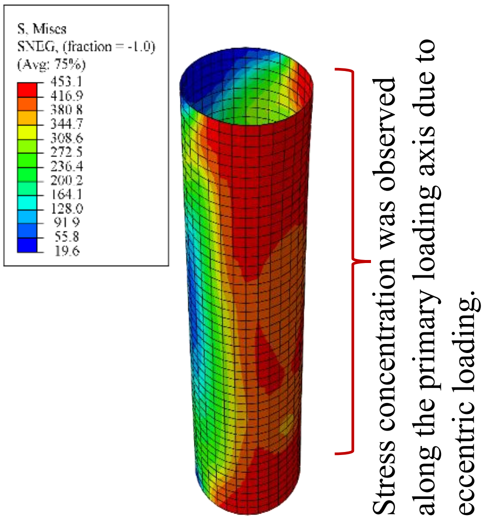


**(c)** Outer steel tube

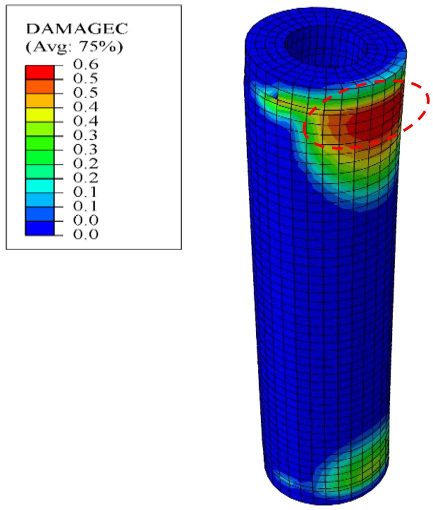


**(d)** Sandwich concrete

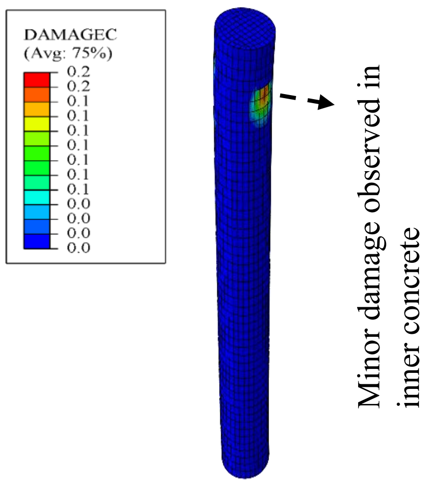


**(e)** Inner concrete

**Fig 4.12** Typical failure behaviour of eccentrically loaded columns

## 4.7 Summary

In summary, this chapter emphasizes the importance of key variables, including the outer steel strength, thickness, and the strength of the sandwich concrete. Several important conclusions can be drawn from the study. The use of high-strength outer steel tubes resulted in a significant strength increase of up to 44% in the stub column. This compressive behaviour was also consistent in full-scale slender columns;

however, in terms of relative strength, columns with normal-strength steel and concrete performed better. For eccentrically loaded columns, the use of a larger diameter inner steel tube helped to maintain stability and reduces the progression of failure. Typical failure patterns were also observed: while the stub column exhibited dispersed failure, both the full-scale and eccentrically loaded columns displayed localized failure. Notably, the eccentrically loaded column highlighted a vulnerable region near the column capital gap, where failure was most pronounced. The axial strength resulted from this chapter will be used in chapter 5 for analytical formulation.

# CHAPTER 5: ANALYTICAL FORMULATION^

## 5.1 Introduction

This chapter focuses on developing an analytical formulation based on the findings from chapter 4, with an emphasis on proposing modifications to existing design standards. Recently, the Bangladesh National Building Code (BNBC 2020) included design guidelines for CFST columns, based on the ANSI/AISC-360-05 (2005) specifications. However, despite this significant step forward, the implementation of CFST columns in Bangladesh's construction industry is still at an early stage, with considerable delays in adoption. This chapter introduces an analytical framework for the DDSTCC column to evaluate axial strength using current standards and propose a modified design formula suited to requirements. By doing so, this chapter sets a benchmark for future research and contributes to the advancement of structural design practices of DDSTCC column in Bangladesh as well as in whole world.

---

^The findings discussed in this chapter have been disseminated through the following publication:

1. Sakib, A. N., & Kabir, Md. I. (2025). Behaviour and design of discontinuous double steel tube confined concrete columns for concentric and eccentric loading. *Structures*, *79*, 109511. https://doi.org/10.1016/j.istruc.2025.109511

## 5.2 Overview of Available Design Standards

Currently, no analytical approach is available for predicting the axial strength of DDSTCC columns. These columns, with their innovative configuration comprising inner and outer steel tubes encasing concrete-filled cores, represent a significant advancement over traditional composite column systems. Although extensive research has been conducted on CFST columns and well-documented design guidelines and analytical formulations are available in standards such as EC4 (1994), AISC (2016), ACI 318 (2014), Chinese Code GB 50936-2014 (2014), local specification DBJ/T 13-51-2010 (2010) and AS 2327 (2017). These formulations can be adapted to DDSTCC columns with certain modifications.

**Key considerations in existing standards for CFST columns**

i. ***EC4 (1994)***: provides a comprehensive framework for the design of CFST columns, incorporating partial interaction theory, confinement effects of concrete by steel tubes and buckling considerations for both axial load and bending moment.
ii. ***AS 2327 (2017)***: is similar to EC4 in several aspects; however, it distinctively accounts for local buckling effects through the application of a form factor $k_f$.
iii. ***Chinese Codes***: include advanced confinement models to predict the behaviour of CFST columns under high axial emphasizing material ductility and localized failure mechanisms.
iv. ***ACI 318 (2014)***: does not consider the composite interaction between steel and concrete, relying solely on the independent plastic contributions of each material to determine strength.

In this study, the axial strength of stub and full-scale DDSTCC columns were calculated using EC4 (1994) and Chinese standards GB 50936–2014 (2014) and DBJ/T 13-51-2010 (2010). The calculated values were then compared with FE simulated results to evaluate the applicability of these codes for DDSTCC columns. Based on the findings, a modified analytical design formula was proposed, emphasizing the confinement ratio to achieve more accurate predictions aligned with the FE results.

### 5.2.1 EC4 (1994) provisions

The axial strength of a DDSTCC column with a circular section is evaluated by considering the confinement effect provided by the concrete. However, this confinement effect is only considered when certain conditions are met, specifically when the relative slenderness $\bar{\lambda}$ is less than equal to 0.5 ($\bar{\lambda} \leq 0.5$) and the eccentricity ratio $\frac{e}{D_o}$ is less than equal to 0.1 $\left(\frac{e}{D_o} \leq 0.1\right)$. For DDSTCC columns, the confinement effect is only applicable in the case of circular sections. In these circular sections, the concrete core is confined by the outer steel tubes, enhancing its strength. This confinement contributes significantly to the axial load-carrying capacity of the column. However, if the conditions for slenderness and eccentricity are not satisfied, then the confinement effect is no longer relevant and the column's behaviour will be dominated by the classic squash load formula, where the axial strength is governed primarily by the material properties of the concrete and steel, rather than the confinement effect as shown in Eq. 5.1

$$P_{EC4} = \begin{cases} A_{cs}f'_{cs}\left(1+\eta_c \frac{t_o}{D_o}\frac{f_{yo}}{f'_{cs}}\right) + A_{si}f_{yi}\eta_s + A_{ci}f'_{ci}\left(1+\eta_c \frac{t_i}{D_i}\frac{f_{yi}}{f'_{ci}}\right) & \bar{\lambda} \leq 0.5 \\ A_{cs}f'_{cs} + A_{si}f_{yi} + A_{ci}f'_{ci} & \bar{\lambda} \geq 0.5 \end{cases} \quad (5.1)$$

here, $A_{cs}$ and $A_{ci}$ represent the area of sandwich and inner concrete while $f'_{cs}$ and $f'_{ci}$ denotes corresponding concrete strength. Yield strength of outer and inner steel tube are represented through $f_{yo}$ and $f_{yi}$ respectively. Composite action is taken into account by two factors, $\eta_s$ for steel and $\eta_c$ for concrete as follows

$$\eta_s = 0.25(3+2\bar{\lambda}) \leq 1 \quad (5.2)$$

$$\eta_c = 4.9 - 18.5\bar{\lambda} + 17\bar{\lambda}^2 \geq 0 \quad (5.3)$$

The steel's strength reduces with increasing slenderness, while the concrete's strength increases due to confinement when slenderness permits. The global buckling effect is taken into account using a slenderness reduction factor $\chi$, as follows:

$$P_{EC4}^{sl} = \chi P_{EC4} \quad (5.4)$$

$$\chi = \frac{1}{\phi + \sqrt{\phi^2 - \bar{\lambda}^2}} \leq 1 \quad (5.5)$$

$$\phi = 0.5\left[1 + 0.21(\bar{\lambda} - 0.2) + \bar{\lambda}^2\right] \quad (5.6)$$

### 5.2.2 Chinese Code GB 50936–2014 (2014) and Local Specification DBJ/T 13-51-2010 (2010)

Both the Chinese Code GB 50936–2014 (2014), and the local specification DBJ/T 13-51-2010 (2010), provides comprehensive guidelines for the design and analysis of CFST columns, integrating both the axial and lateral load capacities of the columns.

These codes adopt a unified theoretical approach for modelling CFST columns, with particular attention to the interaction between the concrete core and the surrounding steel tube. The design of CFST columns is primarily based on the concept of confinement, where the steel tube provides lateral restraint to the concrete, enhancing its strength and overall stability under compressive loads. The confinement effect is typically represented by the confinement factor $\xi$, which depends on the tube's geometry and incorporates complex factors B and C to determine the confined concrete strength in the steel tube as presented in Eq. 5.7.

$$P_{GB} = P_{GB}^{s} + P_{GB}^{i} = [(A_{cs})f_{sc}] + [(A_{si} + A_{ci})f_{sc}] \qquad (5.7)$$

where $f_{sc} = (1.212 + B\xi + C\xi^2)f_c'$ and the coefficient of $B, C$ and $\xi$ can be calculated using the following equations:

$$B = \frac{0.176 f_y}{213} + 0.974$$

$$C = \frac{-0.104 f_y}{14.4} + 0.031$$

$$\xi = \begin{cases} \dfrac{A_{so} f_{yo}}{A_{cs} f_{cs}'} & for\ sandwich\ section \\ \dfrac{A_{si} f_{yi}}{A_{ci} f_{ci}'} & for\ inner\ section \end{cases}$$

Here, $P_{GB}^{s}$ and $P_{GB}^{i}$ are the ultimate resistance on axial compression by sandwich and inner section respectively. The value of $f_{sc}$ was determined using the corresponding confinement ($\xi$) provided by the steel tube and the concrete strength.

The local specification DBJ/T 13-51-2010 (2010) further refines these calculations. This specification simplifies the calculation process for CFST columns by primarily focusing on the confinement effect for determining the confined concrete strength. Unlike the Chinese Code GB 50936–2014 (2014), which uses more complex factors

B and C to account for the detailed interaction between the steel tube and concrete, DBJ/T 13-51-2010 (2010) provides a more straightforward approach as follows:

$$f_{sc} = (1.14 + 1.02\xi)f_c' \tag{5.8}$$

The global buckling effects are considered in the design of columns as per the provisions outlined in the EC4.

$$P_C^{sl} = \chi P_C \tag{5.9}$$

$$\chi = \frac{1}{\phi + \sqrt{\phi^2 - \bar{\lambda}^2}} \leq 1 \tag{5.10}$$

$$\phi = 0.5\left[1 + 0.21(\bar{\lambda} - 0.2) + \bar{\lambda}^2\right] \tag{5.11}$$

### 5.2.3 Modified Analytical Formula

The calculation method for CFST columns, as outlined in different guidelines, has been discussed briefly in previous sections. In EC4, confinement is considered with respect to the global slenderness of the CFST column, focusing on the overall stability and buckling behaviour of the column. However, in the Chinese codes, the confinement effect from the outer and inner steel tubes is assumed to be equal. This assumption does not fully account for the disparity in confinement between the two tubes. Specifically, for DDSTCC columns with a discontinuous outer steel tube, the confinement effect is significantly greater for the outer steel tube than for the inner steel tube, due to the larger interaction between the concrete core and the outer tube. Additionally, the confinement provided by the inner steel tube is reduced under axial load, as the axial forces acting on the tube reduces its ability to confine the concrete.

To address these discrepancies, a modified analytical formula has been proposed, based on regression analysis, which considers the unequal confinement effects between the inner and outer steel tubes. This new formula provides a more accurate prediction of the confined concrete strength and enhances the overall design prediction of DDSTCC columns under axial loads. The procedure for the analytical formulation is depicted in the flowchart shown in Fig. 5.1.

The newly modified analytical formula for predicting the axial strength ($P_{MAN}$) as follows:

$$P_{MAN} = P_{MAN}^{s} + P_{MAN}^{i} = [(1 + 2.38\xi_s)A_{cs}f'_{cs}] + [(1 + 0.65\xi_i)A_{ci}f'_{ci}] \quad (5.12)$$

Here, $P_{MAN}^{s}$ and $P_{MAN}^{i}$ are the ultimate resistance on axial compression by sandwich and inner section respectively. The confinement ratio for the sandwich section is expressed as $\xi_s = (A_{so}f_{yo}/A_{cs}f'_{cs})$ and the confinement ratio for the inner section is given by $\xi_i = (A_{si}f_{yi}/A_{ci}f'_{ci})$. For global buckling failure, the reduction factor provided by EC4 (1994) is slightly modified based on regression analysis as follows:

$$\phi = 0.5\left[1.07 + 0.21\left(\bar{\lambda} - 0.2\right) + \bar{\lambda}^2\right] \quad (5.13)$$

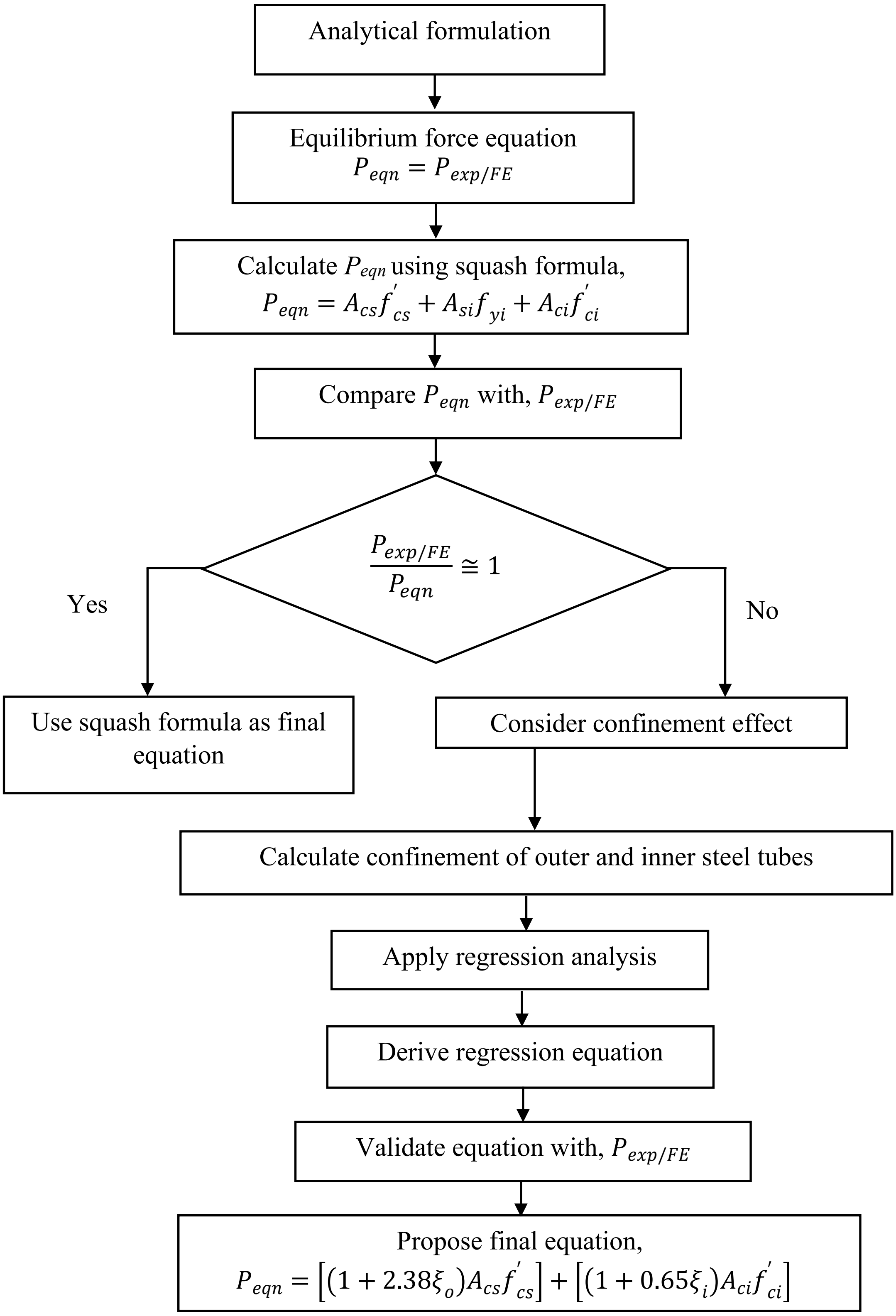


Fig 5.1 Procedure to obtained analytical formulation

## 5.3 Comparison of Axial Strength Prediction

The comparison of axial strength predictions for stub and full-scale slender columns, according to various design standards are presented in **Tables 5.1, 5.2, and 5.3**. These standards include the EC4 (1994), the Chinese standard GB 50936–2014 (2014), the local specification DBJ/T 13-51-2010 (2010) and a modified analytical formulation. Additionally, the comparison between different calculation methods is illustrated in Fig. 5.2 and 5.3.

### 5.3.1 Stub Columns

For stub columns, the predictions from both Chinese standards—GB 50936–2014 and DBJ/T 13-51-2010—were relatively close to the results from FE analysis. The mean prediction ratios for these standards are 0.99 and 1.03 (refer to Table 5.1) respectively, indicating that GB 50936–2014 slightly overestimated the axial strength, while DBJ/T 13-51-2010 slightly underestimated it. However, both standards provided fairly accurate predictions overall. In contrast, the EC4 standard consistently underestimated axial strength, as evidenced by a mean ratio of 1.15 as shown in Table 5.1, which suggested that its predictions were more conservative. The modified analytical formulation aligns closely with the FE results, with a mean ratio of 1.02, slightly underestimating the strength but still showing good agreement with the FE analysis as depicted in Fig 5.2.

**Table 5.1** Comparison of axial load from various standards, modified analytical formula, test data and FE analysis for stub columns

| Dataset type | Column designation | $P_{GB}$ (kN) | $\frac{P_{FE}}{P_{GB}}$ | $P_{DBJT}$ (kN) | $\frac{P_{FE}}{P_{DBJT}}$ | $P_{EC4}$ (kN) | $\frac{P_{FE}}{P_{EC4}}$ | $P_{MAN}$ (kN) | $\frac{P_{FE}}{P_{MAN}}$ |
|---|---|---|---|---|---|---|---|---|---|
| Experimental dataset | ST3-D80-4 | 2805 | 0.99 | 2796 | 1.00 | 2458 | 1.13 | 2764 | 1.01 |
| | ST3-D106-3 | 2921 | 0.96 | 2897 | 0.97 | 2571 | 1.09 | 2814 | 1.00 |
| | ST3-D158-2 | 3119 | 0.92 | 3119 | 0.92 | 2767 | 1.03 | 2923 | 0.98 |
| | ST3-D106-4 | 2895 | 1.03 | 2875 | 1.03 | 2598 | 1.14 | 2797 | 1.06 |
| | ST3-D106-5 | 2866 | 1.08 | 2850 | 1.08 | 2616 | 1.18 | 2778 | 1.11 |
| | ST4-D106-3 | 2915 | 1.05 | 2891 | 1.06 | 2564 | 1.20 | 2801 | 1.10 |
| | ST5-D106-3 | 3052 | 1.16 | 3101 | 1.14 | 2810 | 1.26 | 3375 | 1.05 |
| FE dataset | S1O34-I13-S44-C66 | 6574 | 1.06 | 6334 | 1.10 | 5685 | 1.22 | 6928 | 1.00 |
| | S1O33-I13-S44-C66 | 6263 | 0.98 | 5993 | 1.02 | 5332 | 1.15 | 6115 | 1.00 |
| | S1O32-I13-S44-C66 | 5905 | 0.92 | 5649 | 0.96 | 4984 | 1.09 | 5297 | 1.03 |
| | S1O33-I14-S44-C66 | 6231 | 1.02 | 5969 | 1.07 | 5425 | 1.18 | 6097 | 1.05 |
| | S1O33-I12-S44-C66 | 6294 | 0.95 | 6016 | 0.99 | 5234 | 1.14 | 6135 | 0.97 |
| | S1O33-I13-S74-C66 | 7384 | 1.08 | 6764 | 1.18 | 6044 | 1.32 | 7759 | 1.02 |
| | S1O33-I13-S24-C66 | 5670 | 0.93 | 5522 | 0.95 | 4897 | 1.07 | 5104 | 1.03 |
| | S1O33-I13-S47-C66 | 6851 | 0.96 | 6555 | 1.00 | 5901 | 1.11 | 6411 | 1.02 |
| | S1O33-I13-S42-C66 | 5915 | 0.99 | 5649 | 1.04 | 4979 | 1.18 | 5935 | 0.99 |

| | | | | | | | | |
|---|---|---|---|---|---|---|---|---|
| S1O33-I13-S44-C46 | 5529 | 1.01 | 5273 | 1.06 | 4783 | 1.17 | 5550 | 1.01 |
| S1O33-I13-S44-C96 | 7736 | 0.95 | 7433 | 0.99 | 6447 | 1.14 | 7242 | 1.01 |
| S1O33-I13-S44-C64 | 6004 | 0.96 | 5733 | 1.00 | 5159 | 1.12 | 5934 | 0.97 |
| S1O33-I13-S44-C69 | 6788 | 0.96 | 6512 | 1.00 | 5681 | 1.15 | 6479 | 1.01 |
| S1O33-I23-S44-C66 | 6668 | 1.01 | 6409 | 1.05 | 5941 | 1.14 | 6329 | 1.07 |
| S1O33-I.73-S44-C66 | 5728 | 1.00 | 5578 | 1.03 | 4699 | 1.22 | 5908 | 0.97 |
| S1O33-I13-S77-C66 | 7973 | 1.01 | 7326 | 1.10 | 6582 | 1.22 | 8051 | 1.00 |
| S1O33-I13-S22-C66 | 5322 | 0.94 | 5178 | 0.96 | 4531 | 1.10 | 4923 | 1.01 |
| S1O33-I13-S44-C44 | 5271 | 1.02 | 5013 | 1.07 | 4613 | 1.17 | 5368 | 1.00 |
| S1O33-I13-S44-C99 | 8261 | 0.93 | 7952 | 0.97 | 6805 | 1.13 | 7605 | 1.02 |
| Mean | | 0.99 | | 1.03 | | 1.15 | | 1.02 |
| COV | | 0.06 | | 0.06 | | 0.05 | | 0.03 |

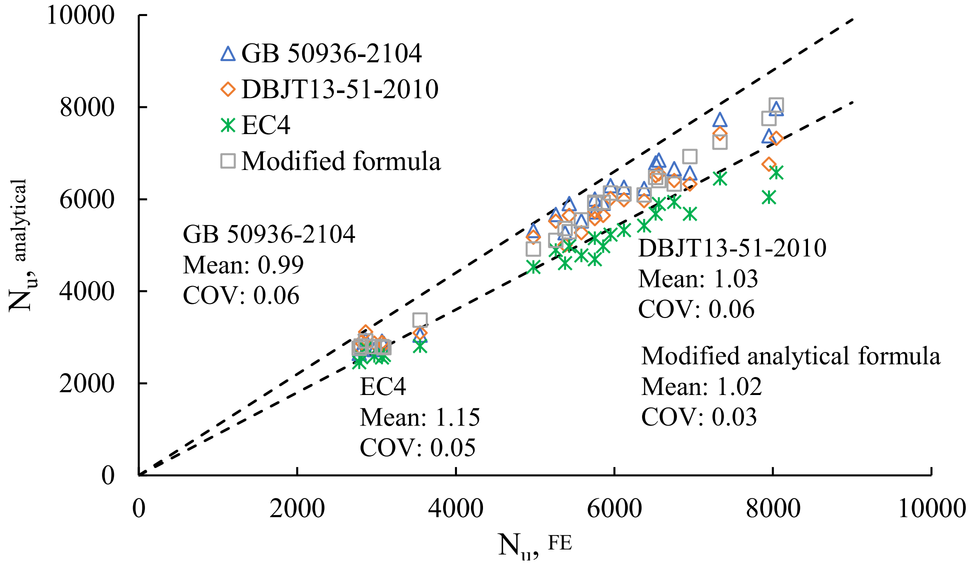


**Fig 5.2** Comparison of axial strength prediction-stub column

In terms of variability, the modified analytical formulation exhibited the lowest coefficient of variation (COV) at 0.03, reflecting the most consistent predictions among the methods. The EC4 standard, while conservative, showed moderate variability (COV = 0.05), suggesting some inconsistency in its strength estimates. Both GB 50936–2014 and DBJ/T 13-51-2010 had COVs of 0.06, indicating similar levels of variability in their predictions. In summary, while the EC4 standard underestimated axial strength, the Chinese standards and the modified analytical formulation provided closer and more consistent predictions relative to the FE results, with the modified analytical formulation demonstrating the highest consistency.

### 5.3.2 Full-Scale Slender Columns

The predictions for full-scale slender columns revealed a similar trend as presented in Table 5.2. The EC4 standard once again had the highest mean ratio of 1.27, significantly underestimating the strength and its COV increased from 0.05 for stub columns to 0.10 for slender columns. This increase reflects a greater degree of variability in the predictions for slender columns, suggesting that EC4 becomes less consistent as the column's slenderness increases. In comparison, the Chinese standards slightly overestimated the axial strength for slender columns, with mean ratios of 0.92 and 0.94 for GB 50936–2014 and DBJ/T 13-51-2010, respectively. These ratios are lower than those for stub columns, which were 0.99 and 1.03, indicating a closer alignment of the Chinese codes with the FE analysis for slender columns. However, both Chinese codes showed higher variability in their predictions for slender columns, with a COV of around 0.10, compared to 0.06 for stub columns as illustrated in Fig 5.3.

The modified analytical formulation provided the most accurate predictions for both stub and slender columns, with a mean ratio of 0.95 for slender columns and 1.02 for stub columns. However, similar to the other standards, the COV for the modified formulation increased from 0.03 for stub columns to 0.08 for slender columns, reflecting decreased consistency in predicting the strength of slender columns due to the influence of buckling and slenderness effects.

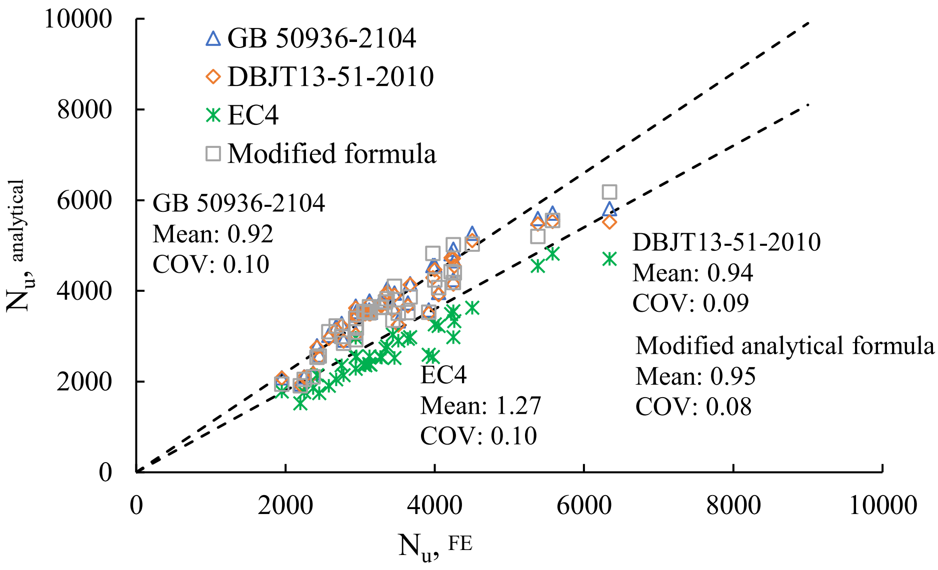


**Fig 5.3** Comparison of axial strength prediction-full scale slender column

### 5.3.3 Summary and Overall Comparison

For both stub and full-scale slender columns, the Chinese codes (GB 50936–2014 and DBJ/T 13-51-2010) and the modified analytical formulation tend to slightly overestimated the axial strength, while the EC4 standard consistently underestimated it. Regarding variability, all prediction methods exhibited an increase in the coefficient of variation, with COV values of approximately 0.09 for all codes when considering both stub and slender columns as shown in Table 5.3. In conclusion, while the EC4 standard was generally conservative and underestimated axial strength, it showed increased variability for slender columns compared to stub columns. The Chinese standards and the modified analytical formulation provided predictions that were more consistent with the FE results, although they showd some overestimation, especially for slender columns. The modified analytical formulation, despite a slight underestimation, stands out for offering the most consistent predictions across all scenarios.

**Table 5.2** Comparison of axial load from various standards, modified analytical formula and FE analysis for full scale columns

| Columns designation | $P_{GB}$ (kN) | $\frac{P_{FE}}{P_{GB}}$ | $P_{DBJT}$ (kN) | $\frac{P_{FE}}{P_{DBJT}}$ | $P_{EC4}$ (kN) | $\frac{P_{FE}}{P_{EC4}}$ | $P_{MAN}$ (kN) | $\frac{P_{FE}}{P_{MAN}}$ |
|---|---|---|---|---|---|---|---|---|
| L3O24-I13-S33-C66 | 3954 | 0.87 | 3905 | 0.89 | 2524 | 1.37 | 4100 | 0.84 |
| L3O23-I13-S33-C66 | 3764 | 0.87 | 3686 | 0.89 | 2545 | 1.28 | 3642 | 0.90 |
| L3O22-I13-S33-C66 | 3546 | 0.83 | 3464 | 0.85 | 2558 | 1.15 | 3176 | 0.93 |
| L3O23-I14-S33-C66 | 3749 | 0.88 | 3677 | 0.89 | 2531 | 1.30 | 3635 | 0.91 |
| L3O23-I12-S33-C66 | 3779 | 0.83 | 3696 | 0.85 | 2560 | 1.22 | 3648 | 0.86 |
| L3O23-I13-S37-C66 | 4160 | 0.88 | 4138 | 0.89 | 2980 | 1.23 | 3868 | 0.95 |
| L3O23-I13-S32-C66 | 3590 | 0.86 | 3494 | 0.88 | 2361 | 1.30 | 3547 | 0.87 |
| L3O23-I13-S73-C66 | 4559 | 0.87 | 4290 | 0.93 | 2545 | 1.56 | 4826 | 0.82 |
| L3O23-I13-S23-C66 | 3463 | 0.85 | 3426 | 0.86 | 2545 | 1.16 | 3094 | 0.95 |
| L3O23-I13-S33-C46 | 3216 | 0.83 | 3145 | 0.85 | 2047 | 1.31 | 3225 | 0.83 |
| L3O23-I13-S33-C96 | 4557 | 0.88 | 4467 | 0.90 | 3263 | 1.23 | 4243 | 0.94 |
| L3O23-I13-S33-C64 | 3578 | 0.87 | 3496 | 0.89 | 2386 | 1.31 | 3516 | 0.89 |
| L3O23-I13-S33-C69 | 4043 | 0.83 | 3965 | 0.85 | 2776 | 1.21 | 3827 | 0.88 |
| L3O23-I1.73-S33-C66 | 3970 | 0.84 | 3895 | 0.86 | 2726 | 1.23 | 3757 | 0.89 |
| L3O23-I.73-S33-C66 | 3533 | 0.86 | 3494 | 0.87 | 2371 | 1.29 | 3544 | 0.86 |
| F1O23-I13-S33-C66 | 4248 | 1.00 | 4149 | 1.02 | 3549 | 1.20 | 4187 | 1.02 |
| F4O23-I13-S33-C66 | 3068 | 0.96 | 3026 | 0.97 | 2278 | 1.29 | 2924 | 1.01 |

| | | | | | | | | |
|---|---|---|---|---|---|---|---|---|
| F6O23-I13-S33-C66 | 2188 | 1.08 | 2174 | 1.09 | 1859 | 1.28 | 2106 | 1.13 |
| F1O23-I13-S22-C66 | 3639 | 0.95 | 3572 | 0.96 | 3034 | 1.13 | 3354 | 1.03 |
| F3O23-I13-S22-C66 | 3284 | 0.84 | 3229 | 0.85 | 2361 | 1.16 | 2993 | 0.92 |
| F4O23-I13-S22-C66 | 2788 | 0.87 | 2753 | 0.88 | 2139 | 1.13 | 2538 | 0.95 |
| F6O23-I13-S22-C66 | 2087 | 0.93 | 2074 | 0.94 | 1783 | 1.09 | 1946 | 1.00 |
| F1O23-I13-S66-C66 | 5813 | 1.09 | 5517 | 1.15 | 4709 | 1.35 | 6183 | 1.03 |
| F3O23-I13-S66-C66 | 4918 | 0.86 | 4711 | 0.90 | 2980 | 1.43 | 5015 | 0.85 |
| F4O23-I13-S66-C66 | 3581 | 1.09 | 3504 | 1.12 | 2589 | 1.51 | 3531 | 1.11 |
| F1O23-I13-S33-C44 | 3342 | 1.05 | 3250 | 1.08 | 2903 | 1.21 | 3509 | 1.00 |
| F3O23-I13-S33-C44 | 3023 | 0.85 | 2949 | 0.87 | 1906 | 1.35 | 3096 | 0.83 |
| F4O23-I13-S33-C44 | 2581 | 0.95 | 2533 | 0.97 | 1748 | 1.40 | 2563 | 0.96 |
| F6O23-I13-S33-C44 | 1948 | 1.13 | 1928 | 1.14 | 1517 | 1.45 | 1907 | 1.15 |
| F1O23-I13-S33-C99 | 5596 | 0.96 | 5473 | 0.98 | 4549 | 1.18 | 5197 | 1.04 |
| F3O23-I13-S33-C99 | 4821 | 0.88 | 4731 | 0.89 | 3484 | 1.21 | 4421 | 0.95 |
| F4O23-I13-S33-C99 | 3660 | 0.80 | 3622 | 0.81 | 2964 | 0.99 | 3392 | 0.87 |
| F1O23-I.73-S33-C66 | 3969 | 1.02 | 3919 | 1.03 | 3225 | 1.26 | 4075 | 0.99 |
| F3O23-I.73-S33-C66 | 3533 | 0.89 | 3494 | 0.90 | 2371 | 1.32 | 3544 | 0.89 |
| F4O23-I.73-S33-C66 | 2914 | 0.95 | 2892 | 0.96 | 2137 | 1.30 | 2846 | 0.98 |
| F6O23-I.73-S33-C66 | 2105 | 1.07 | 2097 | 1.07 | 1766 | 1.27 | 2049 | 1.10 |
| F1O33-I13-S33-C66 | 5718 | 0.98 | 5531 | 1.01 | 4820 | 1.16 | 5554 | 1.00 |

| | | | | | | | | |
|---|---|---|---|---|---|---|---|---|
| F3O33-I13-S33-C66 | 5268 | 0.85 | 5110 | 0.88 | 3624 | 1.24 | 5029 | 0.89 |
| F4O33-I13-S33-C66 | 4663 | 0.91 | 4548 | 0.94 | 3330 | 1.28 | 4396 | 0.97 |
| F6O33-I13-S33-C66 | 3731 | 0.98 | 3674 | 0.99 | 2943 | 1.24 | 3522 | 1.03 |
| Mean | | 0.92 | | 0.94 | | 1.27 | | 0.95 |
| COV | | 0.10 | | 0.09 | | 0.10 | | 0.08 |

**Table 5.3** Overall comparison of axial load from various standards, modified analytical formula and FE analysis

| Columns Type | | $\frac{P_{FE}}{P_{GB}}$ | $\frac{P_{FE}}{P_{DBJT}}$ | $\frac{P_{FE}}{P_{EC4}}$ | $\frac{P_{FE}}{P_{MAN}}$ |
|---|---|---|---|---|---|
| Stub column | Mean | 0.99 | 1.03 | 1.15 | 1.02 |
| | COV | 0.06 | 0.06 | 0.05 | 0.03 |
| Full scale column | Mean | 0.92 | 0.94 | 1.27 | 0.95 |
| | COV | 0.10 | 0.09 | 0.10 | 0.08 |
| Stub and full-scale column | Mean | 0.95 | 0.97 | 1.22 | 0.98 |
| | COV | 0.09 | 0.09 | 0.09 | 0.08 |

## 5.4 Reliability Analysis

### 5.4.1 General Procedure

A statistical evaluation was conducted to assess the reliability of EC4, Chinese codes, and the modified analytical formulation using the standard evaluation procedure outlined in Annex D of EN 1994 (1994). The procedure begins by obtaining theoretical resistance values ($r_t$) from a resistance model, which incorporates measured material and geometric properties. These theoretical values were then compared with FE results ($r_e$) through linear regression analysis. An error term ($\delta_i$) was calculated for each data pair, where the correction factor (b) was determined by the slope of the least squares best fit of the $r_e$ versus $r_t$ plot. To quantify the variability of the resistance model, the coefficient of variation of the error term ($V_\delta$) was computed. The design resistance value ($r_d$) was subsequently derived using the Eq. 5.14 with the mean value of b and the mean values of the basic variables.

$$r_d = b g_{rt}(X_m) \exp\left(-k_{d,\infty}\alpha_{rt}Q_{rt} - k_{d,n}\alpha_\delta Q_\delta - 0.5Q^2\right) \tag{5.14}$$

Weighting factors $\alpha_{rt}$ and $\alpha_{\delta}$ for $Q_{rt}$ and $Q_{\delta}$ were also incorporated through Eq (5.15 to 5.18), to refine the design resistance model, ensuring a reliable design with an associated probability of failure of approximately 0.1%.

$$\alpha_{rt} = \frac{Q_{rt}}{Q} \tag{5.15}$$

$$\alpha_{\delta} = \frac{Q_{\delta}}{Q} \tag{5.16}$$

$$Q_{rt} = \sqrt{ln(V_{rt}^2 + 1)} \tag{5.17}$$

$$Q_{\delta} = \sqrt{ln\left(V_{\delta}^2 + 1\right)} \tag{5.18}$$

$$Q = \sqrt{ln(V_{\mathrm{r}}^2 + 1)} \tag{5.19}$$

$$V_r^2 = V_{\delta}^2 + V_{rt}^2 \tag{5.20}$$

The design fractile for ultimate limit state design was determined by applying the factor $k_{d,\mathrm{n}}$ for a finite population of tests and $k_{d,\infty}$ = 3.04 for an infinite population. This procedure follows the semi-probabilistic approach of EN 1990, which decouples the effects of actions and resistances using the weight factors $\alpha_E$ and $\alpha_R$, set to 0.8 and the reliability index (β) set at 3.8 for a 50-year reference period under ultimate limit state conditions. The analysis incorporated the key parameters essential for evaluating the probability of failure and ensuring compliance with relevant safety standards, as outlined in Table 5.4. The partial safety factors for materials were selected based on established codes: a factor of 1.0 for steel (as per EN 1993-1-1) and 1.5 for concrete (as per EN 1992-1-1). To assess the reliability of the design, the overall partial safety factor for the column (denoted as $\gamma_m$) is calibrated using the following equation:

$$\gamma_m = \frac{\sum_{i=1}^{n} r_n r_d}{\sum_{i=1}^{n} r_d^2} \tag{5.21}$$

In this equation, $r_n$ represents the characteristic resistance, which accounts for material-specific partial safety factors, while $r_d$ refers to the design resistance, including associated error terms. The reliability analysis was based on this relationship to ensure that the designed structure meets the required safety standards under various conditions.

The resulting value of $\gamma_m$ is used to determine whether the existing partial safety factors for concrete and steel are adequate. If $\gamma_m$ is less than or equal to 1.0, it suggests that the current partial safety factors are sufficient to maintain the required level of reliability and these factors can be applied across a broader range of design parameters. However, if the value of $\gamma_m$ exceeds 1.0, it indicates a need for increased partial safety factors in order to achieve the necessary reliability level. This adjustment ensured that the structure will continue to meet safety standards under all expected loading conditions.

### 5.4.2 Partial Safety Factor Analysis

The reliability results are presented in Table 5.4 and Fig 5.4 provide valuable insights into the partial safety factors of various standards and analytical formulations used in the design process.

**Table 5.4** Summary of the parameters for reliability analysis

| Design standards | No of test, n | $k_{d,n}$ | b | $v_r$ | $\gamma_m$ |
|---|---|---|---|---|---|
| EC4 | 64 | 3.28 | 1.19 | 0.179 | 0.850 |
| GB 50936–2014 | 64 | 3.28 | 0.96 | 0.183 | 1.025 |
| DBJ/T 13-51-2010 | 64 | 3.28 | 0.99 | 0.184 | 1.005 |
| Modified analytical formulation | 64 | 3.28 | 0.98 | 0.178 | 0.981 |

Notably, the EC4 standard demonstrated a partial safety factor of 0.85, which was substantially lower than the unity value typically expected for safety factor analysis. In contrast, the other standards—GB 50936–2014, DBJ/T 13-51-2010 and the modified analytical formulation—yield partial safety factors close to unity, with GB 50936–2014 showing the highest value at 1.025. The lower partial safety factor of EC4 (0.85) suggests that the existing safety factors for steel and concrete under this standard provide an ample safety margin, adequately addressing potential uncertainties in material behaviour and loading conditions. This result indicated that the design is highly conservative, yet still maintains the necessary reliability standards. The relatively low value of 0.85 for EC4 signified that the current safety factors are sufficient and there is a no need for additional material safety precautions.

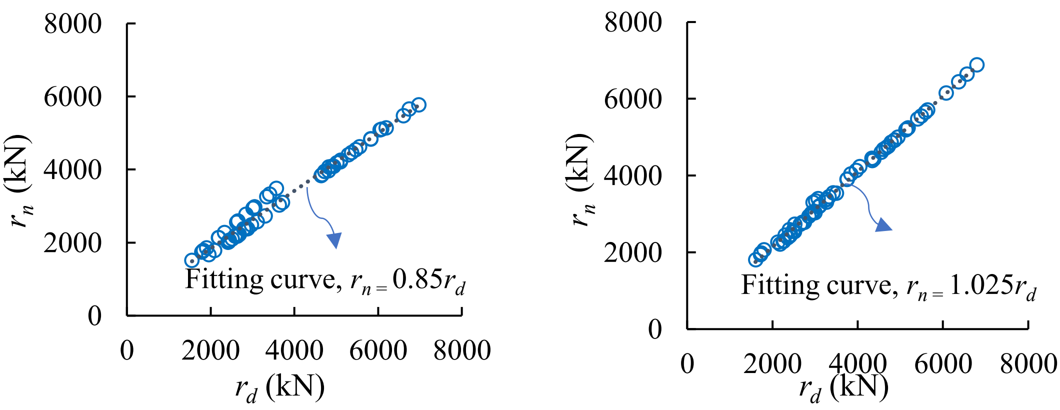


**(a)** EC4 **(b)** GB 50936–2014

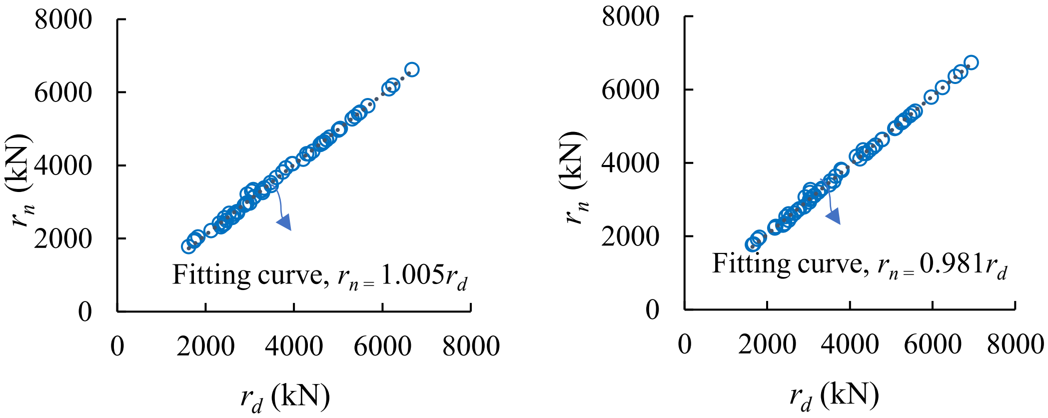


**(c)** DBJ/T 13-51-2010 **(d)** Modified analytical formulation

**Fig 5.4** Reliability analysis

In comparison, the DBJ/T 13-51-2010 and the modified analytical formulation both exhibited partial safety factors near unity, indicating a balanced approach. These formulations provided a compromise between conservatism and efficient use of materials. By setting the partial safety factor close to 1, these standards ensured a moderate safety margin, thereby maintaining structural reliability while allowing for some degree of material optimization. This approach maintains a balance between ensuring safety and minimizing material overuse, which is critical in achieving both performance and cost-efficiency in design. On the other hand, the GB 50936–2014 standard, with a partial safety factor of 1.025, reflected a higher level of uncertainty regarding material performance. The safety factor value above 1 suggested that this standard must incorporates additional caution to account for potential variability or unknowns in material properties, loading conditions, or environmental factors. It also implied that the material usage may be slightly overestimated compared to other standards.

In summary, the analysis of partial safety factors revealed that different design codes and formulations offer varying levels of safety margins, with EC4 providing a more conservative approach, DBJ/T 13-51-2010 and the modified analytical formulation offering a balanced design and GB 50936–2014 adopting a more cautious approach to account for higher uncertainty in material performance.

### 5.5 Summary

In this chapter, various design codes were evaluated, with EC4 proving to be the most conservative approach for both stub (mean: 1.15, COV: 0.05,) and full-scale columns (mean: 1.27; COV: 0.10). Comparisons indicated that the Chinese codes and the modified analytical formulations closely aligned with FE data, with mean values of 0.99, 1.03, and 1.02, respectively. The reliability analysis revealed that among all the design standards, the modified analytical formula offers the highest safety, with a partial safety factor of 0.981, which is lower than 1. This suggested that the modified formula effectively balances material optimization while maintaining an adequate safety margin in the calculation of axial strength for both stub and full-scale columns.

However, there remains potential for further development in formulation for eccentrically loaded columns. To achieve this, additional datasets would be beneficial. In the next chapter, the findings of this study will be discussed in detail, along with potential scope for future research on DDSTCC columns.

# CHAPTER 6: CONCLUSIONS AND RECOMMENDATIONS

## 6.1 Introduction

This chapter presents the key findings from chapters 4 and 5, highlighting significant insights and their implications. This chapter also includes recommendations and guidelines for future work relating to this investigation.

## 6.2 Key Findings

The study employed both numerical and analytical methods to investigate the behaviour of DDSTCC columns subjected to axial and eccentric loading, alongside the performance of full-scale columns. The comprehensive parametric analysis identified the critical parameters influencing the compressive behaviour and failure behaviour of these columns. Based on the results a modified analytical formula was proposed considering differential confinement effect to predict the ultimate strength of the column. The key findings of the study are summarized as follows:

1. FE model developed in this study was validated against the existing test results which consists of wide range of parameter variations. The results showed a mean value of 1.013 and a low variability index of 0.037, indicating excellent predictive accuracy with minimal discrepancies between predicted FE model and test results. Thus, the FE model could reliably replicate the compressive behaviour and failure pattern of DDSTCC columns and also could be used in future analytical studies. However, for high strength material, the FE models predictive accuracy should be considered with cautions over a certain range.

2. The key influencing parameters of stub columns are thickness and strength of outer steel tube, strength of sandwich concrete and diameter of inner steel tubes. Among these the higher strength of the outer steel tube and the sandwich concrete resulted in significant improvements in axial strength capacity, with increases of up to 24% and 20%, respectively. While the reduction in diameter of the inner steel tube has a negative effect on the residual strength capacity.
3. Similar to stub column, in full scale slender column the incorporation of high-strength outer steel and sandwich concrete resulted in 20% to 22% increment in axial strength capacity. Most of the columns showed a reduction in residual strength but only use of high strength outer steel could provide stability. As the slenderness increase, the performance of high-strength materials appeared to be less effective. With the increasing slenderness the columns with high strength constituents are susceptible to buckling and brittle failure suggesting that, under such conditions, normal strength constituents may play a more significant role in maintaining the column's relative axial strength.
4. For eccentrically loaded columns, the key parameters are associated with inner steel tubes; both thickness and diameter led to significant improvements in both load and moment capacity. Notably, inner steel tube with 225 mm diameter (G25) exhibited higher performance compared to 4 mm thick outer steel tube. (G22), particularly at higher eccentricity ratios, where G25 demonstrated a higher relative axial strength. All parameters at an eccentricity ratio of 0.2 shows minimal variations, however, as the eccentricity ratio increases the stability and stiffness provided by the increased dimensions of the inner steel tube better resisted the effects of eccentric loading.

5. Different failure patterns were observed for stub column with concentric and eccentric loading and full-scale slender column with concentric loading. The concentrically loaded stub columns showed a more uniform buckling with dispersed stress distribution at mid height region. For eccentrically loaded stub column, the stress concentration localized at column capital gap at eccentricity axis, suspecting the vulnerability of this region. Additionally, for full scale slender column demonstrated localized stress concentration at mid height region with C shape global buckling pattern.
6. Among all the existing design standards the EC4 standard demonstrated the conservative prediction with consistent lower estimation, while the Chinese codes GB 50936–2014 and DBJ/T 13-51-2010 predicted closed to FE results with less variability. Comparing with the design standards, the modified analytical formulation demonstrated the closed approximation of mean near to 1 with lowest variability showing its accuracy in predictions. In addition, modified formulation considers differential confinement effect which could accurately predict axial strength of column with high strength steel at outer layer than other standards.
7. The reliability analysis indicated that the conservative EC4 standard offered the highest safety margin, followed by the modified analytical formulation and DBJ/T 13-51-2010, both of which offered adequate safety margins. However, the GB 50936–2014 standard reflected some uncertainty in material optimization, as partial safety factor considerably higher than 1, suggesting that its safety margin might not be consistent as that of the other standards.

To conclude, in this study a detail explanation about the compressive behaviour of DDSTCC column were presented under different loading scenarios and geometric configuration. The study identifies the critical parameters which significantly influence the load-bearing capacity and provides a comprehensive assessment of their failure modes. The proposed analytical formulation offers a reliable guideline to evaluate the strength of DDSTCC columns with adequate safety margins for application in future high rise structural designs.

**6.3 Future Recommendations**

The present study on the compressive behaviour of DDSTCC columns highlighted several promising directions for future research which are as follows:

1. To examine the behaviour DDSTCC column under cyclic and fatigue loading conditions to check the response of discontinuous tube configuration to gain insights into their durability and long-term serviceability.
2. To investigate the effect of void defects in DDSTCC column associated with CFT column during construction.
3. To perform a comprehensive life cycle analysis (LCA) to thoroughly assess the sustainability, environmental impact, and economic viability of DDSTCC columns.
4. To develop the analytical formulation for eccentrically loaded stub column.
5. To carry out more experimental investigation using high strength steel and high strength concrete.

These future investigations will significantly expand the understanding and broaden the application of DDSTCC columns, enabling their integration into modern construction practices.

## References


Abed, F., AlHamaydeh, M., & Abdalla, S. (2012). Experimental and numerical investigations of the compressive behaviour of concrete filled steel tubes (CFSTs). Journal of Constructional Steel Research, 80, 429–439.

ACI 318 (2014), "Building Code Requirements for Structural Concrete". American Concrete Institute, Farmington Hills, MI.

Ahmed, M., Ci, J., Yan, X., Lin, S., & Chen, S. (2021). Numerical modeling of axially loaded circular concrete-filled double-skin steel tubular short columns incorporating a new concrete confinement model. *Structures*, *30*, 611–627.

Ahmed, M., Liang, Q. Q., Patel, V. I., & Hadi, M. N. (2019). Behaviour of eccentrically loaded double circular steel tubular short columns filled with concrete. Engineering Structures, 201, 109790.

Ahmed, M., Liang, Q. Q., Patel, V. I., & Hadi, M. N. (2019). Numerical analysis of axially loaded circular high strength concrete-filled double steel tubular short columns. Thin-Walled Structures, 138, 105–116.

Ahmed, M., Liang, Q. Q., Patel, V. I., & Hadi, M. N. (2020). Computational simulation of eccentrically loaded circular thin-walled concrete-filled double steel tubular slender columns. Engineering Structures, 213, 110571.

Albero, V., Ibañez, C., Piquer, A., & Hernández-Figueirido, D. (2020). Behaviour of slender concrete-filled dual steel tubular columns subjected to eccentric loads. Journal of Constructional Steel Research, 176, 106365.

An, Y., Han, L., & Zhao, X. (2012). Behaviour and design calculations on very slender thin-walled CFST columns. *Thin-Walled Structures*, *53*, 161–175.

ANSI/AISC 360-16 (2005), "Specification for Structural Steel Buildings", American Institute of Steel Construction, American National Standard.

AS/NZS 2327 (2017), Composite Structures: Composite Steel-Concrete Construction in Buildings, SA (Standards Australia), Sydney, Australia.

Ayough, P., Sulong, N. R., & Ibrahim, Z. (2019). Analysis and review of concrete-filled double skin steel tubes under compression. Thin-Walled Structures, 148, 106495.

Binici, B. (2005). An analytical model for stress–strain behaviour of confined concrete. Engineering Structures, 27(7), 1040–1051.

Chen, J., Ni, Y., & Jin, W. (2014). Column tests of dodecagonal section double skin concrete-filled steel tubes. Thin-Walled Structures, 88, 28–40.

Chin, C., Ma, C., Tan, J., Ong, C., Awang, A. Z., & Omar, W. (2019). Review on development of external steel-confined concrete. Construction and Building Materials, 211, 919–931.

DBJ/T 13-51-2010 2010. Technical specification for concrete-filled steel tubular structures. Department of Housing and Urban-Rural Development of Fujian Province, Fuzhou, China.

De Oliveira, W. L. A., De Nardin, S., De Cresce El Debs, A. L. H., & Debs, M. K. E. (2009). Evaluation of passive confinement in CFT columns. Journal of Constructional Steel Research, 66(4), 487–495.

Ekmekyapar, T., & Al-Eliwi, B. J. (2017). Concrete filled double circular steel tube (CFDCST) stub columns. Engineering Structures, 135, 68–80.

Ekmekyapar, T., & Hasan, H. G. (2019). The influence of the inner steel tube on the compression behaviour of the concrete filled double skin steel tube (CFDST) columns. Marine Structures, 66, 197–212.

Elchalakani, M., Zhao, X., & Grzebieta, R. (2002). Tests on concrete filled double-skin (CHS outer and SHS inner) composite short columns under axial compression. Thin-Walled Structures, 40(5), 415–441.

Ellobody, E., Young, B., & Lam, D. (2005). Behaviour of normal and high strength concrete-filled compact steel tube circular stub columns. *Journal of Constructional Steel Research*, *62*(7), 706–715.

European Committee for Standardization (1994). “Eurocode 4: Design of Composite Steel and Concrete Structures”. CEN.

Evirgen, B., Tuncan, A., & Taskin, K. (2014). Structural behaviour of concrete filled steel tubular sections (CFT/CFSt) under axial compression. Thin-Walled Structures, 80, 46–56.

Furlong, R. W. (1967). Strength of Steel-Encased concrete beam columns. Journal of the Structural Division, 93(5), 113–124.

Gabel, J., Carver, M., & Gerometta, M. (2015). The Skyscraper Surge Continues in 2015, The ‘Year of 100 Supertalls’. CTBUH Year in Review: Tall Trends of.

Gardner, N. J., & Jacobson, E. R. (1967). Structural behaviour of concrete filled steel tubes. ACI Journal Proceedings, 64(7). https://doi.org/10.14359/7575

GB 50936-2014 (2014), Technical Code for Concrete Filled Steel Tubular Structures, China Building Industry Press, Beijing. (in Chinese).

Han, L., Li, W., & Bjorhovde, R. (2014). Developments and advanced applications of concrete-filled steel tubular (CFST) structures: Members. Journal of Constructional Steel Research, 100, 211–228.

Han, L., Liu, W., & Yang, Y. (2007). Behaviour of thin walled steel tube confined concrete stub columns subjected to axial local compression. Thin-Walled Structures, 46(2), 155–164.

Han, L., Yao, G., & Tao, Z. (2007). Behaviours of concrete-filled steel tubular members subjected to combined loading. Thin-Walled Structures, 45(6), 600–619.

Han, L.-H., Yao, G.-H., & Tao, Z. (2007). Performance of concrete-filled thin-walled steel tubes under pure torsion. Thin-Walled Structures, 45(1), 24–36.

Hassanein, M., Elchalakani, M., & Patel, V. (2017). Overall buckling behaviour of circular concrete-filled dual steel tubular columns with stainless steel external tubes. Thin-Walled Structures, 115, 336–348.

Hassanein, M., Elchalakani, M., Karrech, A., Patel, V., & Daher, E. (2018). Finite element modelling of concrete-filled double-skin short compression members with CHS outer and SHS inner tubes. Marine Structures, 61, 85–99.

Hoang, A. L., & Fehling, E. (2017). Numerical study of circular steel tube confined concrete (STCC) stub columns. Journal of Constructional Steel Research, 136, 238–255.

Hoang, A. L., Fehling, E., Thai, D., & Van Nguyen, C. (2018). Evaluation of axial strength in circular STCC columns using UHPC and UHPFRC. *Journal of Constructional Steel Research*, *153*, 533–549.

Hossain, K. M. A., & Chu, K. (2019). Confinement of six different concretes in CFST columns having different shapes and slenderness. International Journal of Advanced Structural Engineering, 11(2), 255–270.

Hu, H., & Su, F. (2011). Nonlinear analysis of short concrete-filled double skin tube columns subjected to axial compressive forces. Marine Structures, 24(4), 319–337.

Huang, H., Han, L., & Zhao, X. (2013). Investigation on concrete filled double skin steel tubes (CFDSTs) under pure torsion. Journal of Constructional Steel Research, 90, 221–234.

Ibañez, C., Hernández-Figueirido, D., & Piquer, A. (2018). Shape effect on axially loaded high strength CFST stub columns. Journal of Constructional Steel Research, 147, 247–256.

Ibañez, C., Romero, M. L., Espinos, A., Portolés, J., & Albero, V. (2017). Ultra-high strength concrete on eccentrically loaded slender circular concrete-filled dual steel columns. Structures, 12, 64–74.

Jin, K., Zhou, X., Ren, W., Wang, Y., & Li, R. (2024). Axial compressive behavior of concrete-filled double skin steel tubular columns with different stiffening constructions for wind turbine towers. *Structures*, *63*, 106390.

Kabir, M. I., Rehan, M. S., Ahmed, Z., Sakib, A. N., & Shoeb, M. M. (2025). Numerical and analytical evaluation of the compressive performance of steel tube (ST)-Reinforced Concrete filled Stainless Steel tubular (CFSST) columns. *Results in Engineering*, 103904.

Knowles, R. B., & Park, R. (1969). Strength of concrete filled steel tubular columns. Journal of the Structural Division, 95(12), 2565–2588.

Lam, D., Dai, X., Han, L., Ren, Q., & Li, W. (2012). Behaviour of inclined, tapered and STS square CFST stub columns subjected to axial load. *Thin-Walled Structures*, *54*, 94–105.

Li, W., Ren, Q., Han, L., & Zhao, X. (2012). Behaviour of tapered concrete-filled double skin steel tubular (CFDST) stub columns. Thin-Walled Structures, 57, 37–48.

Liang, Q. Q. (2008). Performance-based analysis of concrete-filled steel tubular beam–columns, Part I: Theory and algorithms. Journal of Constructional Steel Research, 65(2), 363–372.

Liang, Q. Q. (2010). High strength circular concrete-filled steel tubular slender beam–columns, Part I: Numerical analysis. *Journal of Constructional Steel Research*, *67*(2), 164–171. https://doi.org/10.1016/j.jcsr.2010.08.006

Liang, Q. Q. (2016). Nonlinear analysis of circular double-skin concrete-filled steel tubular columns under axial compression. *Engineering Structures*, *131*, 639–650.

Liang, Q. Q., & Fragomeni, S. (2009). Nonlinear analysis of circular concrete-filled steel tubular short columns under axial loading. *Journal of Constructional Steel Research*, *65*(12), 2186–2196.

Liew, J. R., & Xiong, D. (2012). Ultra-High strength concrete filled composite columns for Multi-Storey building construction. Advances in Structural Engineering, 15(9), 1487–1503.

Liew, J. R., Xiong, M., & Xiong, D. (2016). Design of Concrete Filled Tubular Beam-columns with High Strength Steel and Concrete. Structures, 8, 213–226.

Liew, J. Y. R., & Xiong, M. (2015). Design Guide for Concrete Filled Tubular Members with High Strength Materials to Eurocode 4.

Lu, S., Wang, J., Yang, J., & Wang, L. (2022). Compressive behaviour of circular steel tubed high-strength concrete columns with embedded steel tubes. Journal of Constructional Steel Research, 193, 107259.

Lu, S., Wang, J., Yang, J., & Wang, L. (2022). Numerical analysis of circular tubed high-strength concrete columns with embedded steel tubes under axial compression. Structures, 45, 1124–1138.

Mander, J. B., Priestley, M. J. N., & Park, R. (1988). Theoretical Stress-Strain model for confined concrete. *Journal of Structural Engineering*, *114*(8), 1804–1826.

Nguyen, T., Thai, H., Li, D., Wang, J., Uy, B., & Ngo, T. (2021). Behaviour and design of eccentrically loaded CFST columns with high strength materials and slender sections. Journal of Constructional Steel Research, 188, 107004.

Nguyen, T., Thai, H., Ngo, T., Uy, B., & Li, D. (2021). Behaviour and design of high strength CFST columns with slender sections. Journal of Constructional Steel Research, 182, 106645.

Nie, J., Wang, Y., & Fan, J. (2013). Experimental research on concrete filled steel tube columns under combined compression-bending-torsion cyclic load. Thin-Walled Structures, 67, 1–14.

O'Shea, M. D., & Bridge, R. Q. (2000). Design of circular Thin-Walled concrete filled steel tubes. Journal of Structural Engineering, 126(11), 1295–1303.

Pagoulatou, M., Sheehan, T., Dai, X., & Lam, D. (2014). Finite element analysis on the capacity of circular concrete-filled double-skin steel tubular (CFDST) stub columns. Engineering Structures, 72, 102–112.

Patel, V. I., Uy, B., Prajwal, K., & Aslani, F. (2016). Confined concrete model of circular, elliptical and octagonal CFST short columns. Steel and Composite Structures, 22(3), 497–520.

Qiyun, Q., Zhaoyuan, Y., & Wanlin, C. (2021). Axial compressive behaviour of stainless-steel tube confined concrete column piers. *Marine Structures*, *78*, 103021.

Reddy, G. S. R., Bolla, M., Patton, M. L., & Adak, D. (2021). Comparative study on structural behaviour of circular and square section-Concrete Filled Steel Tube (CFST) and Reinforced Cement Concrete (RCC) stub column. Structures, 29, 2067–2081.

Ren, Q., Han, L., Lam, D., & Hou, C. (2014). Experiments on special-shaped CFST stub columns under axial compression. Journal of Constructional Steel Research, 98, 123–133.

Romero, M., Espinos, A., Portolés, J., Hospitaler, A., & Ibañez, C. (2015). Slender double-tube ultra-high strength concrete-filled tubular columns under ambient temperature and fire. Engineering Structures, 99, 536–545.

Sakino, K. (1985). Sustaing Load Capacity of Plain Concrete Stub Columns Confined by Circular Steel Tube. In Proceedings of the International Speciality Conference on Concrete Filled Steel Tubular Structures (pp. 112-118)

Samarakkody, D. I., Thambiratnam, D. P., Chan, T. H., & Moragaspitiya, P. H. (2017). Differential axial shortening and its effects in high rise buildings with composite concrete filled tube columns. Construction and Building Materials, 143, 659–672.

Sugimoto, M., Yokota, S., Sonoda, K., & Yagishita, F. (1997, July). A basic consideration on double skin tube-concrete composite columns. In Osaka City University and Monash University Joint Seminar on Composite Tubular Structures, Osaka.

Tang, J., Hino, S., Kuroda, I., & Ohta, T. (1996). Modeling of stress - Strain relationships for steel and concrete in concrete filled circular steel tubular columns. IEEE Journal of Solid-State Circuits, 3(11), 35–46.

Tao, Z., & Han, L. (2005). Behaviour of concrete-filled double skin rectangular steel tubular beam–columns. Journal of Constructional Steel Research, 62(7), 631–646.

Tao, Z., Han, L., & Zhao, X. (2004). Behaviour of concrete-filled double skin (CHS inner and CHS outer) steel tubular stub columns and beam-columns. *Journal of Constructional Steel Research*, *60*(8), 1129–1158.

Tao, Z., Wang, Z., & Yu, Q. (2013). Finite element modelling of concrete-filled steel stub columns under axial compression. Journal of Constructional Steel Research, 89, 121–131.

Tomii, M. (1977). Experimental studies on concrete filled steel tubular stub columns under concentric loading. In Proceedings of international colloquium on stability of structures under static and dynamic loads, SSRC/ASCE/Washington, DC.

Tomii, M. (1985). Lateral load capacity of reinforced concrete short columns confined by stell tube-experimental results of preliminary research. Proceedings of the International Specialty Confernce on Concrete-Filled Steel Tubular Structures, 19-26.

Uenaka, K., Kitoh, H., & Sonoda, K. (2009). Concrete filled double skin circular stub columns under compression. *Thin-Walled Structures*, *48*(1), 19–24.

Wang, F., Han, L., & Li, W. (2018). Analytical behaviour of CFDST stub columns with external stainless steel tubes under axial compression. Thin-Walled Structures, 127, 756–768.

Wang, J., He, J., & Xiao, Y. (2019). Fire behaviour and performance of concrete-filled steel tubular columns: Review and discussion. Journal of Constructional Steel Research, 157, 19–31.

Wang, W., Ji, S., & Shi, Y. (2022). Experimental and numerical investigations on concrete-filled double-tubular slender columns under axial and eccentric loading. Journal of Constructional Steel Research, 201, 107714.

Wang, X., Fan, F., & Lai, J. (2022). Strength behaviour of circular concrete-filled steel tube stub columns under axial compression: A review. Construction and Building Materials, 322, 126144.

Wei, J., Xie, Z., Zhang, W., Luo, X., Yang, Y., & Chen, B. (2020). Experimental study on circular steel tube-confined reinforced UHPC columns under axial loading. Engineering Structures, 230, 111599.

Xiong, M., Xiong, D., & Liew, J. R. (2017). Axial performance of short concrete filled steel tubes with high- and ultra-high- strength materials. Engineering Structures, 136, 494–510.

Xiong, M., Xiong, D., & Liew, J. R. (2017). Behaviour of steel tubular members infilled with ultra high strength concrete. Journal of Constructional Steel Research, 138, 168–183.

Yan, X., Zhao, Y., Lin, S., & Zhang, H. (2021). Confining stress path-based compressive strength model of axially compressed circular concrete-filled double-skin steel tubular short columns. Thin-Walled Structures, 165, 107949.

Yan, X.-F., & Zhao, Y.-G. (2021). Experimental and numerical studies of circular sandwiched concrete axially loaded CFDST short columns. Engineering Structures, 230, 111617.

Yang, Q., Zhao, B., Liu, B., Zhao, Z., & Mo, S. (2024). Influence of corrosion on loading capacity of circular concrete-filled steel tubular column. Journal of Constructional Steel Research, 215, 108564.

Yu, Q., Tao, Z., Liu, W., & Chen, Z. (2009). Analysis and calculations of steel tube confined concrete (STCC) stub columns. Journal of Constructional Steel Research, 66(1), 53–64.

Zhao, H., Wang, R., Lam, D., Hou, C., & Zhang, R. (2020). Behaviours of circular CFDST with stainless steel external tube: Slender columns and beams. Thin-Walled Structures, 158, 107172.

Zhao, X., & Grzebieta, R. (2002). Strength and ductility of concrete filled double skin (SHS inner and SHS outer) tubes. Thin-Walled Structures, 40(2), 199–213.

Zheng, Y., & Tao, Z. (2018). Compressive strength and stiffness of concrete-filled double-tube columns. Thin-Walled Structures, 134, 174–188.

Zheng, Y., He, C., & Zheng, L. (2018). Experimental and numerical investigation of circular double-tube concrete-filled stainless steel tubular columns under cyclic loading. Thin-Walled Structures, 132, 151–166.

Zhu, H., Chen, S., Ahmed, M., & Liang, Q. Q. (2024). Experimental and numerical investigations of circular concrete filled steel double-skin and double-tube columns exposed to fire. Thin-Walled Structures, 198, 111766.

Zhu, J., & Chan, T. (2018). Experimental investigation on octagonal concrete filled steel stub columns under uniaxial compression. Journal of Constructional Steel Research, 147, 457–467.

Zhu, J., & Chan, T. (2019). Experimental investigation on steel-tube-confined-concrete stub column with different cross-section shapes under uniaxial-compression. Journal of Constructional Steel Research, 162, 105729.